ANALYSIS OF FLOW STRUCTURE IN A HELICOPTER CABIN TO IMPROVE THE THERMAL COMFORT USING COMPUTATIONAL FLUID DYNAMICS MODELING

A THESIS SUBMITTED TO
THE GRADUATE SCHOOL OF NATURAL AND APPLIED SCIENCES
OF
MIDDLE EAST TECHNICAL UNIVERSITY

BY

DORUK ŞAHİN

IN PARTIAL FULFILLMENT OF THE REQUIREMENTS
FOR
THE DEGREE OF MASTER OF SCIENCE
IN
MECHANICAL ENGINEERING

MAY 2018

Approval of the thesis:

ANALYSIS OF FLOW STRUCTURE IN A HELICOPTER CABIN TO IMPROVE THE THERMAL COMFORT USING COMPUTATIONAL FLUID DYNAMICS MODELING

submitted by **DORUK ŞAHİN** in partial fulfillment of the requirements for the degree of **Master of Science in Mechanical Engineering Department, Middle East Technical University** by,

Prof. Dr. Halil Kalıpçılar _____
Director, Graduate School of **Natural and Applied Sciences**

Prof. Dr. M. A. Sahir Arıkan _____
Head of Department, **Mechanical Engineering**

Assoc. Prof. Dr. Mehmet Metin Yavuz _____
Supervisor, **Mechanical Engineering Dept., METU**

Examining Committee Members:

Assoc. Prof. Dr. Cüneyt Sert _____
Mechanical Engineering Dept., METU

Assoc. Prof. Dr. Mehmet Metin Yavuz _____
Mechanical Engineering Dept., METU

Prof. Dr. Kahraman Albayrak _____
Mechanical Engineering Dept., METU

Asst. Prof. Dr. Özgür Uğraş Baran _____
Mechanical Engineering Dept., METU

Assoc. Prof. Dr. Murat Kadri Aktaş _____
Mechanical Engineering Dept., TOBB-ETU

Date: 04.05.2018

I hereby declare that all information in this document has been obtained and presented in accordance with academic rules and ethical conduct. I also declare that, as required by these rules and conduct, I have fully cited and referenced all material and results that are not original to this work.

Name, Last name: Doruk Şahin

Signature:

ABSTRACT

ANALYSIS OF FLOW STRUCTURE IN A HELICOPTER CABIN TO IMPROVE THE THERMAL COMFORT USING COMPUTATIONAL FLUID DYNAMICS MODELING

Şahin, Doruk

M.S., Department of Mechanical Engineering

Supervisor: Assoc. Prof. Dr. Mehmet Metin Yavuz

May 2018, 118 pages

Proper distribution of conditioned air inside the cabins of passenger transportation type aircrafts is crucial in terms of passengers' comfort. Low air velocities may cause passengers to feel stuffy whereas high velocities may create disturbance. Moreover, satisfying uniform temperature distribution inside the cabin is also crucial for the passenger comfort. High temperature variation inside the cabin results in feeling of discomfort.

In this thesis, computational fluid dynamics (CFD) models are developed using ANSYS FLUENT to investigate thermal comfort level of the passengers in a newly designed passenger transportation helicopter. The desired air velocities in the vicinity of the faces of passengers are determined by utilizing SAE ARP292, ASHRAE 161-2013 and ASHRAE 161-2007. Moreover, in addition to air velocity, effective distribution of the personalized air flow around the faces of passengers is also considered. On the other hand, SAE ARP292 is used to determine the temperature related comfort parameters. For the analyses, a turbulence model anticipated as suitable for cabin type flows is selected and the competence of its performance is

confirmed by the experimental and numerical results available in the literature. The results reveal that the existing design of personalized air distribution system is inadequate for creating comfortable environment to passengers. For the purpose of enhancing thermal comfort of the passengers, an iterative procedure is followed to redesign personalized air distribution system by evaluating the results of numerical simulations in terms of thermal comfort levels. By the present thesis study, by redesigning personalized air inlets, adjusting their locations and proposing a flow rate ratio between personalized and main inlet flows, an improvement has been shown up in terms of thermal comfort levels of the passengers. The new design provides air velocities between the designated comfort range and effective distribution of the personalized air flow around the faces of passengers. Moreover, the temperature distribution inside the cabin becomes more uniform by the new design.

Keywords: Thermal Comfort, Air Distribution, Computational Fluid Dynamics, Turbulence Model

ÖZ

BİR HELİKOPTER KABİNİNDE TERMAL KONFORU İYİLEŞTİRME AMACIYLA AKIŞ YAPISININ HESAPLAMALI AKIŞKANLAR DİNAMİĞİ MODELLEME İLE İNCELENMESİ

Şahin, Doruk
Yüksek Lisans, Makina Mühendisliği Bölümü
Tez Yöneticisi: Doç. Dr. Mehmet Metin Yavuz

Mayıs 2018, 118 sayfa

Yolcu taşıma amaçlı kullanılan helikopterlerde, koşullandırılmış havanın dağıtımının doğru yapılması yolcu konforu açısından oldukça önemlidir. Düşük hava hızları yolcuların bunaltıcı hissetmesine yol açabilecekken, yüksek hızlar rahatsızlığa neden olabilir. Bunun yanında, kabin içerisindeki sıcaklık dağılımının homojen olması da yolcu konforu açısından oldukça önemlidir. Kabin içerisinde oluşan yüksek sıcaklık farklılıkları yolcuların rahatsız hissetmesine yol açar.

Bu tez çalışmasında, yeni tasarlanmış bir yolcu taşıma helikopteri içerisindeki yolcuların konfor durumlarını incelemek amacıyla ANSYS FLUENT kullanılarak CFD modelleri geliştirilmiştir. Yolcuların yüzleri etrafında olması hedeflenen hava hızları SAE ARP292, ASHRAE 161-2003 ve ASHRAE 161-2007 standartlarından yararlanılarak belirlenmiştir. Ayrıca, hava hızına ek olarak, kişisel hava çıkışlarından üflenen havanın, yolcuların yüzleri etrafında efektif dağılımı konusu da ele alınmıştır. Diğer yandan, sıcaklıkla ilgili olan konfor parametreleri SAE ARP292 standartından yararlanılarak belirlenmiştir. Analizlerde kullanmak amacıyla, kabin tipi akışları için uygun olarak öngörülen bir türbülans modeli seçilmiştir ve modelin

performans yetkinliği, literatürden elde edilen deneysel ve numerik çalışmaların sonuçlarıyla doğrulanmıştır. Araştırma sonuçları, mevcut kişisel hava çıkışı tasarımının, yolcu etrafında konforlu bir ortam oluşturma açısından yetersiz olduğunu ortaya çıkarmıştır. Yolcu konforunu artırma hedefiyle, numerik simülasyonlardan yararlanarak, kişisel hava dağıtım sistemi tasarımını geliştirmek amacıyla iteratif bir süreç takip edilmiştir. Bu tez çalışması ile, kişisel hava çıkışlarını tekrar tasarlayarak, bu çıkışların kabin içindeki yerleşim yerlerini ayarlayarak ve kabin hava girişlerine hava taşıyan hat için konfor açısından uygun olan akış miktarı oranı belirlenerek yolcuların konfor durumları iyileştirilmiştir. Yeni tasarım ile yolcuların yüzleri etrafında hedeflenen hava hızları elde edilmiştir ve havanın efektif dağıtımı da sağlanmıştır. Ayrıca, yeni tasarım ile kabin içerisindeki sıcaklık dağılımı daha homojen bir hale getirilmiştir.

Anahtar Kelimeler: Termal Konfor, Hava Dağılımı, Hesaplamalı Akışkanlar Dinamiği, Türbülans Modeli

To:

My Love Neslihan

My Mother

My Father

My Brother

ACKNOWLEDGEMENTS

I would like to express my gratitude to my supervisor Assoc. Prof. Dr. Mehmet Metin Yavuz, for giving me an opportunity to work with him, allowing me to benefit from his invaluable comments and experiences and his endless patience throughout my study.

My mother İffet, my father Uğur and my brother Alp Emre supported and encouraged me throughout my life. It would never be possible without their help.

I would like to thank to my love Neslihan for her endless support, encourage and patience.

I would like to express my thanks to my dearest friends and family for their supports.

I must also express my gratitude to my colleagues for their guidance.

TABLE OF CONTENTS

LIST OF TABLES

LIST OF FIGURES

LIST OF SYMBOLS

c_p	specific heat capacity, (J/kg-K)
k	turbulent kinetic energy, (m^2/s^2) thermal conductivity, (W/m-K)
k_t	turbulent thermal conductivity, (W/m-K)
L	characteristic length scale, (m)
l_ε, l_μ	length scales, (m)
P_{static}	static pressure, (N/m^2)
$\overline{p}$	mean pressure, (N/m^2)
Pr_t	turbulent Prandtl number
Re	Reynolds number
t	time, (s)
u_i, u_j, u_k	velocity components, (m/s)
$\overline{u_i}, \overline{u_j}, \overline{u_k}$	mean velocity components, (m/s)
$u_i', u_j', u_k{}'$	fluctuating velocity components, (m/s)
u_{wall}	velocity at wall, (m/s)
u_τ	shear velocity, (m/s)
U	characteristic velocity, (m/s)
U_∞	free stream velocity, (m/s)
u^+	dimensionless velocity
V	velocity, (m/s)

y	distance from wall, (m)
y^+	dimensionless distance from wall
β	volumetric thermal expansion coefficient
δ_{ij}	Kronecker delta
ε	turbulent dissipation rate, (m^2/s^3)
μ	molecular viscosity, (Pa.s)
μ_t	turbulent viscosity, (Pa.s)
ν	kinematic viscosity, (m^2/s)
ρ	fluid density, (kg/m^3)
σ_k	turbulent Prandtl number for turbulent kinetic energy
σ_ε	turbulent Prandtl number for turbulent dissipation rate
τ_w	shear stress, (Pa)
ω	specific turbulence dissipation rate, (s^{-1})

ABBREVIATIONS

C	contaminant concentration
CFD	computational fluid dynamics
CTA	constant temperature anemometry
DES	detached eddy simulation
DNS	direct numerical simulation
ECS	environmental control system
EVM	eddy-viscosity model
GS	gas sensor
H	humidity
HFM	heat flux meter
HSA	hot-sphere anemometer
HWA	hot-wire anemometer
LES	large eddy simulation
LRN	low Reynolds number
OAT	outside air temperature
RANS	Reynolds-averaged Navier-Stokes
PIV	particle image velocimetry
RMS	root mean square
RNG	renormalization group
RSM	Reynolds stress model

SA	sonic anemometer
SST	shear stress transport
T	temperature
TC	thermocouple
UA	ultrasonic anemometer
URANS	unsteady Reynolds-averaged Navier-Stokes
V	velocity
VPTV	volumetric particle tracking velocimetry
VS	velocity sensor

CHAPTER 1

INTRODUCTION

Recently, more and more people are travelling via air transportation. In a five-year period from 2012 to 2017, passenger traffic in the European countries' airports has increased by close to 30% [1]**.** As aviation industry develops rapidly, interest of the flying public to the environmental conditions in aircraft cabins is increasing [2]. To make passengers feeling satisfied, a thermally comfortable cabin environment should be created.

Thermal comfort is controlled by two factors, namely, personal factors and environmental factors [3]. Personal factors are related to the physical condition of the occupants like metabolic rate depending on occupants' level of activity and clothing. On the other hand, environmental factors such as temperature, velocity and humidity are controlled by the aircraft system called environmental control system (ECS).

Thermal comfort is influenced mainly by the velocity and temperature distribution inside the passenger cabin compartment [4]. Air distribution system which is a fundamental component of ECS controls the air temperature and velocity fields inside the cabin and; therefore, should properly distribute the conditioned air in order to make passengers feeling comfortable [5]. ECS of a typical passenger aircraft comprises two types of air distribution system; namely, main air distribution system and personalized air distribution system [6]. The primary function of main air distribution system is to satisfy the designated performance requirements throughout the cabin environment; thereby, main air distribution system provides limited contribution in meeting the thermal comfort demands of every passenger. Therefore, a personalized air supply system directly supplying conditioned air to each passenger is highly required to make passengers feeling comfortable. Personalized air

distribution system comprises adjustable type of air inlets, called gaspers which are controlled by passengers. When gaspers are turned on by the passengers, flow field inside the cabin may be dominated by both the main airflow and gasper-induced airflow [7].

Considering the other comfort analysis in literature such as for people in buildings, it has been proved that the personal ventilation can improve thermal comfort with the sensation of cooling as it passes over skin area, resulting in convection and evaporation; however, high velocities in the people's head region supplied by the personal ventilation may cause discomfort [8].

The cabin of an aircraft is such a complex domain, which involves high occupant density with multiple heat sources. Air flow inside the passenger cabin can be significantly influenced by a variety of parameters such as the geometry of the cabin, the positions of the air supply inlets, the supply air jet momentum and flow rate, the blockage by seats and passengers, the heat load in the cabin, the temperature difference between the cabin air and the supplied air, the temperature of the cabin walls, etc. Therefore, the design of environmental systems to ensure thermal comfort in an aircraft cabin is very challenging, especially for passenger transportation type aircrafts where the top performances are required.

1.1 Motivation of the Study

Researchers have investigated thermal comfort in aircraft cabins both numerically and experimentally. Both numerical and experimental methods have their own advantages and disadvantages; however, investigating flow field inside an aircraft cabin is very challenging for both methods because of the high turbulence intensity, unstable flow, complex geometry, high occupant density and high thermal loads.

In the literature, thermal comfort studies generally focus on airplane cabins. Few studies investigate helicopter cabin environment wherein airflow is more complex because of high occupancy in a smaller cabin volume. Moreover, most of the thermal comfort studies focus on main air distribution system by neglecting personalized air

inlets. However, in a helicopter cabin, air flow is dominated by both gaspers and main air supplies whose interaction in small cabin volume is noteworthy.

1.2 Aim of the Study

The aim of the present study is to numerically investigate the flow and temperature fields in a newly designed twelve-passenger capacity passenger transportation helicopter cabin and to propose an air distribution system design to improve thermal comfort conditions of the passengers. For this purpose, computation fluid dynamics (CFD) models of the helicopter cabin are developed.

A suitable turbulence model which is widely used in aircraft cabin simulations is selected. For the purpose of evaluating the performance of the selected turbulence model, a test case is selected from the Günther et al.'s [9] study. By using ANSYS FLUENT, a detailed mesh independence study is performed and followed by turbulence model performance evaluation study considering the experimental results and numerical predictions of Günther et al. [9] for comparison.

Following the confirmation of the performance competence of the selected turbulence model, a CFD model of the investigated helicopter cabin is developed and a detailed mesh independence study is performed. Thermal comfort levels of the passengers are numerically investigated by considering the related requirements obtained from the literature. By an iterative procedure, the design of air distribution system is improved by controlling gasper related parameters such as location, size and shape. Moreover, a flow distribution ratio between main inlets and personalized air inlets is proposed to enhance thermal comfort. Throughout the design iterations, the performance of each new design is investigated by CFD analyses.

With this study, an air distribution system design providing improvement in terms of thermal comfort conditions of passengers is proposed. It is expected from the improved design of this thesis study to have contribution on thermal comfort enhancement studies performed for the other passenger transportation helicopter platforms.

1.3 Structure of the Thesis

This thesis is composed of eight chapters. Chapter 1 provides introductory information about the thermal comfort and the factors influencing it. Motivation and aim of this thesis are stated.

In Chapter 2, previous studies performed on aircraft cabin and a few on enclosed spaces are listed and summarized. In this chapter, both experimental and numerical studies are presented.

In Chapter 3, Reynolds averaging process and governing equations of fluid flow and heat transfer are introduced. The theory behind the standard k-ε turbulence model is explained in detail.

In Chapter 4, the case used in the turbulence model performance evaluation study is described. Mesh independence study is performed for this case and the performance of the selected turbulence model to be used in the aircraft cabin flow simulations is evaluated by using the experimental data and numerical results obtained from the literature.

In Chapter 5, the cabin model of the investigated newly designed helicopter is described. Mesh independence study is performed for the helicopter cabin. The design criteria to satisfy thermal comfort of the passengers are described and thermal comfort levels of the passengers are numerically investigated for the existing air inlet locations.

In Chapter 6, the thermal comfort improvement study performed by controlling gasper locations are described and the procedure followed during the design is explained.

In Chapter 7, the thermal comfort improvement study performed by controlling sizes, shapes and flow rates of the gaspers in addition to controlling locations are described and the procedure followed during the design is explained. The design cases achieving sufficient thermal comfort enhancement are determined and the best design is proposed.

In Chapter 8, conclusions drawn throughout the study is provided and recommendations for possible future works are stated.

CHAPTER 2

LITERATURE REVIEW

In this chapter, the review of the studies conducted on thermal comfort is presented. Although some turbulence model investigation studies performed on general indoor environments are also included, the vast majority of the reviewed studies focus on aircraft cabin environment. In the first section of this chapter, the studies performed on enclosed environments are included to present the comparison of various types of turbulence models. In the second section, investigations considering only main air distribution system are included and in the last section, studies focusing on personalized air flow are presented.

2.1 Turbulence Model Investigation for Enclosed Environments

Several studies have been performed on finding an appropriate CFD approach and turbulence models for numerical simulations of enclosed environments.

Zhai et al. [10] studied on three CFD approaches; namely, Direct Numerical Simulation (DNS), Large Eddy Simulation (LES), and Reynolds-Averaged Navier-Stokes (RANS) modeling to identify turbulence models that are either commonly used or have recently been proposed and which have some potential for indoor air flow applications. The investigated turbulence models and prevalent turbulence models are shown in Table 2-1. Zhang et al. [11] evaluated the performances of eight turbulence models proposed by Zhai et al. [10] in terms of accuracy and computing cost by testing with the experimental data from the literature for four benchmark indoor flow cases. By considering the cases being close to cabin environment, for the forced convection with low turbulence levels in a model room with partitions case; the RNG, LRN-LS, v2f-dav and LES were performed very well. For the mixed

convection with low turbulence levels in a square cavity case; the v2f-dav, the RNG and the indoor zero-equation model showed the best accuracy. Wang and Chen [12] focused on investigating the factors causing complex flow features in indoor environment and identifying promising and advanced turbulence models for such flows. The results of the experimental study based on half of a twin-aisle airline cabin showed that the air inlet jet generates a high turbulence level whereas obstacles decreases velocity and turbulence levels. It is revealed that, buoyancy, generated from heat source, enhances recirculation and thus, the velocity and turbulence levels. By evaluating the performances of eight turbulence models, identified as prevailing by Zhai et al. [10], it is shown that RANS models performed well for simple flows but not for complicated ones. The LES-Dyn performed the best among the eight models. The performance of the DES-SA model was stable.

Table 2-1 List of popular and prevalent turbulence models for predicting airflows in enclosed environments

Model classification			**Primary turbulence models used in indoor air simulations**	**Prevalent models identified**
RANS	EVM	Zero-eqn	0-eq. (Chen and Xu, 1998)	Indoor zero eq.
		Two-eqn	Standard k-ε (Launder and Spalding, 1974) RNG k- ε (Yakhot and Orszag, 1986) Realizable k- ε (Shih et al., 1995)	RNG k- ε
			LRN-LS (Launder and Sharma,1974) LRN-JL (Jones and Launder, 1973) LRN-LB (Lam and Bremhorst, 1981)	LRN-LS
			LRN k-ω (Wilcox, 1994) SST k-ω (Menter, 1994)	SST k-ω
		Multi-eqn	v2f-dav (Davidson et al., 2003) v2f-lau (Laurence et al., 2004)	v2f-dav
	RSM		RSM-IP (Gibson and Launder, 1978) RSM-EASM (Gatski and Speziale, 1993)	RSM-IP
LES			LES-Sm (Smagorinsky, 1963) LES-Dyn (Germano et al., 1991; Lilly, 1992) LES-Filter (Zhang and Chen, 2000, 2005)	LES-Dyn
DES			DES (S-A) (Shur et al., 1999) DES (ASM) (Batten et al., 2002)	DES-SA

2.2 Main Air Distribution System

Several experimental and numerical studies have been performed on the cabins of aircrafts which have only main air distribution system. In Table 2-2, the studies existing in the literature which consider only main air distribution system are tabulated and summarized.

Table 2-2 Studies including only main air distribution system

Owner of the Study	Cabin	Manikins	Tech (s)	Data	CFD
Li et al. [13]	Boeing 737-200 mock-up	Thermal manikins	PIV	V, T	-
Kühn et al. [4]	A380 mock-up	Passenger dummies	PIV, TC	V, T	-
Liu et al. [14]	MD-82	-	HSA, UA	V	-
Liu et al. [15]	MD-82	Thermal manikins	HSA, UA, TC	V, T	RNG k–ε, LES, DES
Bosbach et al. [16]	A380 mock-up	-	PIV	V	Several RANS models
Günther et al. [9]	A380 mock-up	-	PIV	V	Several RANS models
Yan et al. [17]	Boeing 767-300 mock-up	-	VPTV	V, C	Standard k–ε
Zhang et al. [18]	Twin–aisle cabin mock-up	Box manikins	UA, GS	V, T, C	RNG k–ε
Baker et al. [19]	Conference room section of a business jet	-	-	V	Laminar
Liu et al. [20]	MD-82 mock-up	Thermal manikins	HSA, UA, HFM	V, T	RNG k–ε
Yin and Zhang [21]	Wide-body aircraft cabin	Box manikins	-	V, T, C	RNG k–ε

Table 2-2 (Cont'd) Studies including only main air distribution system

Liu et al. [22]	Cabin model	Passenger dummies	-	V, T	RNG k–ε
Wang et al. [23]	Boeing 737-200 mock-up	Thermal manikins	PIV	V	-
Yao et al. [24]	Single–aisle cabin mock-up	Passenger dummies	-	V	LES, several RANS models
Lin et al. [25]	Half of a generic empty cabin mock-up	-	PIV	V	LES
Bianco et al. [5]	Executive aircraft cabin	-	-	V, T	RNG k–ε
Baker et al. [26]	Boeing 747-100, Boeing 747-400	-	SA	V	RANS

Flow field in aircraft cabins have been subjected to many studies. Li et al. [13] investigated flow field within a Boeing 767-200 cabin mock-up by 2D-PIV and compared flow fields of isothermal and cooling conditions. They found that in non-isothermal conditions, thermal plumes from the passengers weaken the jet flows and make overall flow field more stable. Kühn et al. [4] performed PIV and temperature field measurements in a A380 cabin mock-up for isothermal and cooling conditions by varying air inlet configurations and flow rates. The results of experimental study showed that jet-jet and jet-thermal plume interactions significantly affect flow field in aircraft cabins and their relative dominance highly depends on cabin thermal condition and inlet configuration. Liu et al. [14] experimentally investigated flow field in the first-class cabin of a commercial MD-82 airplane under isothermal conditions (unoccupied cabin). They found that in aircraft cabins, air inlet boundary conditions are rather complex and significantly differ from one to another. They measurements showed that cabin flow is of low speed, low turbulence kinetic energy with high turbulence intensity. Liu et al. [15] conducted additional experimental measurements for non-isothermal conditions (occupied cabin) of Liu et al.'s [14]

case and numerically investigated performances of RNG k-ε model, LES and DES for both thermal conditions. According to the results of the simulations, they recommended to use RNG k-ε model for isothermal cabin conditions by considering both accuracy and computing time issues. On the other hand, LES predictions gave the best result for the non-isothermal cabin conditions. Their experimental measurements and numerical predictions showed that the thermal plumes diminish the jet momentum which is also observed by Li et al. [13]. Moreover, by comparing measured flow field for both thermal conditions, they found that thermal plumes from the passengers have significant effect on flow field but little influence on turbulence. Bosbach et al. [16] and Günther et al. [9] investigated flow field of an A380 cabin mock-up under isothermal conditions. By comparing simulation results with their own experimental data obtained by PIV technique, they concluded that low Reynolds number models predict jet diffusion and separation rather well; therefore, they proposed to use low Reynolds number models instead of high Reynolds number and two-layer models for isothermal cabin flow simulations. Yan et al. [17] used standard k-ε model to investigate the flow field within a Boeing 767-300 cabin mock-up and compared with the experimental data obtained by volumetric particle tracking velocimetry (VPTV). They found that standard k-ε model prediction results agree well with the experimental data. They also observed longitudinal flow in the cabin because of the complex flow domain. Zhang et al. [18] investigated airflow and temperature distribution in a half-occupied cabin by both experimental measurements and numerical simulations with RNG k-ε model. They found that the results of temperature distribution agree well with the experimental data while significant discrepancies exist in airflow patterns due to the difficulties in measuring accurate flow boundary conditions from the air supply diffusers. From both experimental data and numerical results, they found that the thermal plumes from passengers break down the most energetic and unstable large eddies. As a result, by comparing with Baker's [27] study for isothermal cabin, they found that the cabin domain is more stable in occupied cabin than in unoccupied cabin, as concluded by Li et al. [13]. According to this inference, they propose to use time averaging method for the occupied cabin flows.

CFD has been used to modify and/or optimize the ventilation system in aircrafts to improve passengers thermal comfort. Baker et al. [19] numerically investigated thermal comfort levels of occupants in the cabin of a business jet with a laminar flow model. Liu et al. [20] validated RNG k-ε model with the experimental data of airflow in MD-82 aircraft cabin and used to study passengers' thermal comfort in a newly designed aircraft cabin. Yin and Zhang [21] validated and used RNG k-ε model to investigate the performance of a new air distribution system for wide body aircrafts in terms of lessening CO2 concentration and enhancing moisture level. Liu et al. [22] used CFD-based adjoint method by RNG k-ε model to find air supply conditions that would provide the most comfortable thermal environment in a fully occupied single-aisle airliner cabin under summer and winter conditions. They found that airflow pattern and thermal comfort level in the cabin highly depends on air supply location and temperature and less on size and velocity. The reason was explained by comparable magnitudes of inertial forces from the inlets jets and buoyancy forces from the thermal plumes. They also found that the optimal air supply temperature differs under summer and winter conditions because of the varying thermal resistance of the passengers' clothing whereas the optimal air supply location, size and velocity is same for both thermal conditions.

Unsteady nature of cabin flow structures has been subject of many researchers. Wang et al. [23] experimentally investigated instantaneous airflows in collision regions generated by jets of diffusers in a Boeing 767-200 cabin mock-up by PIV technique. They found that the airflow in the collision region is highly turbulent with a low velocity magnitude and a high fluctuation. The results showed that although the average airflow fields in an aircraft cabin are uniform and having a small velocity gradient, the instantaneous airflow fields are remarkably unstable. Yao et al. [24] showed instability of the airflow field in an aircraft cabin both theoretically and numerically by LES. They performed unsteady RANS (URANS) by using RNG k-ε model, realizable k-ε model and V2f turbulence model and concluded that these models cannot effectively simulate the instability of flow field. Lin et al. [25] performed experiments in a model of one-half of a twin-aisle aircraft cabin by PIV technique and validated LES. Both the experimental data and LES predictions

showed the temporally occurring reversal of the primary flow direction. Bianco et al. [5] used RNG k-ε model to investigate the transient behavior of the cabin of an executive aircraft by two-and three-dimensional models and compared these models. The results of two-dimensional and three-dimensional models show a good qualitative agreement and two-dimensional models are proposed for pre-optimization analysis because of the computational time effectiveness. Baker et al. [26] focused on validating CFD methodology for prediction of cabin ventilation velocity vector fields by three-dimensional experimental measurements performed in the cabins of Boeing 747-100 and Boeing 747-400. The results of experimental measurements showed that the main cabin flow is unsteady with isotropic, homogeneous and time-independent turbulence structure.

2.3 Personalized Air Distribution System

In the literature, several experimental and numerical studies exist which focus on personalized air distribution system. These studies are tabulated and summarized in Table 2-3.

Flow field of aircraft cabins having personalized air distribution system have been subjected to several experimental and numerical studies. Li et al. [28] conducted experimental measurements in the cabin of an MD-82 airplane in two of five gaspers on condition and compared the obtained data with the Liu et al.'s [15] study which is performed for all gaspers are off condition. The results revealed that although having lower flow rate than diffusers, gaspers have much larger effect on air motion since they have far higher momentum flux. Moreover, gaspers increase the airflow in the cabin and make air distribution more uniform. Zhang and Chen [29] used RNG k-ε model to compare the performance of a seat-back located personalized air distribution system with the two typical air distribution systems, namely, mixing and under-floor displacement in a section of Boeing 767-300 cabin. They found that, by considering combined results of air velocity, temperature and contaminant distribution, personalized air distribution system created the best environment. Fiser and Jícha [30] validated and used SST k-ω model to investigate ventilation quality of

Table 2-3 Studies focusing on personalized air distribution system

Owner of the Study	Cabin	Manikins	Tech (s)	Data	CFD
Li et al. [28]	MD-82	Thermal manikins	HWA, UA, TC, GS	V, T, C	-
Zhang and Chen [29]	Boeing 767-300	Box manikins	-	V, T, C	RNG k–ε
Fiser and Jícha [30]	Nine-passenger small aircraft	Thermal manikins	CTA, TC	V, T	SST k-ω
You et al. [7]	Boeing 737 mock-up	Heated box	PIV, HSA, TC	V, T	RNG k–ε, SST k-ω
You et al. [31]	Boeing 737 mock-up, MD-82	Heated box, thermal manikins	-	V, T, C	SST k-ω
Lin et al. [32]	Boeing 767-300	Passenger dummies	-	V	RNG k–ε, LES
Fang et al. [6]	A320 mock-up	Passengers	Survey	V, T	-
Du et al. [2]	A320 mock-up	Passengers	HWA, VS, Survey	V, T	-
Zitek et al. [33]	Boeing 767-300	Thermal manikins	PIV, Thermometer	V, T, H	Standard k-ε
Zhang et al. [34]	A cabin mock-up	Thermal manikins	UA, TC, GS	V, T, C	RNG k–ε
Khalifa et al. [35]	-	Thermal manikins	HSA, TC, GS	V, T, C	-
Russo et al. [36]	-	Thermal manikins	-	V, T, C	Realizable k-ε
You et al. [37]	Boeing 767, Boeing 737	Heated box, thermal manikins	-	V, C	Hybrid (Standard k-ω, RNG k–ε)

three different types air distribution system, two of which including personalized air flow, in a small, nine-passenger aircraft cabin for cold, mild and hot ambient conditions. The results revealed that ventilation performances of distribution systems highly depend on ambient conditions. You et al. [7] focused on identifying a suitable turbulence model to calculate airflow distribution in an aircraft cabin while both personalized and main air distribution systems are operating. To investigate flow field in more detail, they take experimental measurements by dividing cabin into two as critical region where gasper-induced airflow, main flow and thermal plume mix and the region where gasper-induced jet have limited effect. The results showed that the SST k-ω model is more accurate than the RNG k-ε model for predicting the airflow distribution in gasper-induced flow dominant region whereas in regions where gasper-induced airflow has limited impact on the airflow pattern, the RNG k-ε model provided slightly better airflow predictions than does the SST k-ω model. You et al. [31] validated SST k-ω model by experimental data for two cases; a cabin mock-up [7] and a real cabin [30] and used to explore the possibility of simplifying the gasper geometry as a round nozzle for CFD simulations. The results showed that simplified gasper model gave acceptable results in predicting air velocity, air temperature and contaminant concentrations and reduces grid number, hence, computing cost. Lin et al. [32] used LES and standard k-ε model to investigate flow field in a Boeing 767-300 cabin and compared the results with the available test data. The results show that LES agrees fairly good with test data whereas standard k-ε model underpredicts turbulence levels.

The effect of personalized air flow on thermal comfort and air quality have been investigated by many researchers. Fang et al. [6] conducted a survey in an experimental chamber to examine nozzle utilization rate over a period of time in different occupancy conditions. The utilization rate and adjustment observation results revealed the significance of the personalized air distribution in passengers' comfort. Du et al. [2] carried out thermal survey and performed flow field measurements in an experimental three-row aircraft cabin to obtain an optimized personalized air flow rate and velocity for varying cabin temperatures. The results showed that increasing personalized air flow makes passengers feeling cooler in

addition to the feeling of air movement. Zítek et al. [33] validated standard k-ε model with the experimental measurements and used it in study of forming a separate environment for each passenger by designing a seat-back located personalized ventilation system. The results showed that personalized ventilation system protects each passenger from undesirable sharing of the breathed air with her/his neighbors. Moreover, the results showed that using personalized ventilation in addition to main flow provides a greater cooling effect for passenger. Zhang et al. [34] validated RNG k-ε model with the experimental measurements and used it in study of improving aircraft cabin environment by proposing a novel personal chair-armrest-embedded air distribution system. Khalifa et al. [35] experimentally investigated the performance characteristics of a personalized ventilation system design with a novel nozzle design which deliver high quality air to the breathing zone and Russo et al. [36] validated their CFD model, using realizable k-ε model, by Khalifa et al.'s [35] experimental data. You et al. [37] developed a hybrid turbulence model which uses standard k-ω model in the near wall regions and a transformed RNG k-ε model in the bulk air regions to investigate the impact of gaspers on the cabin air quality in a seven-row section of economy-class cabin of a Boeing 767 and Boeing 737 airplanes. The developed turbulence model was validated with two experimental data; one of which is from a mock-up of half of a full-scale, one-row, single-aisle aircraft cabin with one gasper turned on, from You et al.'s [7] study and one is from fully occupied first-class cabin of a real MD-82 commercial airliner, from Liu et al.'s [15] study. The result revealed that the overall effect of turning on a passenger's gasper on the mean infection risk for the passenger is neutral.

CHAPTER 3

TURBULENCE MODELING

In this chapter, Reynolds averaging process is introduced and the governing equations of the fluid flow and heat transfer are presented. One of the closing methods of Reynolds-Averaged Navier Stokes (RANS) equations, Boussinesq approach, and the standard k-ε turbulence model along with the near wall approach are explained in detail.

3.1 Reynolds Averaging

Reynolds averaging process divides flow variables of Navier-Stokes equations into mean and fluctuating components. To illustrate, for the velocity components:

$$u_i = \overline{u_i} + u_i' \tag{3.1}$$

where u_i and u_i' are the mean and fluctuating velocity components, respectively.

Similarly, for other scalar quantities such as pressure and energy:

$$\varphi = \bar{\varphi} + \varphi' \tag{3.2}$$

By substituting above expressions for the flow variables into the instantaneous continuity and momentum equations and taking a time average, the Reynolds-Averaged conservation equations can be written in the form as:

Conservation of mass:

$$\frac{\partial \rho}{\partial t} + \frac{\partial}{\partial x_i}(\rho \overline{u_i}) = 0 \tag{3.3}$$

where ρ is density of the fluid and $\overline{u_i}$ is the time average velocity.

Conservation of momentum:

$$\frac{\partial}{\partial t}(\rho\overline{u_i}) + \frac{\partial}{\partial x_j}(\rho\overline{u_i}\,\overline{u_j}) = -\frac{\partial\overline{p}}{\partial x_i} + \frac{\partial}{\partial x_j}\left[\mu\left(\frac{\partial\overline{u_i}}{\partial x_j} + \frac{\partial\overline{u_j}}{\partial x_i} - \frac{2}{3}\delta_{ij}\frac{\partial\overline{u_k}}{\partial x_k}\right)\right] + \frac{\partial}{\partial x_j}(-\rho\overline{u_i{}'u_j{}'}\ ) + S_i \tag{3.4}$$

where $\overline{p}$ is the mean pressure, μ is the dynamic viscosity of the fluid, δ_{ij} is the Kronecker delta, $-\rho\overline{u_i{}'u_j{}'}$ is the unknown Reynolds stress tensor and S_i is the source term.

Source term of the Equation 3.4, S_i represents body forces and the only body force is due to gravity. In this thesis study, gravitational force acts in negative z-direction and is included into the z-momentum equation as "ρg", in the generalized form of the gravity term.

Including the effect of buoyancy; pressure gradient and source (body force) terms of Equation 3.4 for z-momentum becomes:

$$-\frac{\partial\overline{p}}{\partial x_i} + \rho g = -\frac{\partial\overline{P}}{\partial x_i} + (\rho - \rho_0)g \tag{3.5}$$

where;

$$\overline{P} = \overline{p} - \rho_0 g x_i \tag{3.6}$$

The second term on the right-hand side of the Equation 3.5 is the buoyancy force accounting for natural convection.

To model natural convection, for the simplification of the simulations, Boussinesq approximation is used which is valid when the temperature differences in the domain are not too high as in the case of cabin flow. Boussinesq model of ANSYS FLUENT treats density as a constant value in all solved equations, except the buoyancy term in

the momentum equation. That is, temperature dependency of density is confined into the buoyancy term.

$$(\rho - \rho_0)g \approx -\rho_0\beta(T - T_0)g \tag{3.7}$$

where β is volumetric thermal expansion coefficient, a measure of density change tendency of a gas according to a temperature change.

By applying Boussinesq approximation, buoyant force is related to temperature difference.

Equation 3.4 with the terms having overbar representing ensemble averaged values of solution variables have the same form as classical Navier-Stokes equations except the Reynolds Stress term, $-\rho\overline{u_i{'}u_j{'}}$, arising in the momentum equation. This term represents the effect of the turbulence and should be modeled since turbulent fluctuations can be small scale and directly simulating them would be computationally expensive. ANSYS FLUENT provides various types of turbulence models to model Reynolds stresses.

ANSYS FLUENT models energy equation using the concept of Reynolds' analogy. The modeled equation with the absence of viscous heating is given by:

$$\frac{\partial}{\partial t}(\rho\overline{E}) + \frac{\partial}{\partial x_i}\left[\overline{u_i}(\rho\overline{E} + \overline{p})\right] = \frac{\partial}{\partial x_j}\left(k_{eff}\frac{\partial T}{\partial x_j}\right) \tag{3.8}$$

where k_{eff} is the effective thermal conductivity and calculated by ANSYS FLUENT for standard k-ε model as:

$$k_{eff} = k + k_t \tag{3.9}$$

where k_t is the turbulent thermal conductivity and calculated as:

$$k_t = \frac{c_p\mu_t}{Pr_t} \tag{3.10}$$

where Pr_t is the turbulent Prandtl number.

It should be noted that, viscous heating term is neglected since it gains importance for high-velocity, compressible flows and when the working fluid is highly viscous.

3.2 Boussinesq Approach

In Reynolds Averaging approach, Reynolds stresses term of Equation 3.4 must be appropriately modeled to close system of governing equations. Boussinesq hypothesis is one of the most widely used methods to link Reynolds stresses to the mean velocity gradients.

$$-\rho\overline{u_i{}'u_j{}'} = \mu_t\left(\frac{\partial\overline{u_i}}{\partial x_j}+\frac{\partial\overline{u_j}}{\partial x_i}\right)-\frac{2}{3}\left(\rho k+\mu_t\frac{\partial\overline{u_k}}{\partial x_k}\right)\delta_{ij} \tag{3.11}$$

Using Boussinesq hypothesis has low computational cost; therefore, advantageous in calculating turbulence viscosity, μ_t. The Spalart-Allmaras model, k-ε models and k-ω models use Boussinesq hypothesis. To calculate turbulence viscosity, one additional transport equation is solved in Spalart-Allmaras model. On the other hand, in the case of k-ε and k-ω models, two additional transport equations are solved; one is for turbulence kinetic energy, k, the other is turbulence dissipation rate, ε, for k-ε models and specific dissipation rate, ω, for k-ω models.

3.3 Standard k-ε Turbulence Model

In the present study, standard k-ε model proposed by Launder and Spalding [38] is used. Two additional transport equations; one is for turbulence kinetic energy, k, and the other is for its dissipation rate, ε, are solved to determine turbulent length and time scales.

The transport equations to be solved are the followings:

$$\frac{\partial}{\partial t}(\rho k) + \frac{\partial}{\partial x_i}(\rho k \overline{u_i}) = \frac{\partial}{\partial x_j}\left[\left(\mu + \frac{\mu_t}{\sigma_k}\right)\frac{\partial k}{\partial x_j}\right] + G_k + G_b - \rho\varepsilon - Y_M \quad (3.12)$$

and

$$\frac{\partial}{\partial t}(\rho\varepsilon) + \frac{\partial}{\partial x_i}(\rho\varepsilon \overline{u_i}) = \frac{\partial}{\partial x_j}\left[\left(\mu + \frac{\mu_t}{\sigma_\varepsilon}\right)\frac{\partial \varepsilon}{\partial x_j}\right] + C_{1\varepsilon}\frac{\varepsilon}{k}(G_k + C_{3\varepsilon}G_b) - C_{2\varepsilon}\rho\frac{\varepsilon^2}{k} \quad (3.13)$$

In these equations, G_k and G_b terms account for turbulent kinetic energy generation due to the mean velocity gradients and the buoyancy, respectively. Fluctuating dilation in compressible turbulence contribution to overall dissipation rate term is indicated with the term Y_M. Equation constants are represented by $C_{1\varepsilon}$, $C_{2\varepsilon}$ and $C_{3\varepsilon}$ and turbulent Prandtl numbers for k and ε are represented by σ_k and σ_ε, respectively.

By solving above two transport equations for k and ε, turbulent (eddy) viscosity, μ_t, can be computed by the following equation:

$$\mu_t = \rho C_\mu \frac{k^2}{\varepsilon} \quad (3.14)$$

where Cμ is a constant.

3.4 Near Wall Treatment

In wall bounded flow simulations, near wall treatment strategy is a key issue since solution gradients are high in viscosity-affected region and solid walls are one of the main sources of turbulence. Moreover, correct prediction of separation and reattachment, highly observed in cabin flows, depends on the success of near wall treatment.

In this point, it is worthwhile to introduce the dimensionless wall distance parameter for wall bounded flows, y^+, which describes how fine or coarse the mesh near the wall region and defined as:

$$y^+ = \frac{yu_\tau}{v} \tag{3.15}$$

where y is the distance from wall to the centroid of the wall adjacent cell, u_τ is the shear velocity and ν is the kinematic viscosity of working fluid.

To find first cell height, it is necessary to calculate shear velocity.

$$u_\tau = \sqrt{\frac{\tau_w}{\rho}} \tag{3.16}$$

where ρ is the density of the working fluid which is air in this study.

Wall shear stress term in Equation 3.16, τ_w is calculated from skin friction coefficient, C_f, such that:

$$\tau_w = \frac{1}{2} C_f \rho {U_\infty}^2 \tag{3.17}$$

where U_∞ is the free stream velocity and C_f can be estimated for internal flows by the following empirical formula:

$$C_f = 0.079(Re)^{-0.25} \tag{3.18}$$

where Re is the Reynolds number which is a dimensionless term defining the ratio of inertial forces to viscous forces. Reynolds number can be calculated as:

$$Re = \frac{UL}{\nu} \tag{3.19}$$

where U is the characteristic velocity of the flow, ν is the kinematic viscosity and L is the characteristic length scale of the flow.

Mainly two approaches exist to model near-wall region. One is "wall function" approach where centroids of the wall adjacent cells should be located in the log-layer (fully turbulent region). In this approach, viscosity-affected region is not resolved,

instead solution variables at the near wall cells are bridged to the corresponding quantities on the wall by semi-empirical formulae called "wall functions" [39]. In the wall function approach, there is no need to modify turbulent models to account for the presence of the wall. As another approach, viscosity-affected region is resolved with a fine mesh all the way down to the wall. In this approach, turbulence models are modified to resolve viscosity-affected region.

Indeed, it is impossible to keep y^+ in a certain limit in the case of having complex geometry like aircraft cabin wherein too much wall bounds exist representing passengers and seats. Moreover, as a result of the complex air flow pattern, flow velocity varies too much throughout the domain; hence, in the near wall regions. ANSYS FLUENT's Enhanced wall treatment approach comes into existence to handle variable y^+ values.

Enhanced wall treatment combines a two-layer zonal model with enhanced wall functions. When the first near-wall node is at around $y^+=1$, two-layer zonal model is applied which divides the whole domain into two as viscosity-affected region and fully-turbulent region. In the fully turbulent region, k-ε model is employed while in the viscosity-affected region, the low Reynolds one-equation model of Wolfstein [40] is employed. In the one equation model, momentum equations and k-equation are retained as described formerly and turbulent viscosity is calculated by:

$$\mu_{t,viscous\ layer} = \rho C_\mu l_\mu \sqrt{k} \tag{3.20}$$

where l_μ is the length scale.

Two-layer formulation of turbulent viscosity is smoothly blended with high-Reynolds number turbulent viscosity, μ_t, formerly defined in Equation 3.14 for the outer region.

In the viscosity-affected region, turbulence dissipation rate is calculated algebraically by Equation 3.21 and similar blending procedure is employed to ensure smooth transition with ε obtained from the transport equation of the fully-turbulent region.

$$\varepsilon = \frac{k^{3/2}}{l_\varepsilon} \tag{3.21}$$

where l_ε is the length scale.

To have a method which is applicable throughout the near-wall region (viscous sublayer, buffer region, fully-turbulent), enhanced wall functions were derived by using the single wall law function suggested by Kader [41], Equation 3.22, which smoothly blends linear (laminar) and logarithmic (turbulent) wall laws. This formula correctly represents velocity profiles for small and large values of y^+ and provides reasonable representation of velocity profiles where y^+ falls inside the buffer region.

$$u^+ = e^{\Gamma} u^+_{lam} + e^{1/\Gamma} u^+_{turb} \tag{3.22}$$

where Γ is the blending function.

CHAPTER 4

PERFORMANCE EVALUATION OF THE SELECTED TURBULENCE MODEL

In this chapter, mesh independence study and the performance evaluation of the selected turbulence model to be used in aircraft cabin flow simulations are conducted.

4.1 Description of the Test Case

The geometric configuration used for turbulence model performance evaluation is based on Günther et al.'s [9] study. In the study, an empty cabin representing the region between the passengers and overhead luggage compartment of a modern mega liner, indicated in Figure 4-1, is configured. The thermal condition inside the cabin is isothermal.

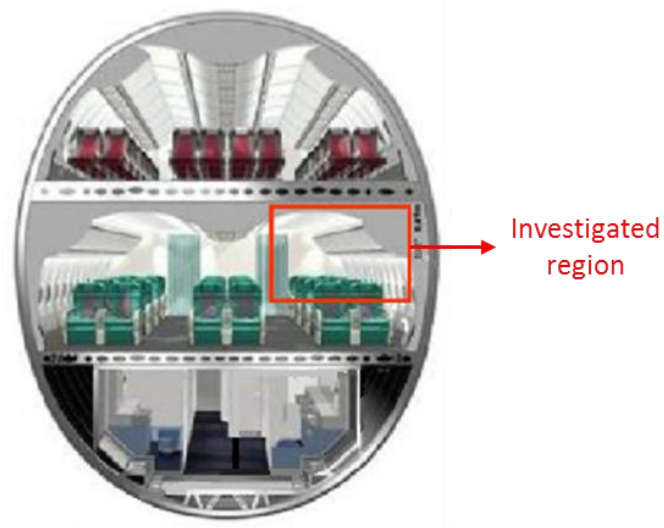

Figure 4-1 Centre cross section of the modern mega liner investigated by Günther et al. [9]

The main reason of selecting Günther et al.'s [9] study for performance evaluation purpose is that all geometrical dimensions and required boundary conditions are provided. In addition, this study includes both the experimental data and numerical results of various turbulence models. By utilizing the symmetry conditions of the domain, one sixth of the experimental mock-up is used in the numerical simulations to reduce computation effort. The experimental mock-up and computational domain of Günther et al. [9] are shown in Figure 4-2 and Figure 4-3, respectively.

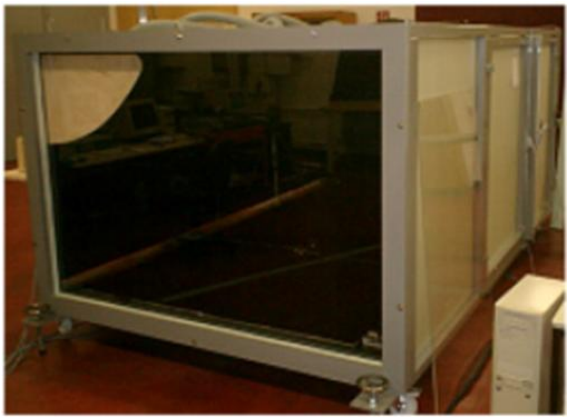

Figure 4-2 Experimental mock-up of Günther et al. [9]

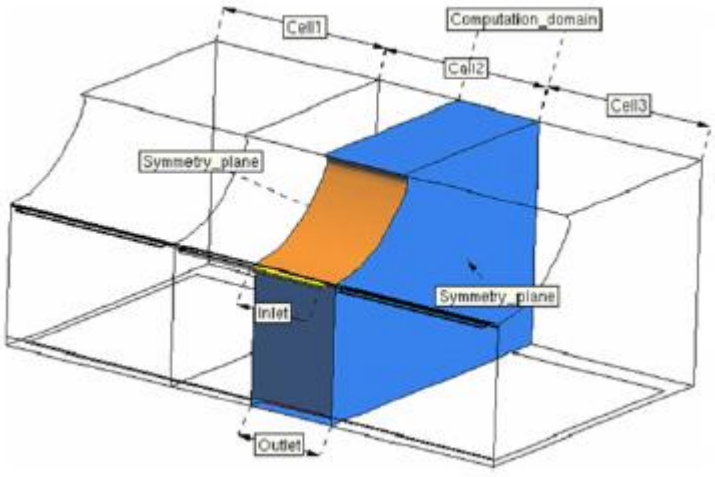

Figure 4-3 Computational domain of Günther et al. [9]

Figure 4-4 shows the modeled cabin configuration used in the turbulence model performance evaluation study.

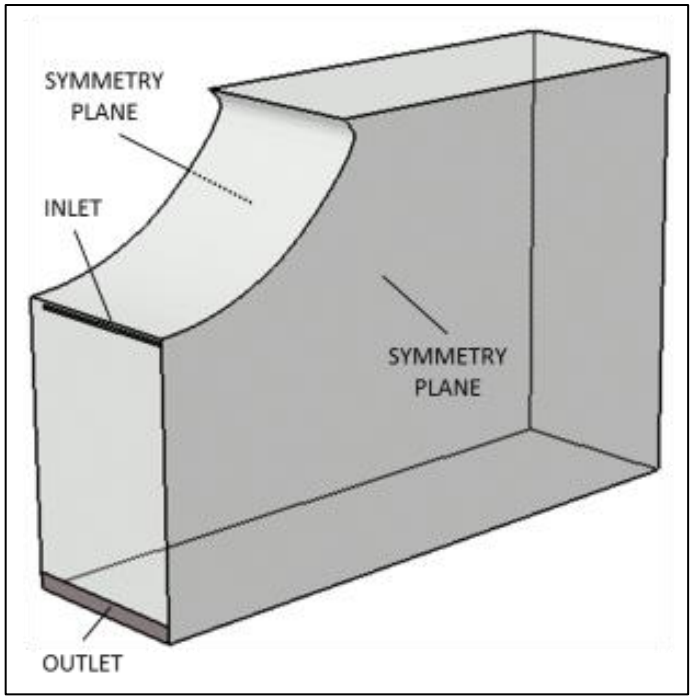

Figure 4-4 Modeled cabin configuration of the test case

4.2 Development of CFD Model

By using ANSYS FLUENT, a CFD model is developed to simulate cabin flow for isothermal and non-occupied conditions. Boundary conditions are defined in this section. For the cabin inlet, air velocity magnitude of the Günther et al. [9] is directly specified. Inlet velocity profile is defined as perpendicular to inlet area and constant magnitude throughout the area. Moreover, turbulence intensity and turbulence length scale are directly specified for the inlet section. For the outlet section, zero gage static pressure is applied as boundary condition. Two symmetric wall conditions are applied to the symmetry planes which are indicated in Figure 4-4. No slip boundary conditions are applied to the other walls. The applied boundary conditions are summarized in Table 4-1.

Table 4-1 Boundary conditions of the test case

Inlet	Velocity (m/s)	1.32
	Turbulence Intensity (%)	15
	Turbulence Length Scale (mm)	1
Outlet	Pressure (Pa)	$P_{static\_gage}=0$
Wall	Velocity (m/s)	$u_{wall}=0$
	Symmetry	2 planes

The standard k-ε model is preferred for this thesis's study since it is robust, computationally economic and reasonably accurate for a wide range of industrial flows [39]. Moreover, well convergence behavior of standard k-ε model is considered when selecting the turbulence model since the further investigation of this thesis study, helicopter cabin investigation, comprises an iterative design procedure wherein boundary conditions; therefore, flow structures are variable from case to case. Moreover, the existence of a total number of eight air inlets, free and wall bounded air jets emerging from them and high occupant density of the cabin make flow domain rather complex.

As the near wall treatment, Enhanced wall treatment is selected to resolve up to all viscous-affected regions. The viscous-affected regions are resolved since in an aircraft cabin, the domain is highly dense with a high number of physical boundaries and as a result of complex domain, various types of fluid flow phenomena exist like separation, recirculation, vortices, attachment to or detachment from physical boundary, etc. which should be correctly predicted by CFD model. Simulations are performed as steady-state. The pressure-based coupled algorithm is employed to couple the pressure and velocity. First-order scheme is used for pressure discretization and second-order upwind scheme is used for discretizing all other variables. Such discretization strategy has been proven to be effective by many previous studies [7], [11], [12], [15].

To ensure that the computation has been performed completely, convergence has to be checked. Convergence can be judged by examining the residuals of various transport equations and checking mass flux conservation [42]. As rules of thumb, for continuity, momentum and transport equations, residual level of 10^{-3} and below can be accepted as a sign of convergence and the net mass flux imbalance should be less than 1% of the smallest mass flux. A residual plot for one simulation is illustrated in Figure 4-5.

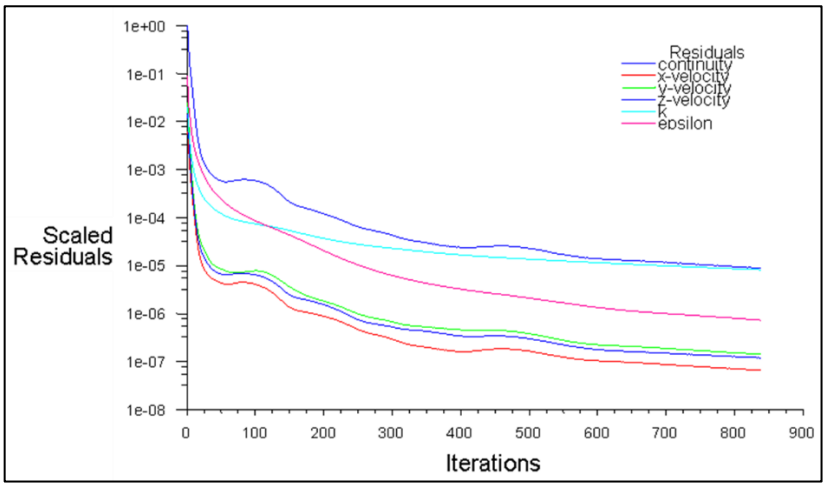

Figure 4-5 Residual plot of a sample calculation to judge the convergence

However, examining residuals is not sufficient to guarantee convergence. For example, depending upon the initial conditions, despite a residual value to decrease up to at most i.e. 10^{-2}, the solution may converge. Conversely, decrement up to i.e. 10^{-4} value may occur for a non-convergent solution. Therefore, as a second method, monitoring key variables on points located in the flow domain is crucial to judge convergence. For this purpose, five monitor points are used and velocity magnitudes are monitored throughout the calculations. The locations of monitor points are shown in Figure 4-6. One monitor point is located near the curved part of the cabin to monitor the jet velocity at the downstream of the air inlet. Two monitor points are located in the first detachment-attachment region and the other two monitor points are located at the corner region of the cabin which is located across the air inlet and can be considered as second detachment-attachment region. For the monitoring

process, if steady fluctuations occur as calculation processes, convergence is examined by considering relative magnitudes of amplitudes of fluctuations to mean values of velocities. Figure 4-7 shows velocity magnitude convergence history of three of monitor points for a sample simulation.

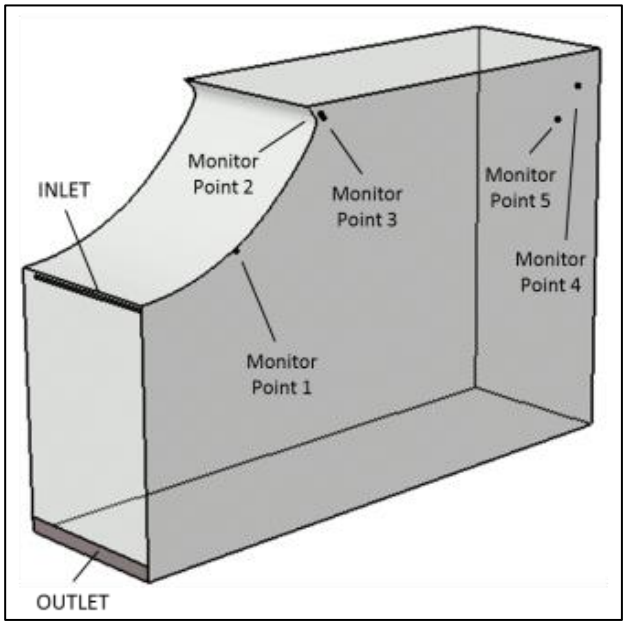

Figure 4-6 Monitor point locations for judging the convergence of the simulation

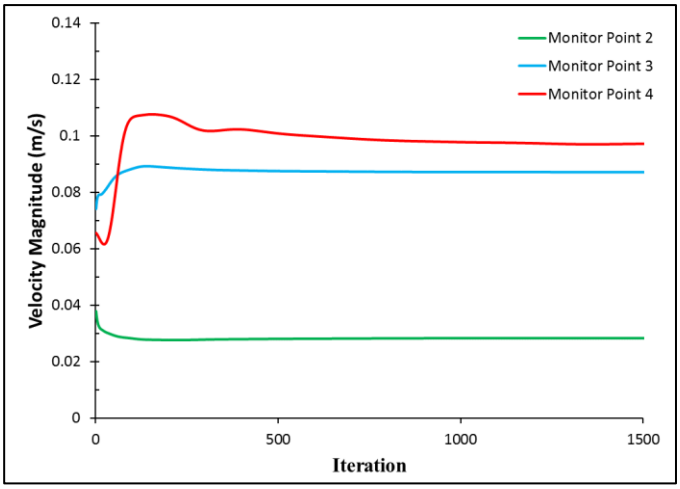

Figure 4-7 Convergence history of three of the monitor points for a sample calculation

4.3 Mesh Independence Study

To evaluate the performance of the selected turbulent model, firstly a mesh independent solution must be obtained. In the turbulence model performance evaluation study, tetrahedral mesh is used for volume fill.

Four different meshes are examined in the mesh independence study. Three main parameters control the mesh independence study, namely, surface mesh size, global mesh size and inflation layer. As a general treatment, mesh sizes are gradually decreased to obtain a finer mesh. For inflation layer, first layer thickness is gradually decreased to obtain a finer mesh in the near wall region by keeping total inflation layer thickness close to each other for all meshes. When determining first layer thicknesses, y^+ values are kept close to 1 to resolve viscous sublayer.

After the simulations, y^+ values are checked. Percentage distribution of y^+ values of the coarsest mesh which also has the highest first layer thickness is illustrated in Figure 4-8. The histogram shows that more than 95% of wall adjacent cells have y^+ value less than 2.

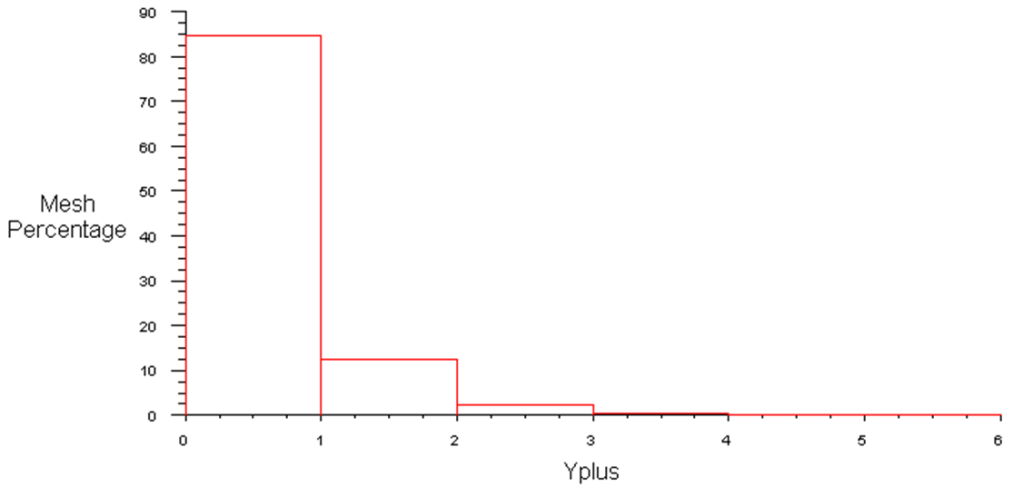

Figure 4-8 Y^+ histogram of the coarsest mesh of the mesh independence part of the turbulence model performance evaluation study

In Figure 4-9, y^+ contour of the coarsest mesh is shown. It can be observed that, the meshes having the highest y^+ values are the ones located at near the air inlet and outlet. The type of these meshes is tetrahedral since they are located at the transition region between prism meshes of the walls and tetrahedral meshes of the inlet/outlet boundary. In fact, because of their type, y^+ values of the wall adjacent tetrahedral meshes located at the transition region do not make any sense in terms of y^+ evaluation of the CFD model.

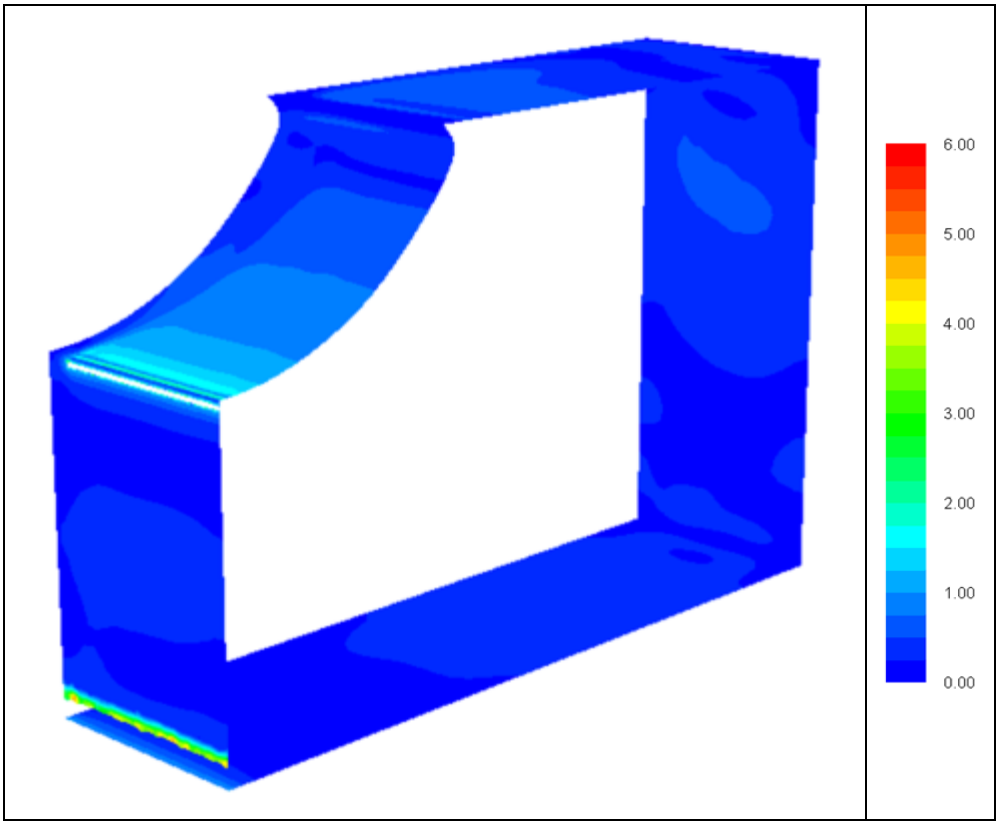

Figure 4-9 Y^+ contours of the coarsest mesh of the mesh independence part of the turbulence model performance evaluation study

The details of the parameters used in the mesh independence study are summarized in Table 4-2.

Table 4-2 Summary of the parameters used in the mesh independence part of the turbulence model performance evaluation study

		Mesh 1	**Mesh 2**	**Mesh 3**	**Mesh 4**
Surface	Global Sizing	60 mm	60 mm	60 mm	50 mm
	Inlet	3 mm	3 mm	2 mm	1.5 mm
	Outlet	13 mm	10 mm	8 mm	6 mm
	Surface Region 1	16 mm	10 mm	7 mm	5 mm
	Surface Region 2	36 mm	25 mm	18 mm	13 mm
	Surface Region 3	45 mm	32 mm	22 mm	15 mm
	Sharp Corner – 1st Zone (Local Improvement)	3 mm	3 mm	2 mm	1.5 mm
	Sharp Corner – 2nd Zone (Local Improvement)	5 mm	5 mm	4 mm	3 mm
	Corner Across the Inlet (Local Improvement)	16 mm	10 mm	7 mm	5 mm
Inflation	First Layer Thickness	0.5 mm	0.3 mm	0.25 mm	0.2 mm
	Maximum # of Layers	13	15	16	17
	Growth Rate	1.2	1.2	1.2	1.2
	Total Thickness of Inflation Layer	24.2 mm	21.6 mm	21.9 mm	21.2 mm

Accuracy of numerical simulations is affected from mesh quality; therefore, should be checked to ensure accuracy of simulations. Mesh quality can be evaluated by maximum and average values of skewness. Skewness value 0 corresponds to best quality whereas 1 corresponds to the worst. Moreover, minimum and average values of orthogonal quality can be used to judge mesh quality. Converse to skewness, orthogonal quality value 1 corresponds to best quality whereas 0 corresponds to the worst. In a numerical simulation, it is crucial not to have many elements having low quality. Also, average quality of all elements should be sufficiently high.

Statistics of all meshes used in mesh independence study are tabulated in Table 4-3. By examining mesh statistics, for all mesh alternatives, maximum skewness is less than 0.941 and minimum orthogonal quality is more than 0.053. Moreover, average skewness values are in the order of 0.2 and average orthogonal quality values are more than 0.849 for all mesh alternatives. Thus, mesh quality used in the mesh independence study is sufficiently high.

Table 4-3 Statistics of the meshes used in the mesh independence part of the turbulence model performance evaluation study

	Mesh 1	**Mesh 2**	**Mesh 3**	**Mesh 4**
Number of Elements	575000	1055000	2010000	3524000
Maximum Skewness	0.805	0.877	0.941	0.807
Average Skewness	0.227	0.196	0.181	0.170
Minimum Orthogonal Quality	0.078	0.054	0.059	0.053
Average Orthogonal Quality	0.849	0.878	0.889	0.898

In the mesh independence study, mesh count is increased in the order of 2 times in each step. The coarsest mesh (Mesh 1) has 575,000 elements and it is figured out in Figure 4-10. The finest mesh (Mesh 4) used in this study has 3,524,000 elements and it is shown in Figure 4-11.

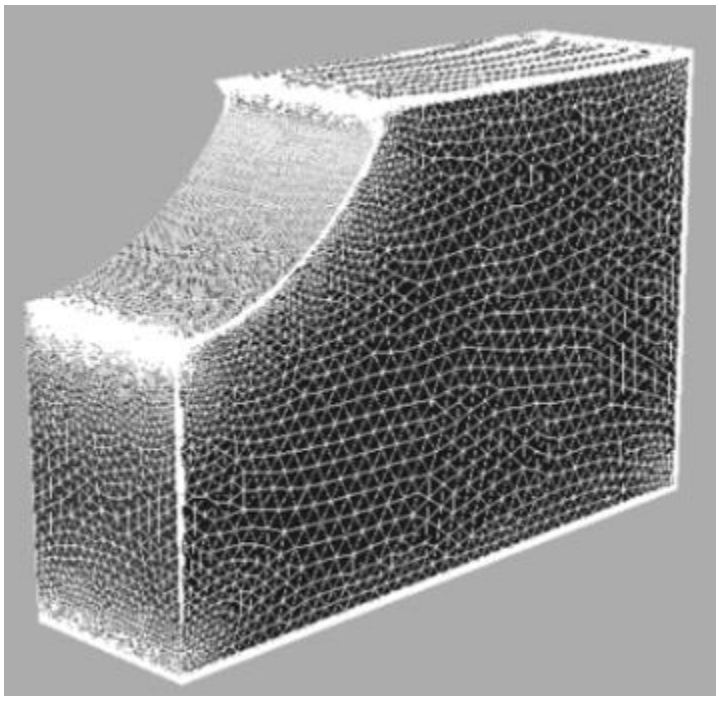

Figure 4-10 The coarsest mesh used in the mesh independence part of the turbulence model performance evaluation study

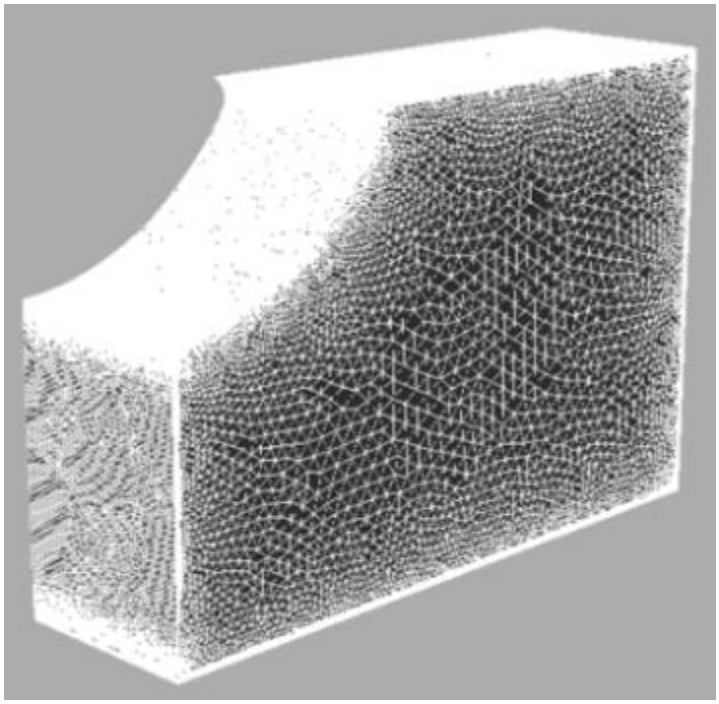

Figure 4-11 The finest mesh used in the mesh independence part of the turbulence model performance evaluation study

In the mesh independence study, velocity magnitudes are compared on three lines which are located on symmetry plane. Locations and coordinate information of the lines are presented in Figure 4-12. In the information part of the figure, "start" position of a line corresponds to the location where the line intersects the cabin wall and "end" position corresponds to the free end of the line.

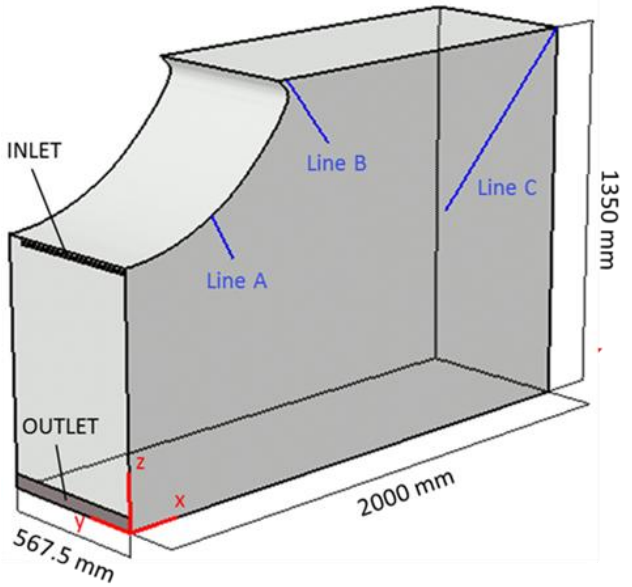

		Coordinate (mm)		
Line		**x**	**y**	**z**
A	**Start**	357.5	0	961.7
	End	446	0	805
B	**Start**	682.7	0	1350
	End	868.9	0	1114.7
C	**Start**	2000	0	1350
	End	1434.3	0	784.3

Figure 4-12 Locations and coordinate information of the lines on which velocity magnitudes are compared

It is important to note that Line A, Line B and Line C are the lines of Günther et al.'s [9] study on which experimental and numerical data are provided and turbulence model performance evaluation study of this thesis is performed. Resultant velocity magnitude profiles on Line A, Line B and Line C are presented in Figure 4-13 to Figure 4-15, respectively. In these figures, x-axis shows the distance from the wall and y-axis shows the velocity magnitude.

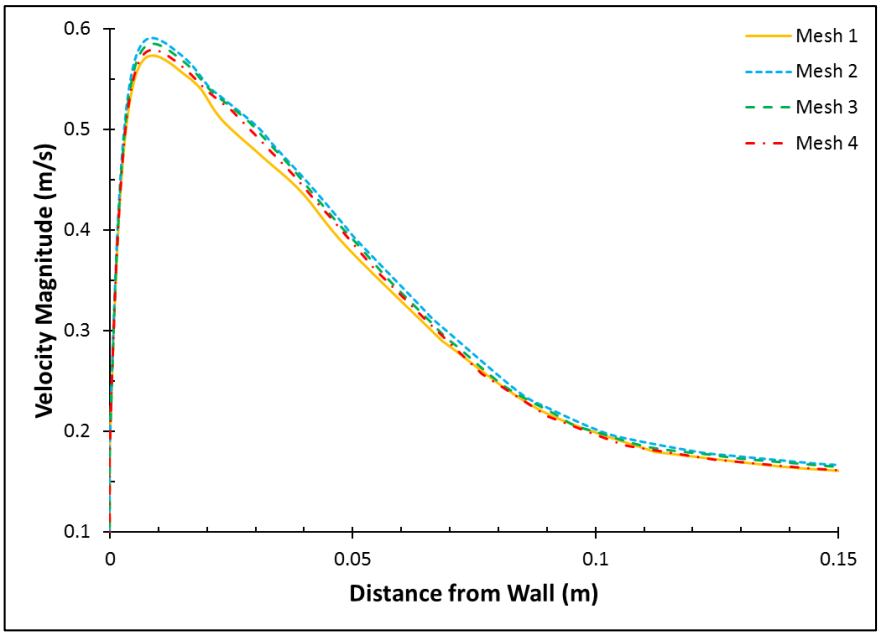

Figure 4-13 Velocity magnitudes on Line A

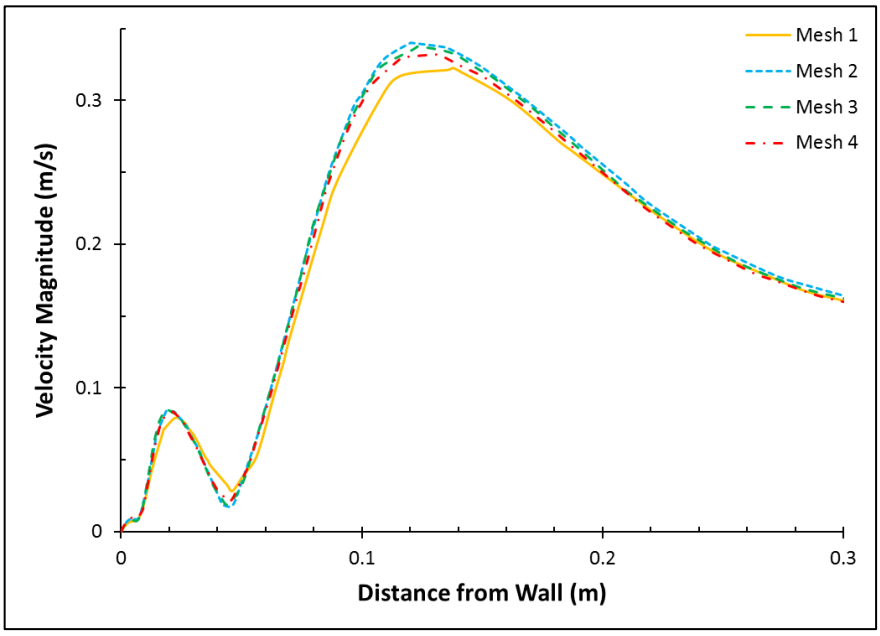

Figure 4-14 Velocity magnitudes on Line B

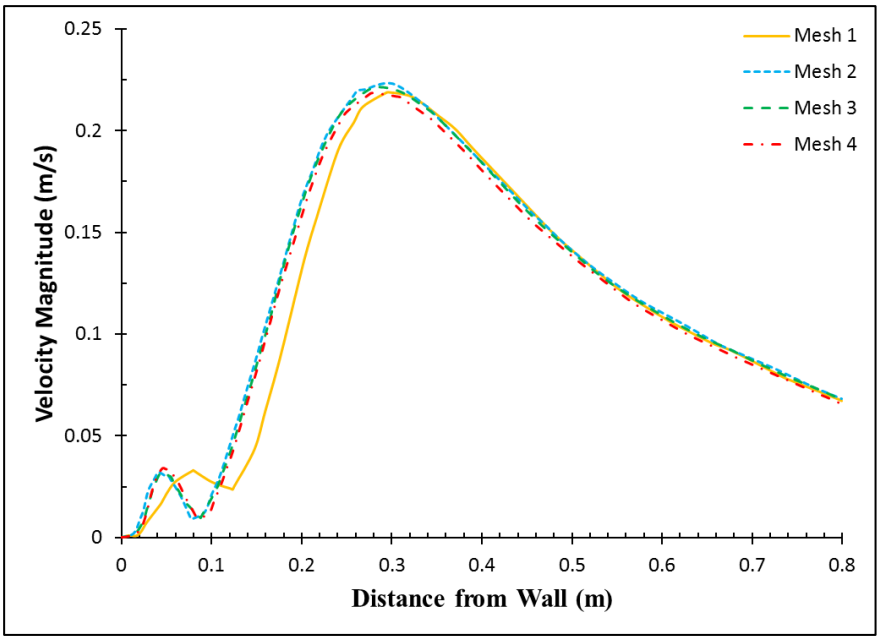

Figure 4-15 Velocity magnitudes on Line C

The comparison of velocity magnitude profiles shows that discrepancy in results does not change with further refinement after Mesh 2. This can be observed from velocity profiles of Line 2 and Line 3 more clearly. Therefore, Mesh 2 is used in the turbulence model performance evaluation study.

4.4 Performance Evaluation of the Selected Turbulence Model

In this section, performance evaluation study of the turbulence model which is selected to be used in forthcoming studies is presented.

In turbulence model performance evaluation study, the experimental and numerical results obtained from Günther et al.'s [9] study are used. In the study, experimental data are obtained by means of PIV and numerical results are obtained by the simulations which are performed by using three different groups of k-ε turbulence models; standard low Reynolds number, standard high Reynolds number with wall function approach and two-layer RNG. The results of Günther et al. [9] are presented in Figure 4-16 on Line A, Line B and Line C, respectively, which are formerly used in the mesh independence study.

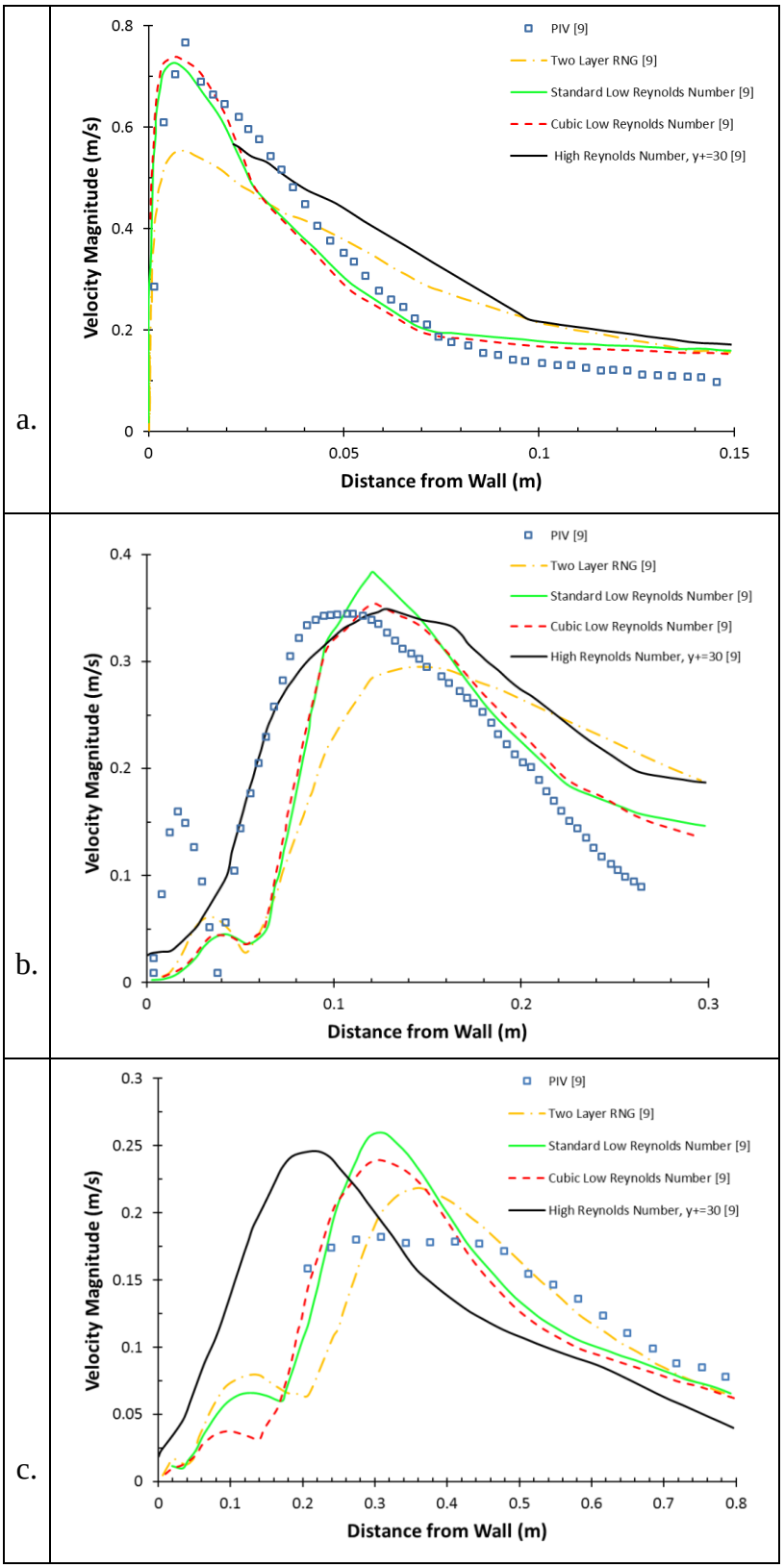

Figure 4-16 Experimental data and numerical results of Günther et al. [9] on; (a) Line A; (b) Line B; (c) Line C

Figure 4-17 to Figure 4-19 show velocity profile comparison of the results predicted by Mesh 2 of this thesis's study with the experimental data and numerical results obtained by cubic low Reynolds number model of Günther et al. [9] on Line A, Line B and Line C, respectively. It should be mentioned that, in these figures, cubic low Reynolds number model results are presented since they are proposed by Günther et al. [9] as the best numerical approach among others.

On Line A, by comparing with the experimental results of Figure 4-17, it can be observed that standard k-ε model with Enhanced wall treatment predicts general velocity magnitude profile pretty well. It also predicts the location of jet peak and width of jet successfully. The only discrepancy occurs in terms of magnitude of peak velocity, which is underestimated by standard k-ε model.

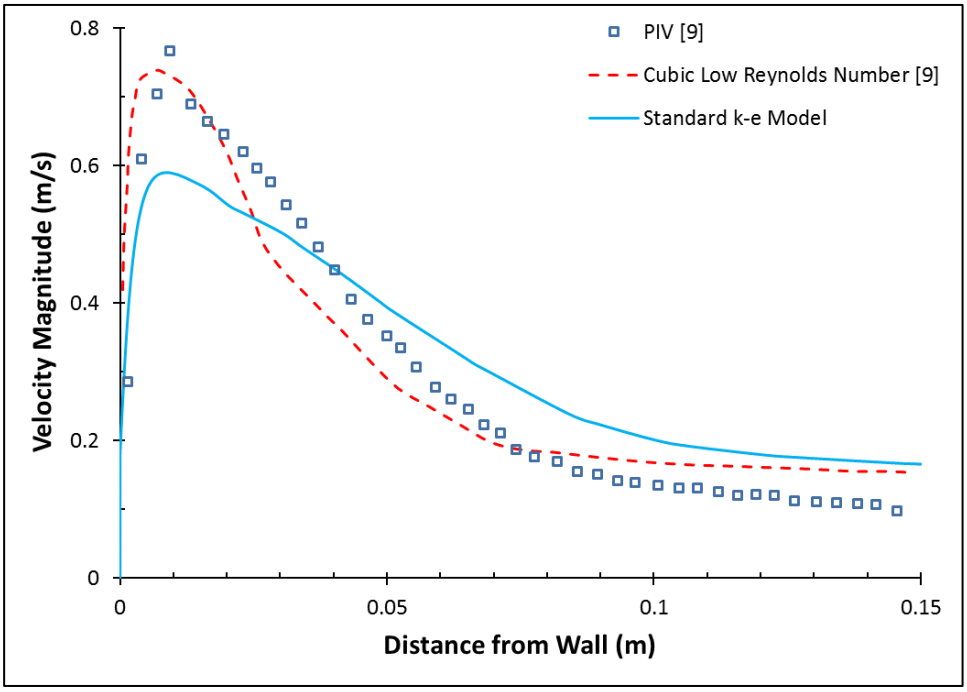

Figure 4-17 Velocity magnitude comparison on Line A – Standard k-ε turbulence model with Günther et al.'s [9] experimental data and the best numerical result

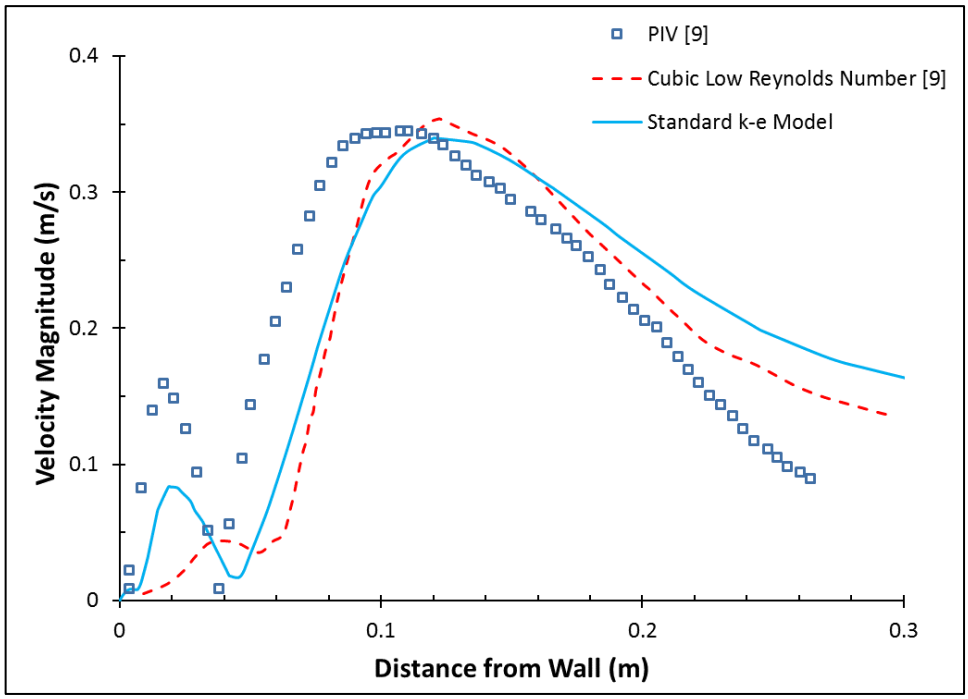

Figure 4-18 Velocity magnitude comparison on Line B – Standard k-ε turbulence model with Günther et al.'s [9] experimental data and the best numerical result

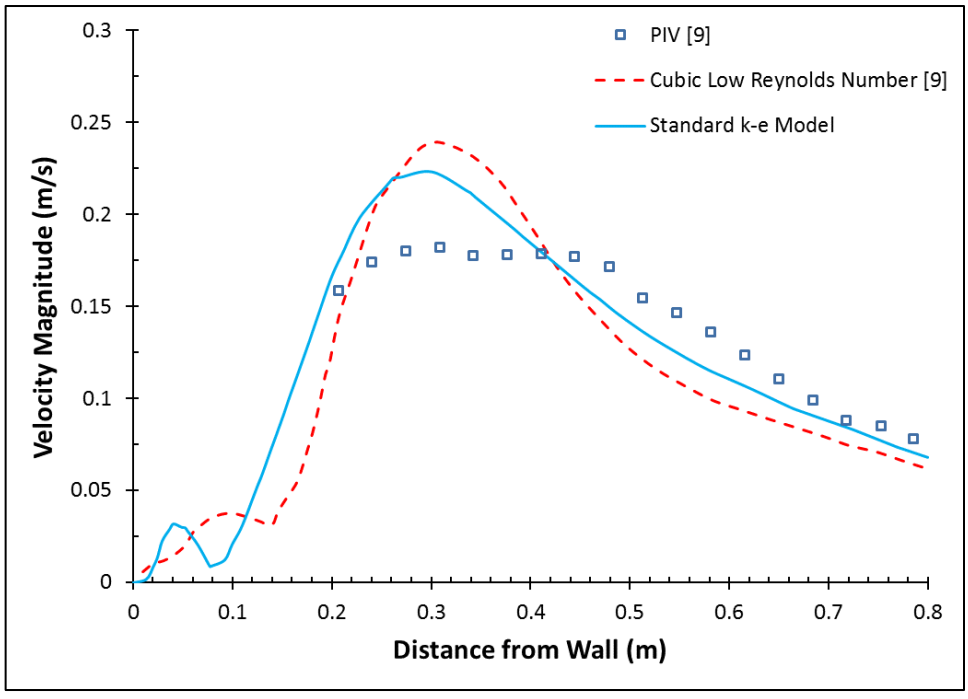

Figure 4-19 Velocity magnitude comparison on Line C – Standard k-ε turbulence model with Günther et al.'s [9] experimental data and the best numerical result

On Line B, in Figure 4-18, it can be observed that the velocity magnitude profile predicted by standard k-ε model with Enhanced wall treatment is quite similar with the experimental results. Jet width and peak velocity magnitude predictions of standard k-ε model are coherent with the experimental data. Comparing the results of the present study with the cubic low Reynolds number model results of Günther et al. [9], it can be observed that, the velocity magnitude profile of the present study demonstrates a better coherence with the experimental results. Moreover, standard k-ε model successfully predicts the location of reversed flow occurring as a result of separation in the sharp corner region.

On Line C, in Figure 4-19, it is observed that the experimental results are not in accordance with the numerical simulation results of the present study and cubic low Reynolds number model of the Günther et al.'s [9] study. This can also be observed for the other numerical results of Günther et al. [9] by examining the Line C part of Figure 4-16. The reason is explained by Günther et al. [9] as since the experimental data of that region have been obtained from large scale measurement with large interrogation windows as large as 70 x 70 mm^2, it was unable to capture smaller flow structures. Consequently, experimental study cannot reproduce the recirculation existing in the corner region, slightly underestimates the peak velocity and overestimates jet width. By considering deficiency of the experimental data, for the performance evaluation purposes, comparison is done only with the cubic low Reynolds number model simulation of Günther et al. [9]. Considering velocity magnitude profiles, although having slight differences, it can be interpreted that the deviation between the results are not significant. Jet location, width and peak velocity magnitude predictions of both models are in coherence.

For the performance evaluation purposes, it is also utilized from velocity magnitude contours. In Figure 4-20, velocity magnitude contours on symmetry plane are presented for the present study and cubic low Reynolds number k-ε model of Günther et al. [9]. Considering both contours, it can be observed that velocity distributions are quite coherent throughout all cross section.

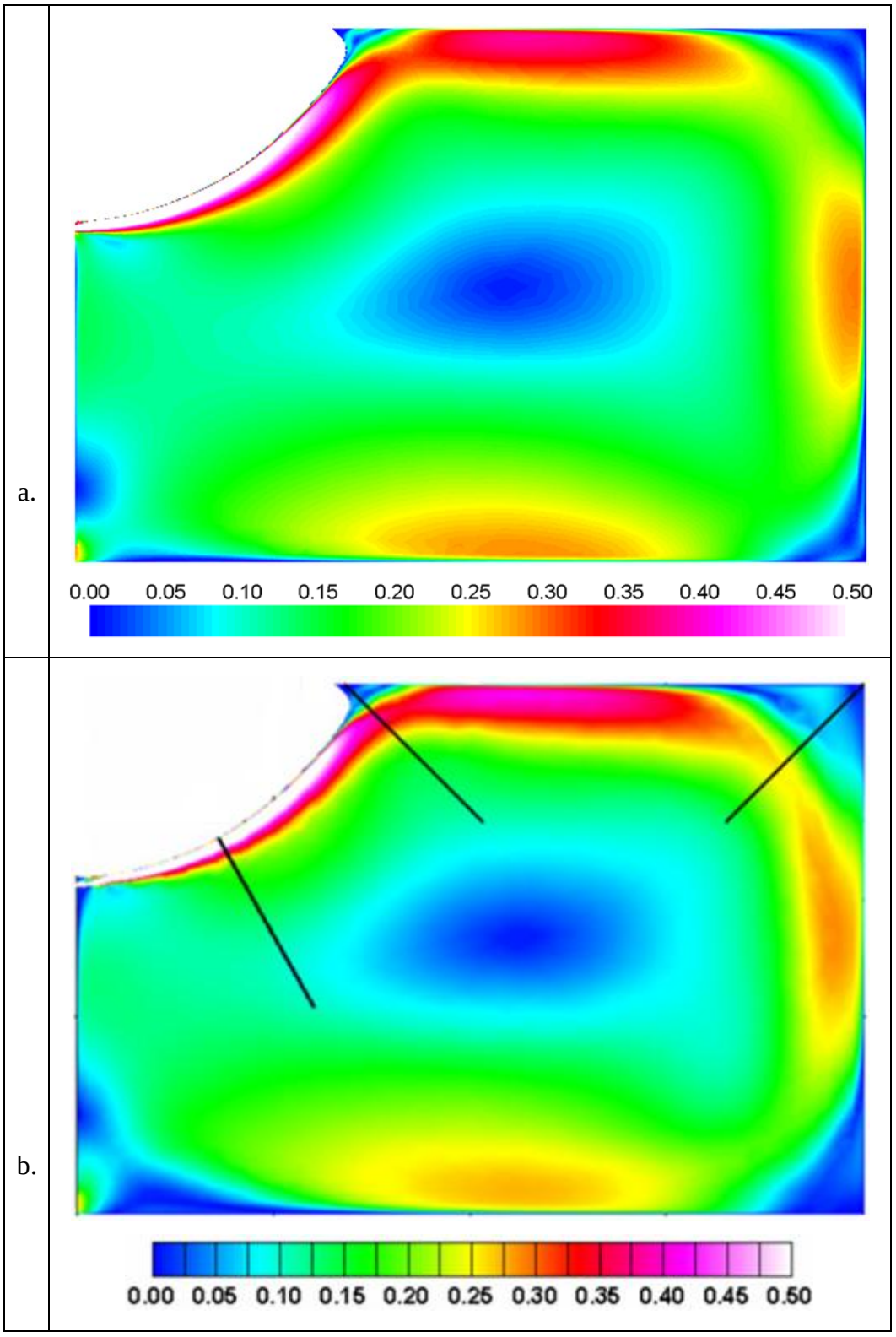

Figure 4-20 Velocity magnitude contours on symmetry plane predicted by; (a) Standard k-ε model of the present study; (b) Cubic low Reynolds number k-ε model of Günther et al.'s [9] study

To detail the coherent results obtained by velocity contours, additionally, velocity vector fields are used to observe the flow structure. In Figure 4-21, it is observed that the jet arising from the inlet, located at the uppermost part of the left wall of the figure, attaches to the curved wall in a short distance due to Coanda effect and remains attached up to upstream of the sharp corner where the first separation occurs. After passing through the sharp corner region, the flow reattaches to the upper wall. The flow repeats successive detachment and reattachment at every corner until it leaves from the outlet, located at the lowermost part of the left wall of the figure. Since the jet follows sidewalls until it leaves through the outlets, velocity magnitudes are very low at the core of the domain.

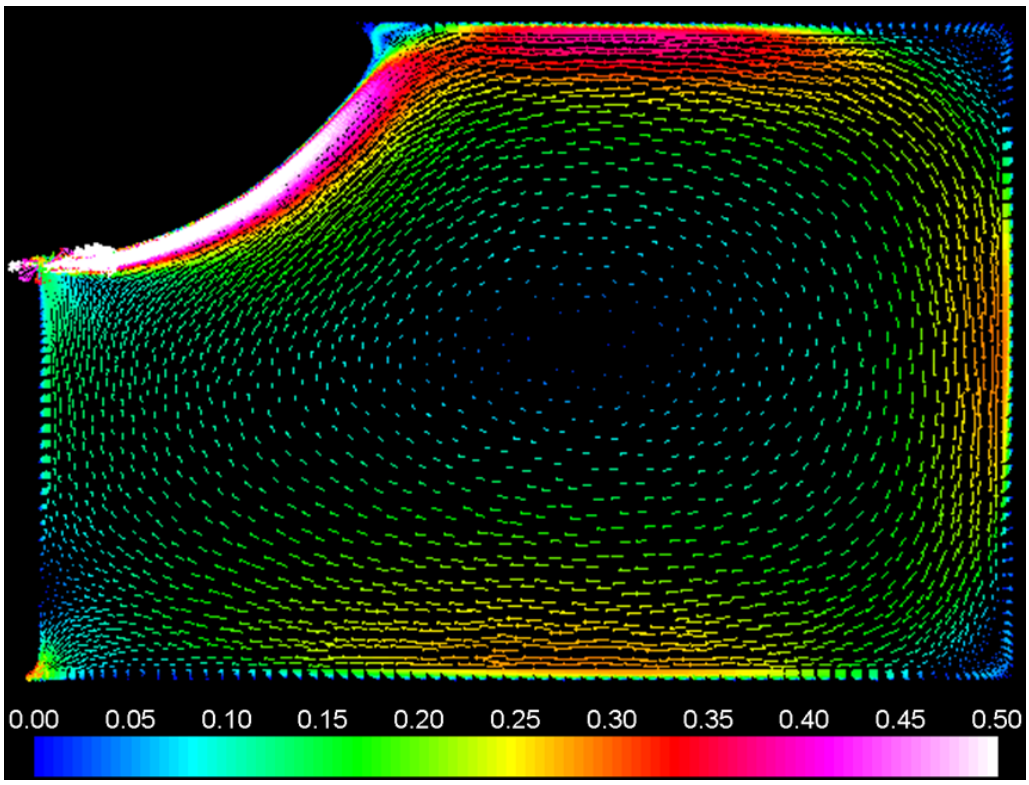

Figure 4-21 Velocity vector fields on symmetry plane predicted by standard k-ε model of the present study

In Figure 4-22, velocity vector field in sharp-edged region is presented wherein also Line B exists. As the curvature of the wall increases, the jet flow expands faster and encounters with adverse pressure gradient. As the boundary layer travels far enough against adverse pressure gradient, the particles having low momentum are forced away to reverse their direction. Therefore, the region of recirculation flow develops. It should be recalled that, the sharp corner region presented in Figure 4-22 are captured quite well by standard k-ε model.

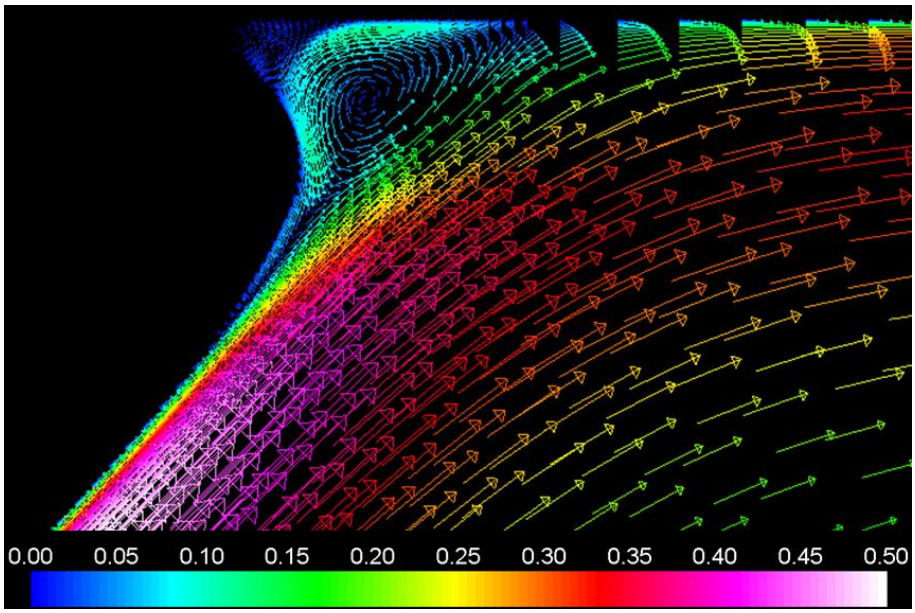

Figure 4-22 Velocity vector fields on symmetry plane, sharp-edged region predicted by standard k-ε model of the present study

By considering as a whole the velocity magnitude plots in Figure 4-17 to Figure 4-19, the velocity magnitude contours in Figure 4-20 and the velocity vector fields in Figure 4-21 and Figure 4-22, it can be concluded that standard k-ε model is superior in predicting the flow field and capturing flow phenomena in an aircraft cabin flow. Therefore, standard k- ε model is used for the further modeling of the numerical simulations of this thesis.

CHAPTER 5

THERMAL COMFORT INVESTIGATION IN THE HELICOPTER CABIN WITH THE EXISTING AIR SUPPLY INLETS

In this chapter, for a newly designed passenger transportation helicopter, flow structure is examined to investigate thermal comfort conditions of the passengers by considering the related requirements obtained from the literature.

5.1 Description of the Helicopter Model

The investigated helicopter has a capacity of twelve passengers. Three rows of seat exist in the cabin and four passengers sit on each row. Foremost row is orientated as faces of passengers are pointing the aft of the cabin whereas the other two rows are orientated as faces of passengers are pointing forward. The reason of such an orientation is to create a space for passengers to get on and off the helicopter without discomfort.

Cooled air is supplied to the cabin by two types of air inlets, namely, main inlets and gaspers. In cabin, totally four main air inlets exist as two are located in each of the port and starboard sides of the cabin. Main inlets are non-adjustable type since their objective is to satisfy thermal comfort requirements related to the general cabin environment. Therefore, air flow of the main inlets can only be controlled by pilot/copilot and main inlets blow air to the cabin all the time through ECS is operated. Moreover, since main inlets are not designed by an objective of creating thermally comfortable environment in the vicinity of the passengers, they blow air horizontally to the sides of the cabin as airflow does not have a direct impact on the occupants. The two main inlets of the port side blows air to the port wall and in the same way, two located at the starboard side blows to the starboard wall. On the other

hand, totally twelve gaspers exist in the cabin as each passenger has one. Gaspers are adjustable type of air inlets which can be opened, closed and adjusted between two extremes by the passengers. In default position, gaspers blow air directly vertically down; however, air blowing directions of gaspers can also be controlled by the passengers. The simplified model of the helicopter cabin with the existing air inlets is shown in Figure 5-1.

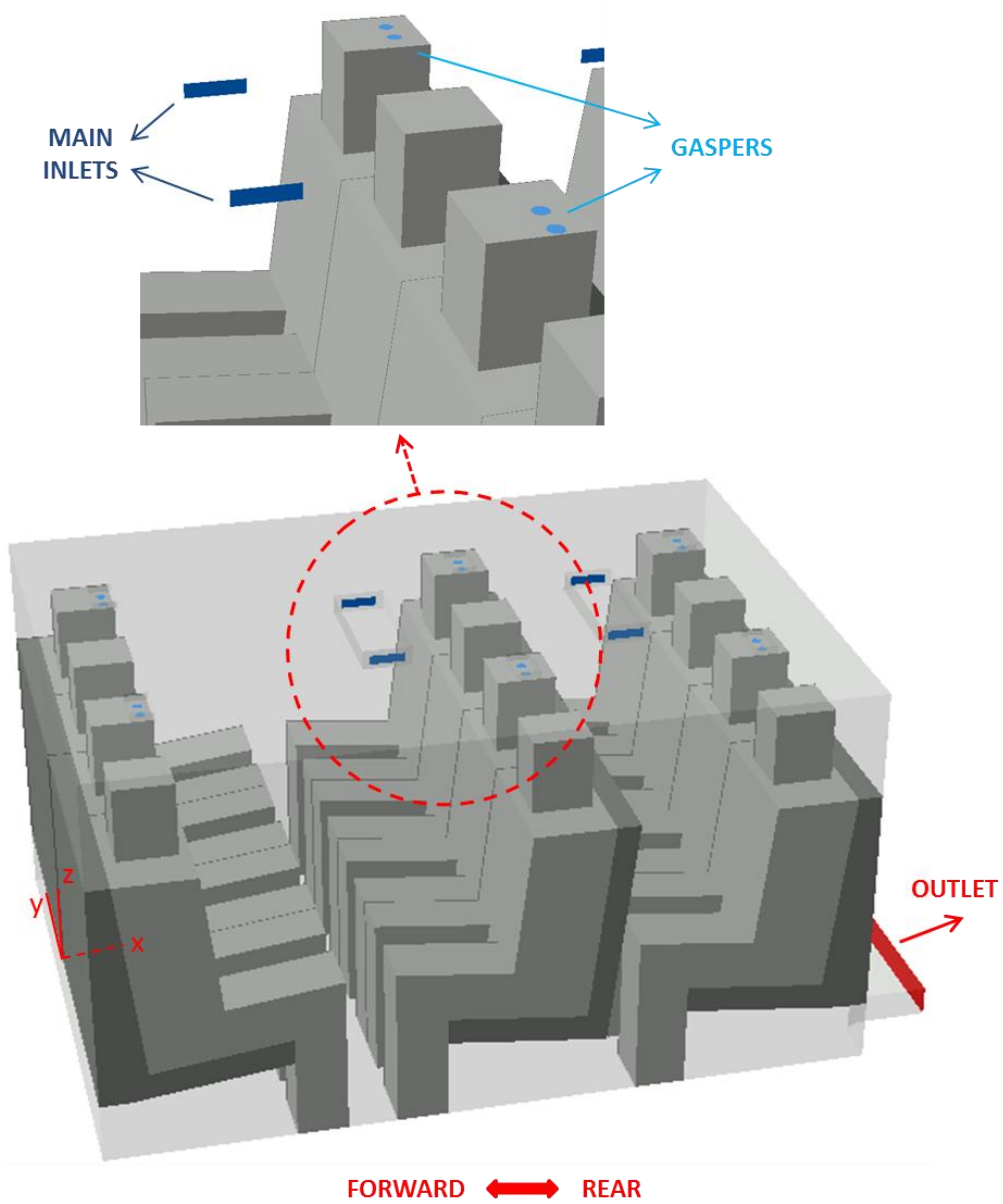

Figure 5-1 Simplified model of the investigated helicopter cabin

To observe the locations of the air inlets and flow of the main inlets, overview of the occupied second-row seats is illustrated in Figure 5-2 from the top.

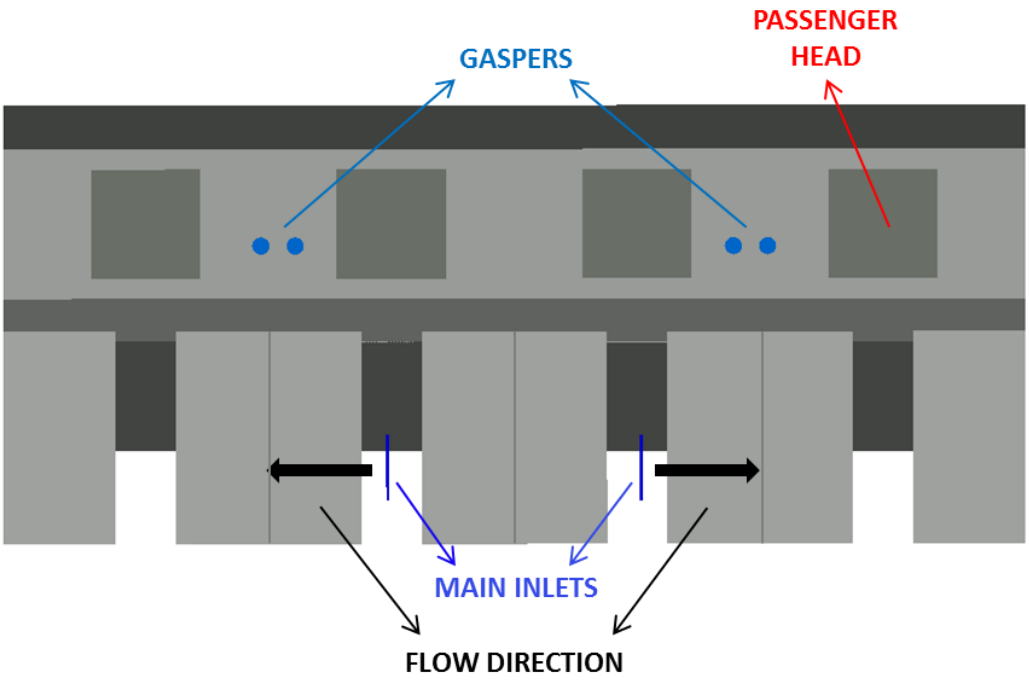

Figure 5-2 Overview of the occupied second-row seats – Top view

5.2 Development of CFD Model

To investigate, the thermal comfort conditions of the passengers, by using ANSYS Fluent, CFD models are developed to simulate cabin flow and temperature for fully occupied conditions.

The cabin model generated to be used in the simulations is half of the real cabin model since the helicopter cabin is symmetric according to the plane which is parallel to zx plane, indicated in Figure 5-1, and passing through the middle of the cabin. By utilizing the symmetry condition, mesh count is decreased. Moreover, in the simulations, simplified models of the main inlets and gaspers are used to reduce computational cost. The accuracy of the simulations performed by using simplified round nozzle instead of real complex gasper geometry has been proven by You et al. [31]. The generated cabin model is shown in Figure 5-3.

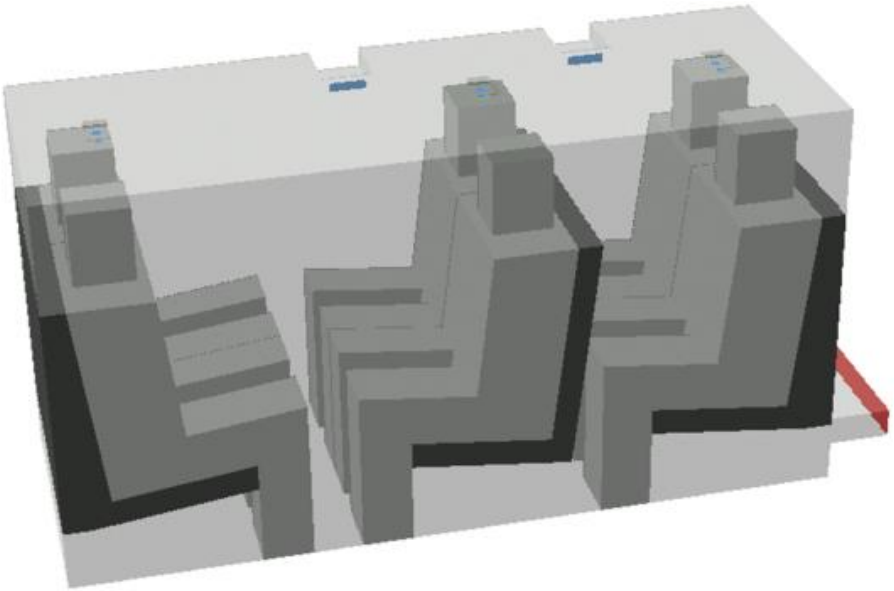

Figure 5-3 The generated cabin model used in the simulations

Simplified passenger dummies are modeled to investigate thermal comfort condition of the passengers. On the other hand, passengers also themselves affect the flow structure. When the helicopter cabin is occupied by twelve passengers, cabin environment becomes highly dense; therefore, flow patterns are highly influenced by the physical occupancy of passengers. Moreover, passengers have also effect on the cabin flow structure as being heat sources.

When developing CFD model, some assumptions are made to focus on to the scope of the study. Since the main purpose of the present study is to investigate the effect of the air inlet locations and the amount of the flow released from the inlets on passenger comfort, solar irradiation is not considered since it would be highly effective in the regions where the sun ray meets with the helicopter surface and where transparencies like windows exist. Therefore, it would manipulate the results of the study as becoming the dominating factor. Considering the cabin boundaries, since transparencies like windows have much lower area than the aluminum surface; they are not included into the model to perform simulations in a more convenient way. In real conditions, there exist slight differences between air flow rates of each of the same inlet type. However, when developing CFD model, all main inlets are

assumed to release the same amount of air and all gaspers to release the same amount by considering that as a general procedure, air ducting design is finalized by adjusting the flow rates of the same inlet types as to be nearly equal. The cabin volume is separated from the cockpit volume by assuming the same target temperature is selected for the cockpit and the cabin by pilot/copilot and no interaction occurs among them.

It should be mentioned that, a design point approximation is made for performance investigations. When modeling the problem, gaspers are handled as being in fully open position. Moreover, they are assumed to be blowing air directly vertically down without specific direction adjustment. This approximation can be considered as the investigation is performed according to the default conditions.

Boundary conditions are defined in this section. In terms of flow conditions, for the main inlets and gaspers, air velocity magnitude is specified. For the investigation of the helicopter cabin with the existing air supply inlets, velocity magnitude is varied for different investigation cases, explained in further on. For all cases, inlet velocity profiles are defined as perpendicular to inlet area and velocity magnitudes are defined as constant throughout the area. Moreover, turbulence intensity according to [43] and hydraulic diameter for the inlet sections are directly specified. For the outlet section, zero gage static pressure is applied as boundary condition. Symmetric wall condition is applied to the symmetry plane which is formerly presented in the chapter. No slip boundary conditions are applied to the other walls. In terms of thermal conditions, outside air temperature (OAT) is defined as 44°C, which is the hottest extreme environment temperature of the helicopter operation envelope. The same air temperature is applied outside of the upper, lower and aft walls of the cabin by assuming that the internal parts of the helicopter are in thermal equilibrium with the ambient. For the heat transfer from ambient to cabin outer surface, convective heat transfer coefficient, defined by [44], is applied according to ground static conditions representing the most challenging condition for the cooling system. For the heat transfer through the cabin walls, thin wall model of ANSYS Fluent is applied and Aluminum, with a thickness of 1 mm, is defined as the wall material

which covers the majority of the helicopter surface and is dominant in heat transfer because of having high conductivity. Adiabatic wall boundary condition is applied to the boundary between the cockpit and the cabin since the cockpit volume is assumed as a separate zone from the cabin volume with the same temperature. The temperatures of the air inlets are specified according to downstream air temperature of the cooling system. For each passenger, heat flux type boundary condition is uniformly applied to all faces and body surfaces as satisfying passenger heat load value described by [28], [31], [34] and [37]. The applied boundary conditions are summarized in Table 5-1.

Table 5-1 Boundary conditions of the helicopter cabin investigation

Outside	Temperature (°C)	44
	Convective Heat Transfer Coefficient (W/m^2-K)	50.6
Main Air Inlet	Velocity (m/s)	Varied according to different cases
	Turbulence Intensity (%)	5
	Hydraulic Diameter (mm)	48.05
	Temperature (°C)	11.8
Personalized Air Inlet	Velocity (m/s)	Varied according to different cases
	Turbulence Intensity (%)	5
	Hydraulic Diameter (mm)	31
	Temperature (°C)	11.8
Outlet	Pressure (Pa)	$P_{static\_gage}=0$
Wall	Velocity (m/s)	$u_{wall}=0$
	Material	Aluminum
	Thickness (mm)	1
	Symmetry	1 longitudinal plane
	Adiabatic	Between cabin and cockpit
Passenger	Heat Generation Rate (W)	75

Standard k-ε model, whose performance competence is confirmed for cabin type flows, is used in the simulations. Simulations are performed as steady state since investigation focuses on the comfort conditions of the passengers in a prolonged period of time. To simulate the buoyancy effect, Boussinesq approximation is adopted. The pressure-based coupled algorithm is adopted to couple the pressure and velocity. For the discretizing the flow variables, the same strategy used in the turbulence model performance evaluation case is applied.

It should be mentioned that to ensure that the computation has been performed completely, as performed in the turbulence model performance evaluation study in Chapter 4, residuals of various transport equations are examined, mass flux conservation is checked and monitor points are used for velocity magnitude and temperature. The only difference is that for the energy equation which is not solved in the turbulence model performance evaluation case, residual value of 10^{-6} is accepted as a sign of convergence as a rule of thumb [42].

5.3 Mesh Independence Study

To investigate the thermal comfort conditions of the passengers, firstly a mesh independent solution must be obtained. For the thermal comfort investigation studies performed on the helicopter cabin, polyhedral mesh is used for volume fill.

Five different meshes are examined in the mesh independence study of the helicopter cabin investigation. Surface mesh size, global mesh size and inflation layer are the three main parameters which controls the mesh independence study and the control strategy is similar to the one performed in Chapter 4. The main difference of the current mesh independence study is in terms of inflation layer. In this part's study, although inflation layer parameters differ from region to region in the domain of a particular mesh count case, first layer thicknesses and number of layers of a particular region are kept same for all five different meshes with a small number of exceptions. The reason is the convergence issues encountered during the study. Moreover, it should be mentioned that although the sizes of surface meshes are determined before the mesh independence study, they also take shape during the

study according to flow field post-processing, convergence status and mesh count, aimed to be arranged as to be compatible with a general mesh independence study refining procedure.

To resolve viscous sublayer, y^+ values are kept as close as to 1. After the simulations, y^+ values are checked. Percentage distribution of y^+ values of the coarsest mesh is illustrated in Figure 5-4. The histogram shows that more than 99% of wall adjacent cells have y^+ value less than 2.

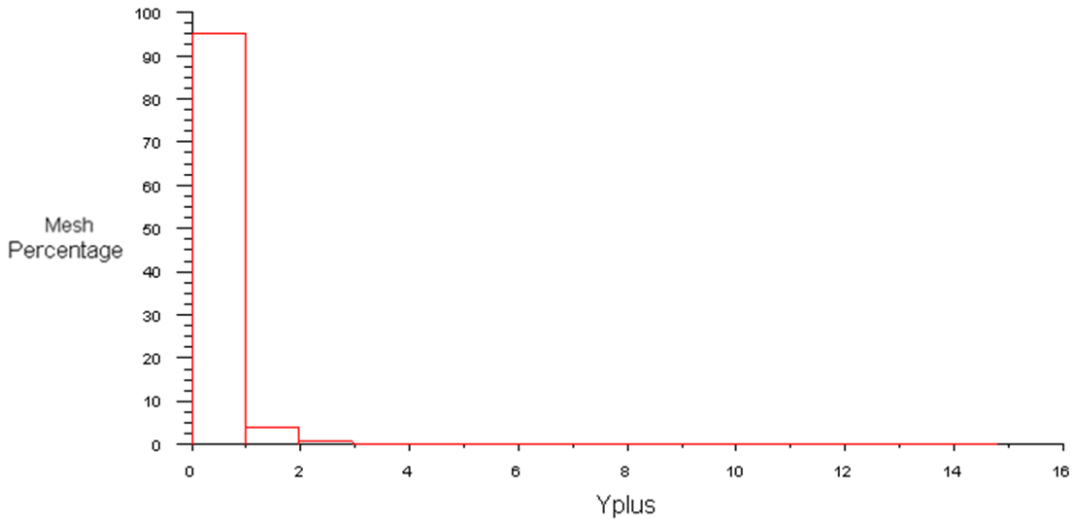

Figure 5-4 Y^+ histogram of the coarsest mesh of the mesh independence part of the helicopter cabin investigation

In Figure 5-5, y^+ contour of the coarsest mesh is shown. It is observed that higher y^+ values arise at the downstream of the air inlets where air velocities are the highest of the domain.

Detailed information about mesh generation parameters of the mesh independence part of the helicopter cabin investigation study is tabulated in Table 5-2. It can be clearly observed from Table 5-2 that the helicopter cabin is divided into various regions for surface meshing because of the complexity of the domain and the flow structure.

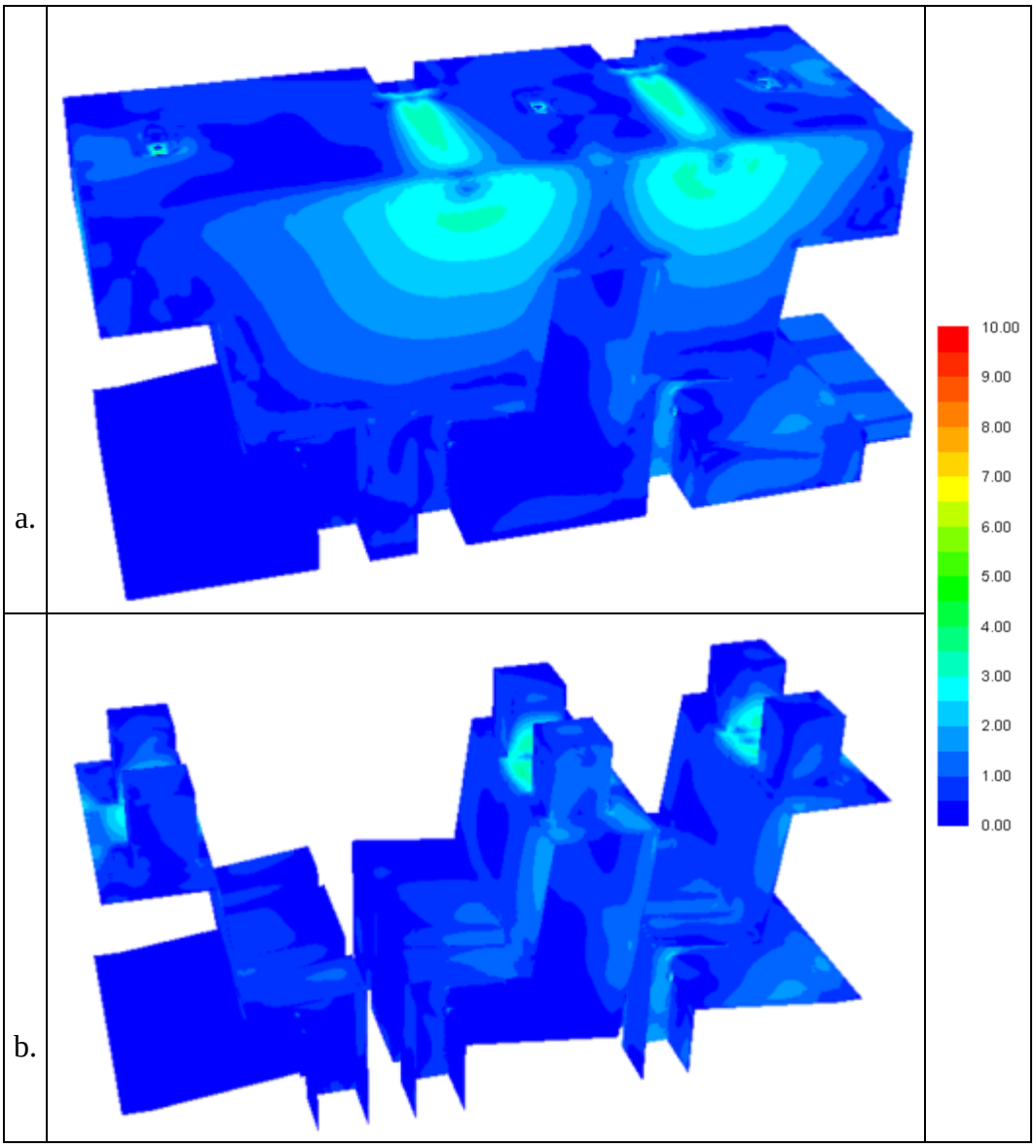

Figure 5-5 Y^+ contours of the coarsest mesh of the mesh independence part of the helicopter cabin investigation; (a) All no-slip boundaries are shown; (b) Helicopter surface is removed

Table 5-2 Summary of the parameters used in the mesh independence part of the helicopter cabin investigation

		Mesh 1	**Mesh 2**	**Mesh 3**	**Mesh 4**	**Mesh 5**
Surface	Global Sizing	80 mm	75 mm	25 mm	20 mm	14 mm
	Gaspers	6 mm	4 mm	2 mm	1 mm	1 mm
	Main Inlets	8 mm	4 mm	3 mm	2 mm	2 mm
	Outlet	20 mm	20 mm	10 mm	6 mm	3 mm
	Cabin Surfaces - General	60 mm	60 mm	20 mm	15 mm	11 mm
	Cabin Lower Surface & Upper Face Near the Outlet	60 mm	60 mm	15 mm	10 mm	7 mm
	Local Improvement Along Main Inlet Jets' Flow Path	41 mm	11 mm	10 mm	8 mm	8 mm
	Passenger Surface Contacting with Gasper Jet	25 mm	13 mm	10 mm	8 mm	6 mm
	Side Surfaces of Main Inlets	5 mm	5 mm	5 mm	5 mm	3 mm
	Surfaces of Main Inlets' and Gaspers' Cases	20 mm	20 mm	12 mm	8 mm	5 mm
	Bottom Surfaces of Main Inlets' Cases	35 mm	35 mm	12 mm	8 mm	5 mm
	Side Surface Near the Outlet	25 mm	25 mm	12 mm	7 mm	5 mm
	Curved Parts in the Outlet Section	15 mm	15 mm	8 mm	5 mm	5 mm
	Forward Faces of Seats	25 mm	25 mm	8 mm	5 mm	5 mm
	Edges of Forward Faces of Seats	5 mm	5 mm	5 mm	5 mm	3 mm

Table 5-2 (Cont'd) Summary of the parameters used in the mesh independence part of the helicopter cabin investigation

			Mesh 1	**Mesh 2**	**Mesh 3**	**Mesh 4**	**Mesh 5**
Inflation	First Layer Thickness		0.35 mm	0.35 mm	0.35 mm	0.35 mm	0.35 mm
	Prism Layer 1 - General	Maximum # of Layers	10	10	10	10	10
		Growth Rate	1.2	1.2	1.2	1.2	1.2
		Total Thickness of Inflation Layer	9.08 mm	9.08 mm	9.08 mm	9.08 mm	9.08 mm
	Prism Layer 2 – Related to Main Inlet Jet Flow Path	Maximum # of Layers	9	9	9	9	9
		Growth Rate	1.2	1.2	1.2	1.2	1.2
		Total Thickness of Inflation Layer	7.27 mm	7.27 mm	7.27 mm	7.27 mm	7.27 mm
	Prism Layer 3 – Related to Gasper	Maximum # of Layers	-	-	5.77 mm	5.77 mm	5.77 mm
		Growth Rate	-	-	5.77 mm	5.77 mm	5.77 mm
		Total Thickness of Inflation Layer	-	-	5.77 mm	5.77 mm	5.77 mm

Mesh quality is checked to ensure the accuracy of the simulations. Since polyhedral type of mesh is used in the simulations, mesh quality can be evaluated by the cell squish index. Maximum cell squish value of 1 corresponds to worst quality whereas 0 corresponds to best. It is recommended to keep maximum cell squish index lower than 0.99 [45].

By examining statistics tabulated in Table 5-3, among all mesh alternatives, Mesh 5 has the highest maximum cell squish index with a value of 0.982 which is below 0.99. The other mesh alternatives have maximum cell squish indexes close to 0.95 or less. Therefore, quality of meshes used in the mesh independence study is adequately high.

Table 5-3 Statistics of the meshes used in the mesh independence part of the helicopter cabin investigation

	Mesh 1	**Mesh 2**	**Mesh 3**	**Mesh 4**	**Mesh 5**
Number of Elements	985000	2066000	3040000	4488000	7359000
Maximum Cell Squish Index	0.949	0.951	0.873	0.946	0.982

In the mesh independence study, five mesh alternatives are compared in terms of velocity magnitude and temperature by utilizing line plots. Locations and features such as length and direction of the lines are determined according to thermal comfort requirements which are explained in the following section of this chapter in detail. When presenting thermal comfort parameters for passengers, indexed which are shown in Figure 5-6 are used throughout the thesis study.

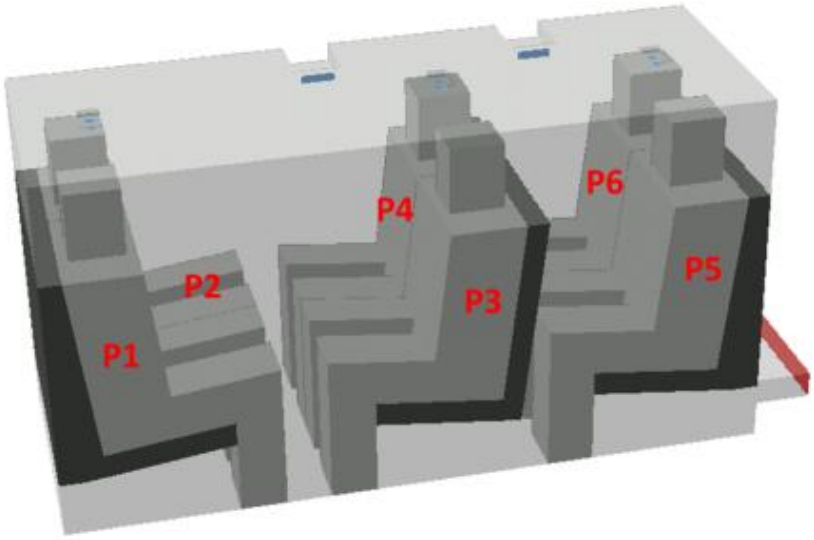

Figure 5-6 Passenger indexes

Velocity magnitudes in the vicinity of each passenger's face are compared on one vertical and one horizontal line. The locations and features of the vertical and horizontal velocity lines are shown in Figure 5-7 for any passenger.

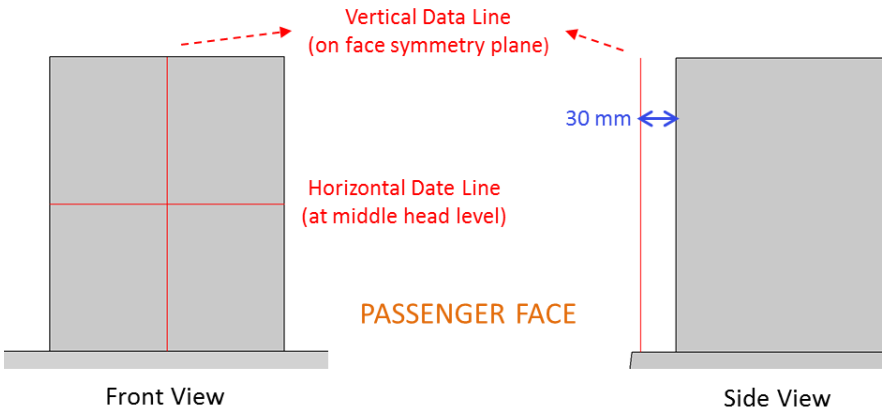

Figure 5-7 Locations and features of the vertical and horizontal velocity lines for any passenger

To illustrate, for P1 and P5, the resultant velocity magnitudes on vertical and horizontal lines are presented in Figure 5-8 and Figure 5-9, respectively. In these figures, for vertical lines, x-axis shows the height from the floor and for horizontal

lines, it shows the y-coordinate, shown in Figure 5-1, whose origin is at the symmetry plane. In both figures, y-axis shows the velocity magnitude. Figures of the other passengers are presented in Appendix A.1.

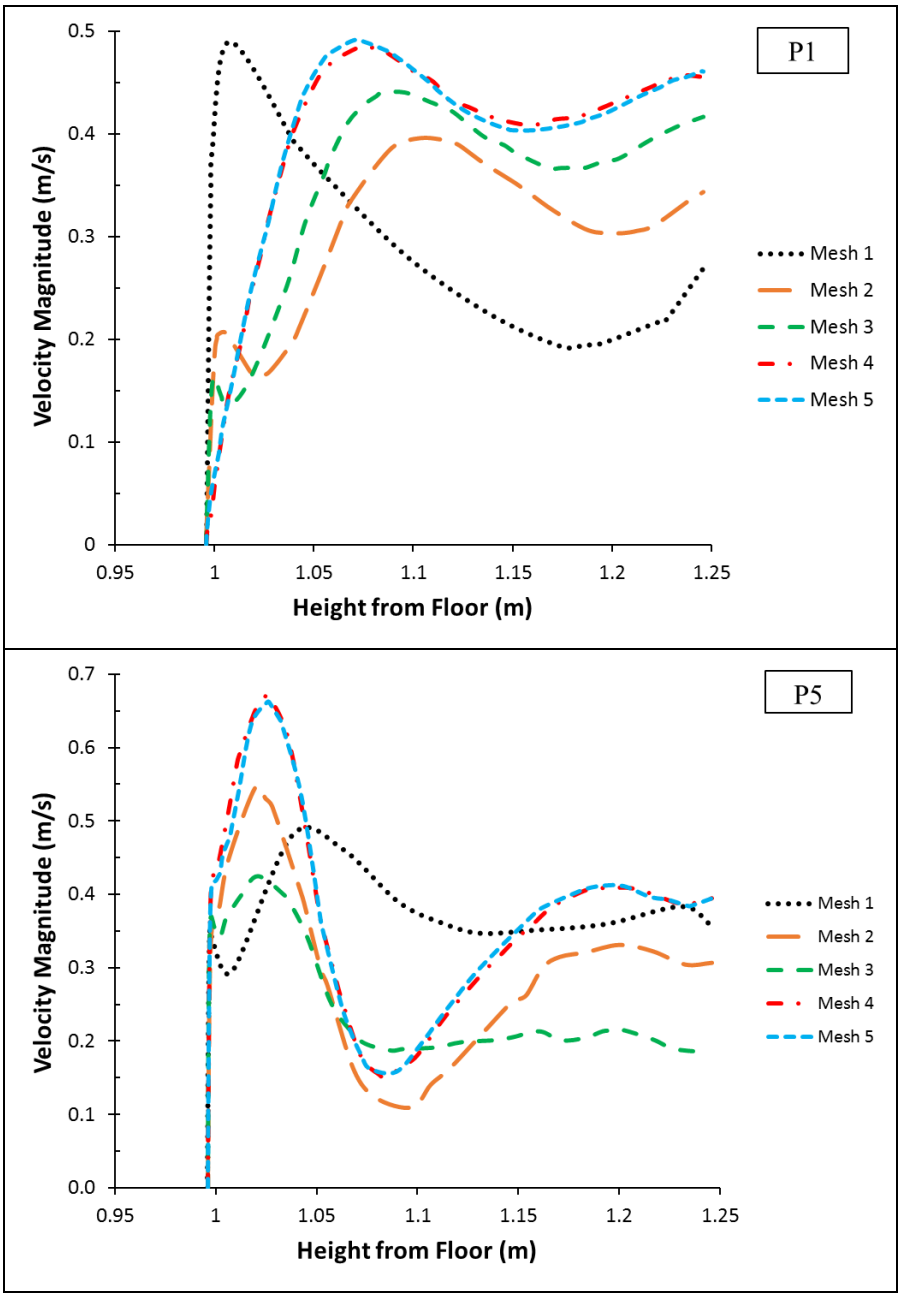

Figure 5-8 Mesh independence results of P1 and P5 for velocity magnitude on vertical lines

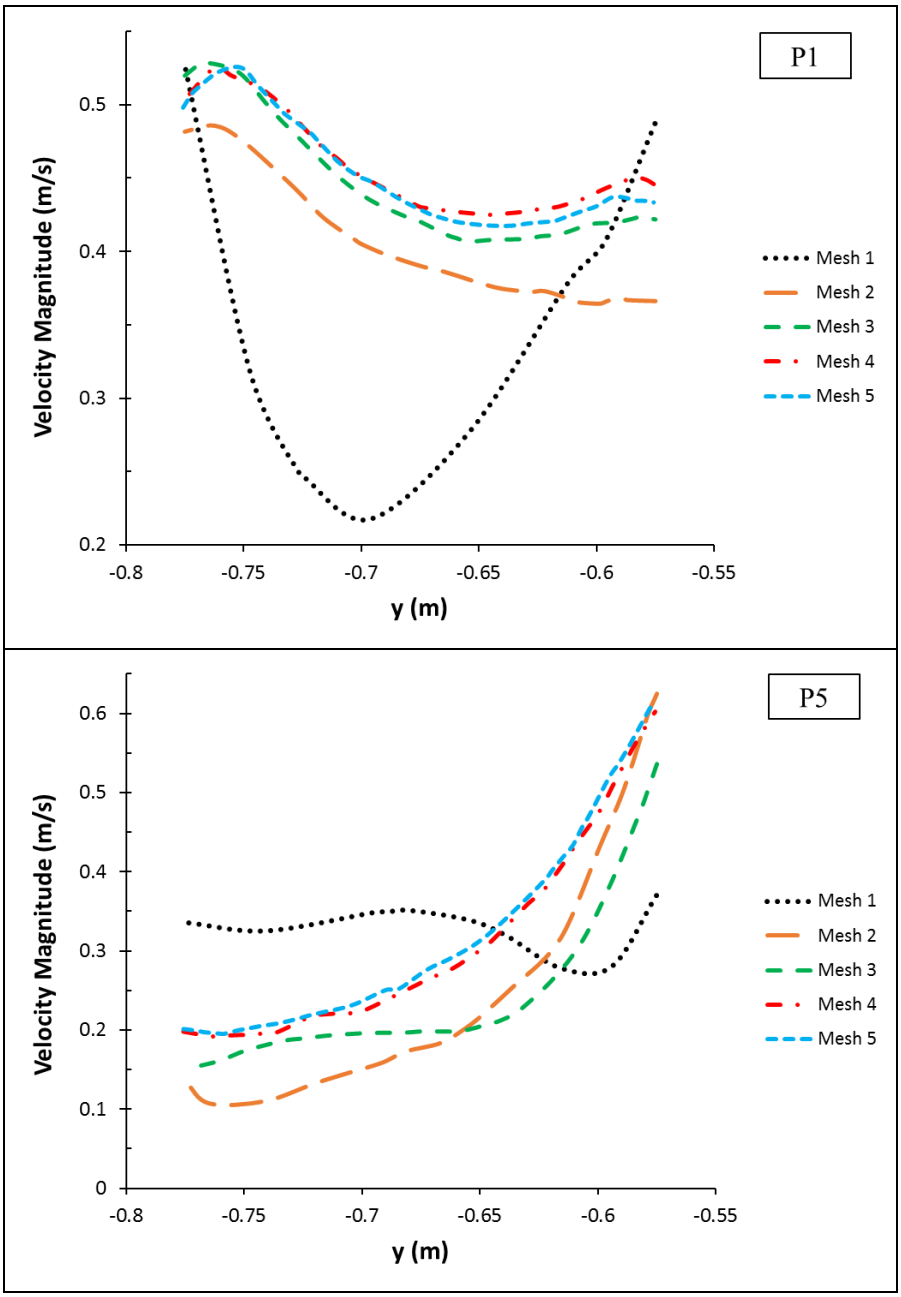

Figure 5-9 Mesh independence results of P1 and P5 for velocity magnitude on horizontal lines

Temperature values are investigated on six vertical lines. The locations and features of the temperature lines are shown in Figure 5-10. In this figure, coordinate information is provided according to the axis system which is defined in Figure 5-1. In the information part of the figure, "start" position of a line corresponds to the lowest point and "end" position corresponds to the highest point.

General View

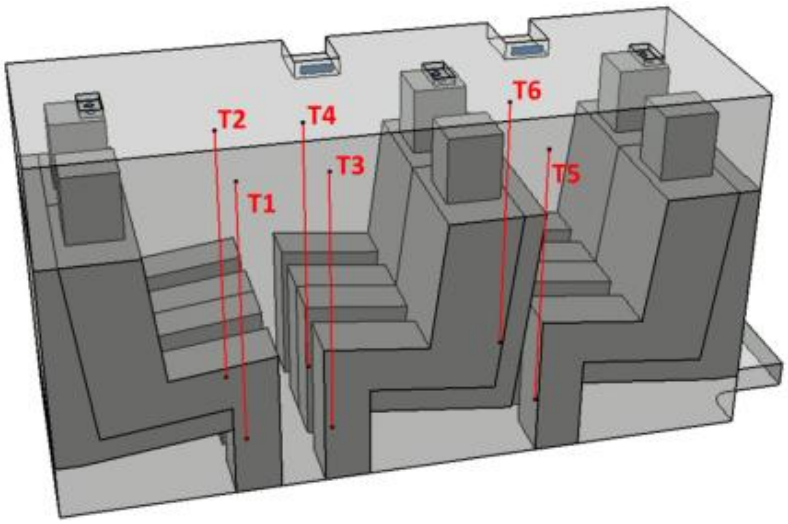

Top View

		Coordinate (mm)		
Line		**x**	**y**	**z**
T1	**Start**	720.5	-675.7	50
	End	720.5	-675.7	1120
T2	**Start**	720.5	-225.1	50
	End	720.5	-225.1	1120
T3	**Start**	1053	-675.7	50
	End	1053	-675.7	1120
T4	**Start**	1053	-225.1	50
	End	1053	-225.1	1120
T5	**Start**	1865.7	-675.7	50
	End	1865.7	-675.7	1120
T6	**Start**	1865.7	-225.1	50
	End	1865.7	-225.1	1120

Figure 5-10 Locations and coordination information of the temperature lines

To illustrate, for P1 and P5, the resultant temperature values are presented in Figure 5-11. In these figures, x-axis shows the height from the floor for and y-axis shows the temperature value. Figures of the other passengers are presented in Appendix A.1.

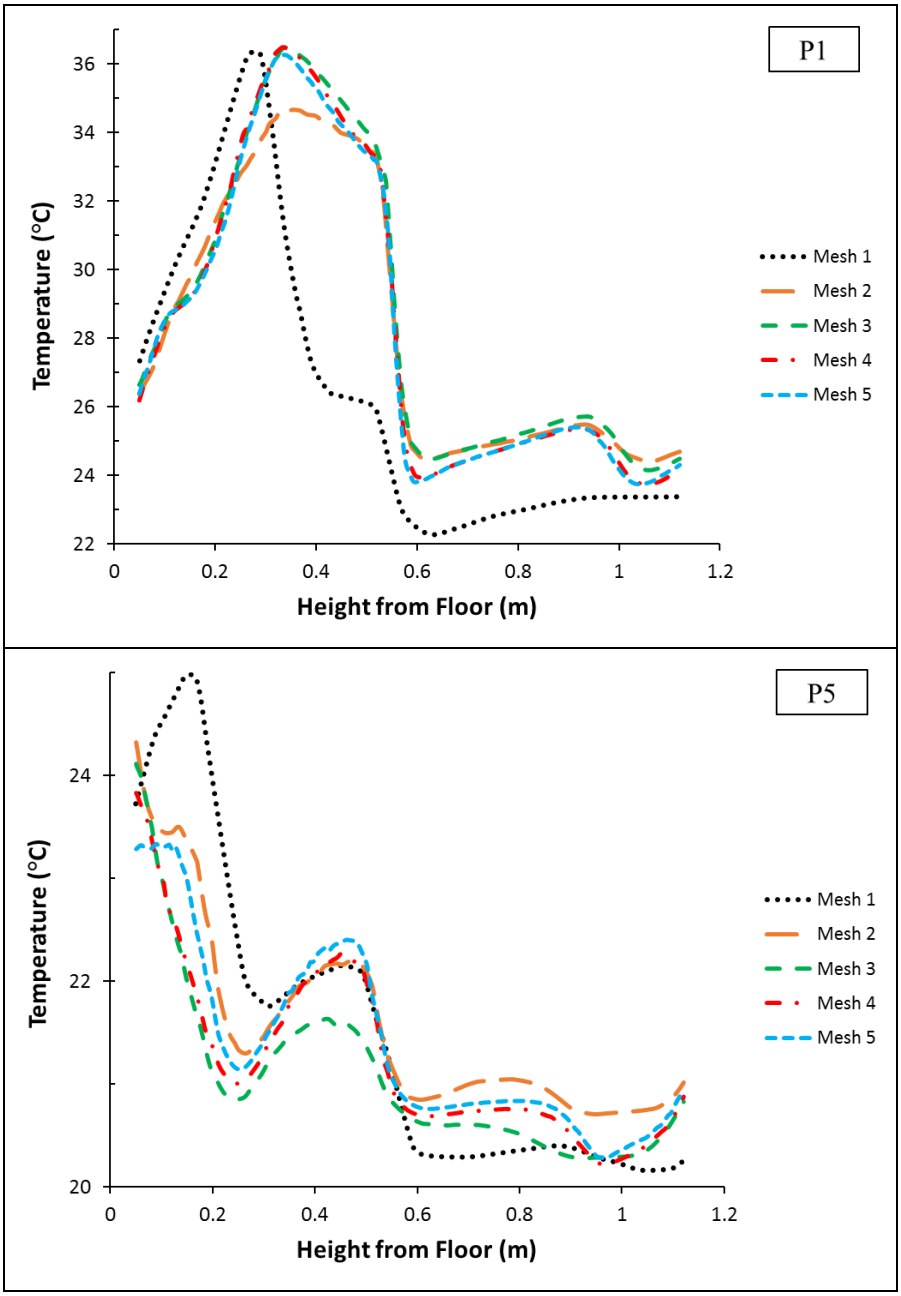

Figure 5-11 Mesh independence results for temperature value

The comparison of the velocity magnitudes and temperature values show that the discrepancy in results does not change with further refinement after Mesh 4. Therefore, Mesh 4 parameters will be used in the further modeling for the thermal comfort investigation of the helicopter cabin.

5.4 Thermal Comfort Investigation of the Existing Design

In this section, the details of the thermal comfort investigation study are presented. The investigation is performed by considering the information obtained from the literature whose sources are highly accepted in the fields of aviation and thermal comfort.

In terms of defining desired velocity magnitudes around the passengers, there exist sufficient information in the literature. SAE ARP292 [46] states, "Where individual air supplies are provided, the recommended jet velocity at seated level should be at least 200 ft/min (1 m/s)." ASHRAE 161-2013 (as cited in Du et al. [2]) recommends that the designed local air velocity at head level should be greater than 1 m/s with personal air outlets. ASHRAE 161-2007 (as cited in Li et al. [28]) stipulates that in the head region of a passenger, the air velocity should be in the range of 1 to 3 m/s when the gasper is turned on.

In terms of defining temperature distribution in the cabin, SAE ARP292 [46] states, "The variation in temperature should not exceed 5°F (2.8°C) measured in a vertical plane from 2 in (5 cm) above floor level to seated head height."

According to the information obtained from the literature, it is considered that the air velocity magnitudes around the faces of passengers should be between 1 m/s and 3 m/s to make passengers feeling comfortable without exposing to drought or stagnation. On the other hand, in terms of temperature distribution, it is inferred that excessive vertical variation should be avoided in the cabin for the comfort of the passengers.

In thermal comfort investigation, since air movement has as a direct effect on the feeling of passengers, air flow in the vicinity of the faces of passengers is determined

as the primary concern. As the secondary concern, temperature distribution throughout the cabin is investigated.

According to the existing locations of the air inlets and the design of the air ducting system carrying air from the cooling system to the inlets, in default conditions when gaspers are fully opened, almost half of the total air flow is directed to the main inlets and the other half is directed to the gaspers. In this part of the thesis study, in addition to the existing air distribution system, different alternative flow rate combination cases are also investigated by keeping the air inlet locations as assuming modifications to be applied only to the upstream ducting portions.

When determining the alternative cases, the limitations existing on account of ECS performance requirements and spatial limitations of the ducting system design are considered. Throughout the ducting portion, modifications can be applied by reducing the sizes of ducting portions since the existing ducting system is designed as wide as possible and no more enlargement can be applied because of the spatial constraints.

It is important to mention that the design of the ducting portions located at the upstream of the main inlets is done to provide sufficient amount of air flow to the cabin. Moreover, the pressure loss characteristic of the existing design of the main inlet upstream ducting is close to the limit; therefore, reducing the size of that ducting portion is not applicable since it would result in ECS performance degradation related to satisfying selected cabin target temperature. By considering all of the mentioned above, it can be concluded that the different alternatives can be created only by reducing the flow rate percentage of the personalized air inlets.

Thermal comfort investigation is performed for three different flow rate combination cases. In addition to the default air flow case, %50-%50, two more cases are investigated in which the %60 and %70 of the total air is directed to the main air inlets, respectively. It should be noted that, for all cases, the same amount of total air is supplied to the cabin since ECS adjusts the amount of air to be supplied to the cabin according to the selected target cabin temperature which is not varied in the

investigation to focus on the scope of the thesis. The total amount of air used in this investigation is determined according to the cabin zone temperature requirements of the investigated helicopter at 44°C OAT. The investigated cases and the corresponding mass flow rate percentages and inlet velocity magnitudes are tabulated in Table 5-4.

Table 5-4 Properties of the investigated three cases for the existing locations of air inlets

	Mass Flow Rate Percentage (%)		**Inlet Velocity (m/s)**	
	Main Air Inlets	**Gaspers**	**Main Air Inlets**	**Gaspers**
Case 1	50	50	7.2	11
Case 2	60	40	8.6	8.8
Case 3	70	30	10.1	6.6

Velocity magnitudes in the vicinity of faces of passengers are investigated on vertical and horizontal lines which are previously introduced in the mesh independence part of this chapter. The velocity lines are located at 30 mm in front of the faces of passenger dummies. When determining the line locations, attention is paid to the positions of the lines relative to the passenger dummies as to be sufficiently close to the faces of passengers but without penetrating into or being so close to the boundary layer. For the three investigated cases, the resultant velocity profiles in the vicinity of each passenger's face are shown in Figure 5-12.

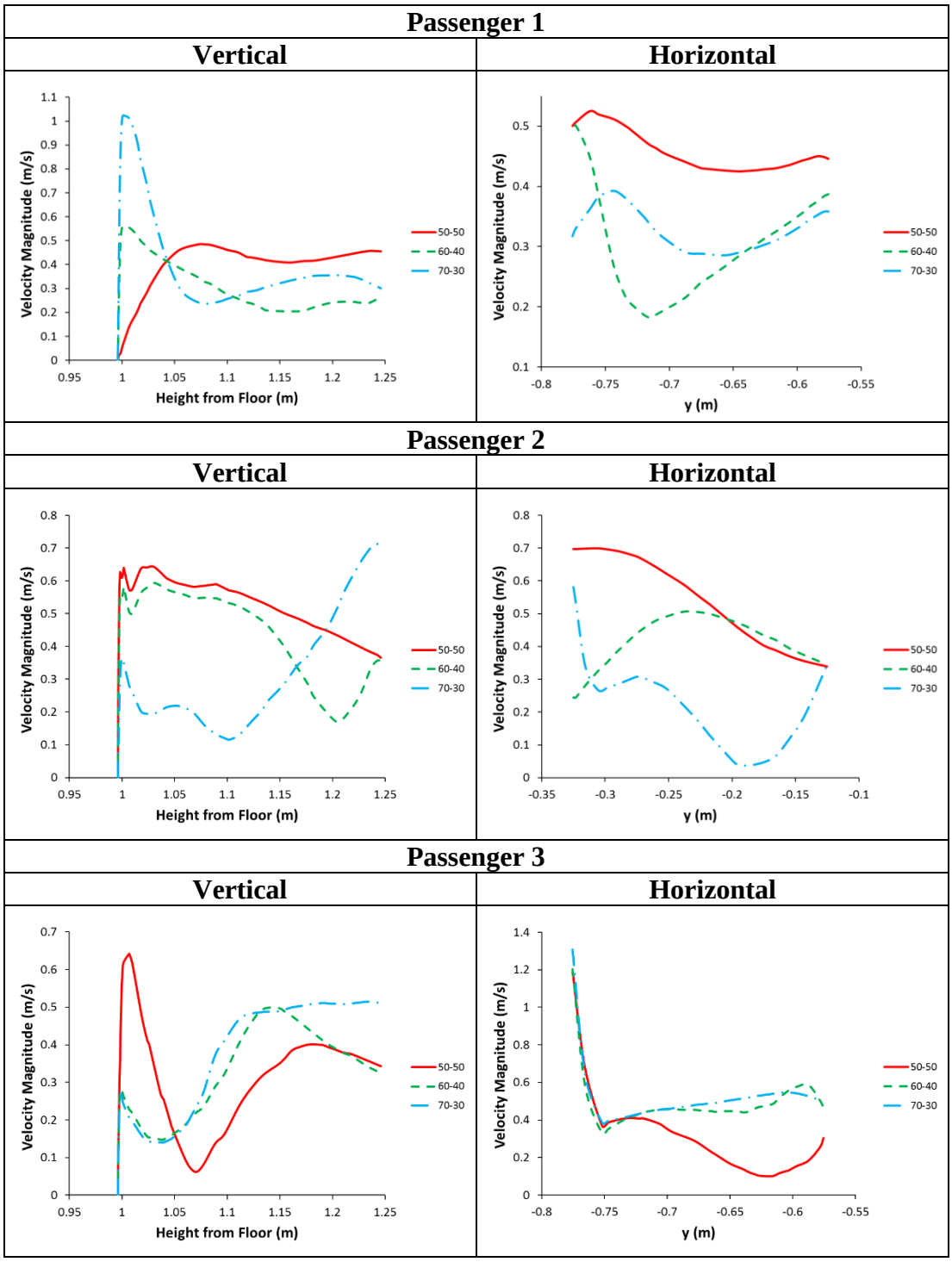

Figure 5-12 Velocity magnitudes on vertical and horizontal lines for three investigated cases

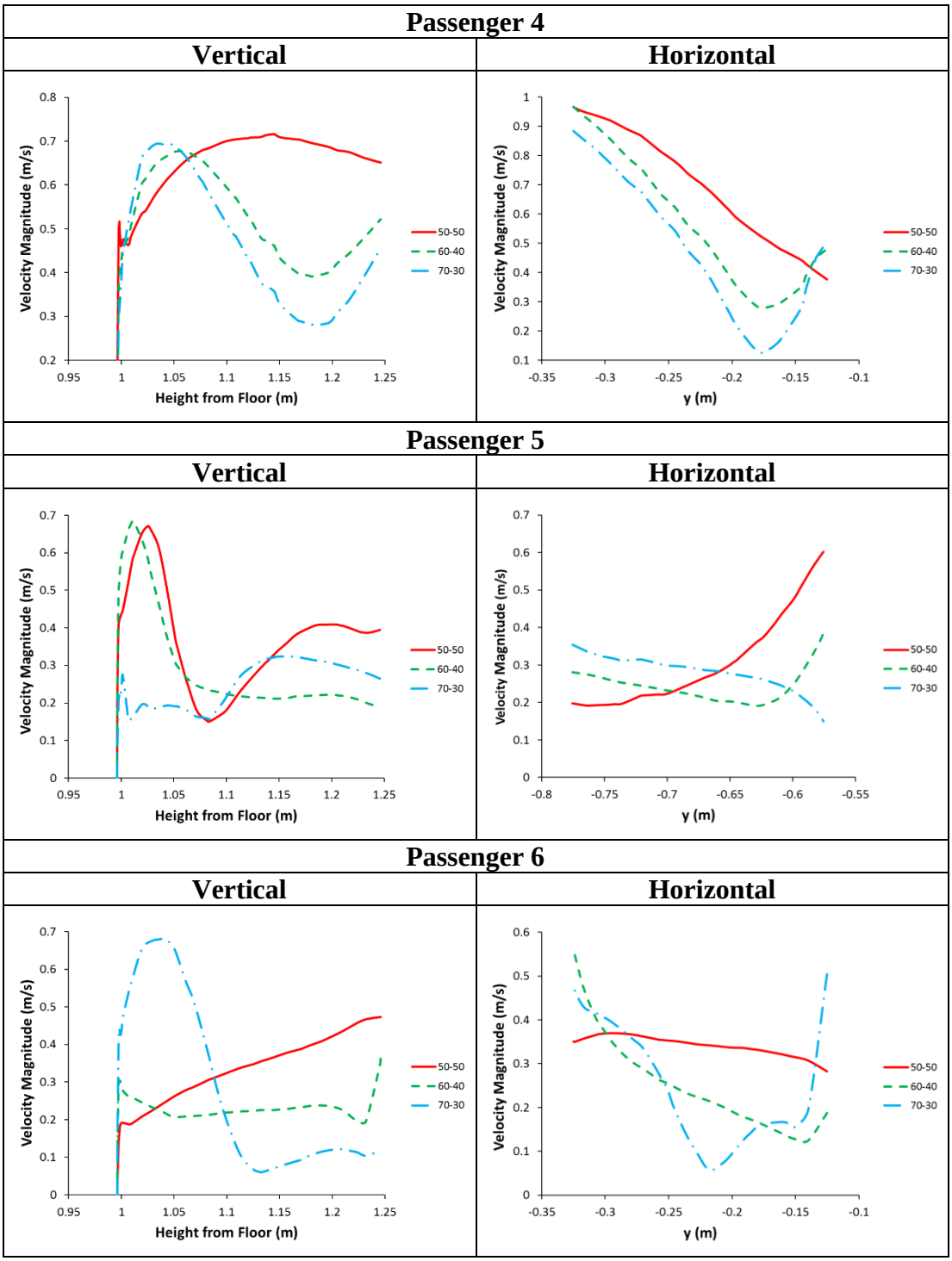

Figure 5-12 (Cont'd) Velocity magnitudes on vertical and horizontal lines for three investigated cases

By analyzing the resultant velocity profiles, it can be observed that for all cases, velocity magnitudes around the faces of the passengers are not in the determined comfort range. In fact, they are much lower than 1 m/s, the lowest value of the comfort range.

By the current locations of the air inlets, a high stagnation risk exists around the faces of passengers which would result in feeling of discomfort.

To illustrate, velocity contours on the horizontal plane passing through the middle of the faces of passengers are shown in Figure 5-13 for %50-%50 flow case; that is, existing case. It is obvious that the effect of jet flow is quite lost in the vicinity of the occupants' faces.

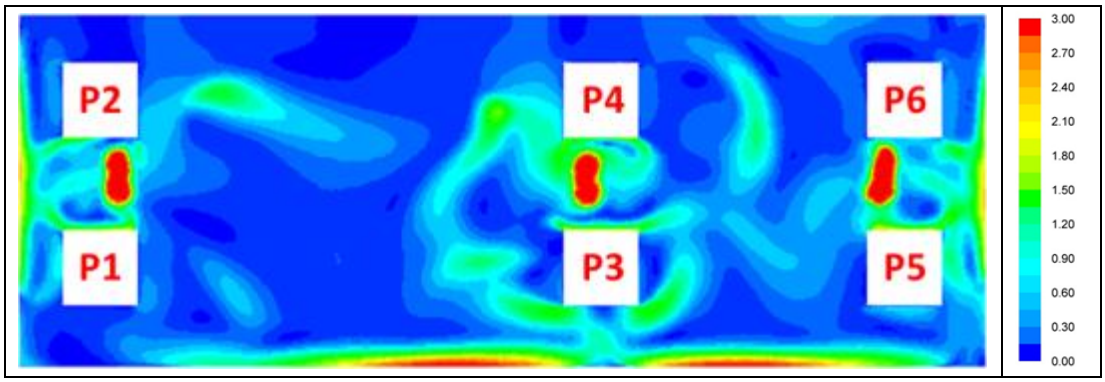

Figure 5-13 Velocity magnitude contours on the horizontal plane passing through the middle of the faces of passengers - %50-50 flow case

Comparing the three cases, velocity magnitudes are mostly higher for %50-%50 flow case than the other two cases. That is, although the locations of gaspers are not sufficiently well in the existing design according to the air flow requirement, gaspers have higher impact on the local comfort of the passengers than main inlets in terms of air movement. It is concluded that, for the existing locations of the air inlets, increasing flow rate of the main inlets by flow balancing process does not make sense; even it would worsen the passengers' comfort conditions.

Since the investigation for the existing locations of the air inlets do not give satisfactory results in terms of air movement which is determined as the primary concern for the thermal comfort conditions of the passengers, it does not make any sense to investigate the resultant temperature profiles. To enhance the thermal comfort of the passengers, air distribution system design should be improved.

It is necessary to emphasize again that the main inlets together with their upstream ducting are designed to provide sufficient amount of air flow to the cabin according to the target temperature requirements. By considering that issue and the inferences obtained from the velocity profiles, it is decided to perform thermal comfort improvement study by modifying the locations of the personalized air inlets.

CHAPTER 6

THERMAL COMFORT IMPROVEMENT STUDY IN THE HELICOPTER CABIN BY ADJUSTING THE LOCATIONS OF THE GASPERS

In this chapter, details of the study performed on the purpose of improving thermal comfort conditions of the passengers are explained. The study is performed by modifying the locations of the gaspers by using the existing gasper design.

6.1 Details of the Gasper Location Improvement Study

During the thermal comfort improvement study, an iterative procedure is followed. For a determined gasper location case, CFD analysis is performed to investigate passengers' comfort condition. The result of the analysis is evaluated by focusing on the thermal comfort related parameters and according to that, the following gasper locations which is anticipated as improving thermal comfort are determined. By processing successive designs and simulations, providing an improvement in the thermal comfort conditions of the passengers is aimed.

During the design process, it is paid attention to keep the locations of gaspers as close as possible to the personalized air inlet main ducting line which is installed in longitudinal direction, nearly at the middle of each symmetric side of the cabin. The main reason of this consideration is that, as locating gaspers further away from the center, the harder the installation of the ducting system becomes. As another concern, locating gaspers further away from the centerline creates additional pressure loss because of the extended ducting portions and may result in decrement of the flow rate of the personalized air flow.

For the cabin inlet location design process, five different gasper locations are studied. Cabin air distribution system case of %50-%50 is used throughout the design stage which corresponds to the existing air ducting design. Five gasper locations are labeled from L1 to L5, respectively according to design iteration order. The investigated gasper locations and the path followed during the design are figured out in Figure 6-1 for P1 and P2.

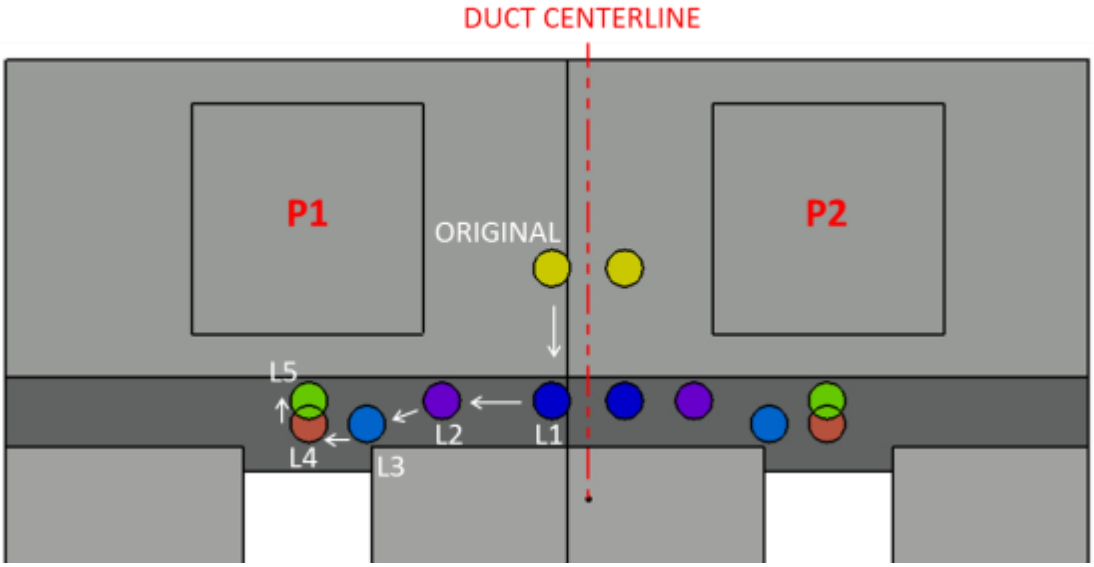

Figure 6-1 Existing and newly investigated locations of the gaspers for P1 and P2 and the followed design path

Position parameters of the existing and newly investigated gasper locations are summarized in Table 6-1. For conformity, during the design, it is paid attention to keep position of a gasper relative to the passenger whom it is dedicated same for all passengers. On the other hand, this arrangement makes the horizontal distance of each of the two neighbor passengers from the main ducting line different since the ducting does not pass right in the middle of the two neighbor passengers as shown in Figure 6-1. That is, for the newly designed cases, gaspers of P1, P3 and P5 have the same position parameters and P2, P4 and P6 have the same. Therefore, to present the data in a more convenient way, in Table 6-1, for the newly investigated locations,

position parameters are presented only for the gaspers dedicated to P1–P2 pair. The only exception of the foregoing design process exists for L1, the first of the newly examined locations. The reason of the exception is that as the first design iteration, modification is applied only in longitudinal direction not to deviate from main ducting line. It should also be stated that when calculating the distances presented in Table 6-1, centers of the gaspers are considered.

Table 6-1 Position parameters of the existing and newly investigated gasper locations

GASPERS			**Horizontal Distance from Pipe Centerline in y-direction (mm)**	**Horizontal Distance from Center of Passengers' Faces in y-direction (mm)**	**Horizontal Position in x-direction; Origin => Passenger Face, (+) Value => To Front of Passengers (mm)**
ORIGINAL GASPERS		P1	31.5	211.3	-57.9
		P2		176.3	
		P3		211.3	-59,6
		P4		176.3	
		P5		211.3	-51.9
		P6		176.3	
NEWLY DESIGNED GASPERS	L1	P1	31.5	211.3	57.5
		P2		176.3	
	L2	P1	126.5	116.3	57.5
		P2	91.5		
	L3	P1	191.5	51.3	77.5
		P2	156.5		
	L4	P1	242.8	0	77.5
		P2	207.8		
	L5	P1	242.8	0	57.5
		P2	207.8		

6.2 Results of the Gasper Location Improvement Study

When examining the thermal comfort conditions of the passengers for a gasper location design case, it is utilized from various types of post processing methods. The vertical and horizontal velocity lines, introduced in Chapter 5, are used to evaluate passengers' comfort conditions by observing velocity magnitude values and profiles around the faces of the passengers. Moreover, profiles of the free jet flow spreading from the gaspers are examined by the line plots to comprehend the flow structure and obtain necessary information to use in the design stage. Furthermore, it is also utilized from velocity contours and velocity vector fields to observe flow structure and various types of fluid flow phenomena occurring in the cabin flow in detail.

6.2.1 Velocity Profiles

Velocity profile comparison of the five newly investigated gasper location designs on vertical and horizontal lines are presented in Figure 6-2 for each passenger. In these figures, for vertical lines, x-axis shows the height from the floor and for horizontal lines, it shows the y-coordinate, whose origin is at the symmetry plane. In both figures, y-axis shows the velocity magnitude.

Evaluation of the vertical velocity lines show that, for gasper locations of L1, L2 and L3, velocity magnitudes are mostly less than the lower limit of the comfort range, 1 m/s, almost at all locations along the vertical lines. For L1, the furthest located one to the faces of passengers, velocity magnitudes are such low that they merely do exceed 0.5 m/s throughout the line. For L2 and L3, velocity magnitudes are close to or just over 1 m/s only at lower head levels and for only some passengers. For L4, velocity magnitudes are higher around the lower head levels of the passengers as reaching up to 1.5 m/s. Moreover, L4 creates velocity magnitude values of more than 1 m/s along most of the head level for all passengers. Considering L5, although velocities are higher than the comfort range upper velocity limit of 3 m/s almost at all locations along the vertical lines, it can be interpreted as by locating gaspers at L5 or its surroundings, the desired velocity magnitudes can be obtained around the faces of passengers. For all gasper locations except L1, a velocity increment is observed in

the lower regions of the vertical lines. This increment with considering the whole velocity profiles can be explained by the conic shape flow profile of the gasper jets.

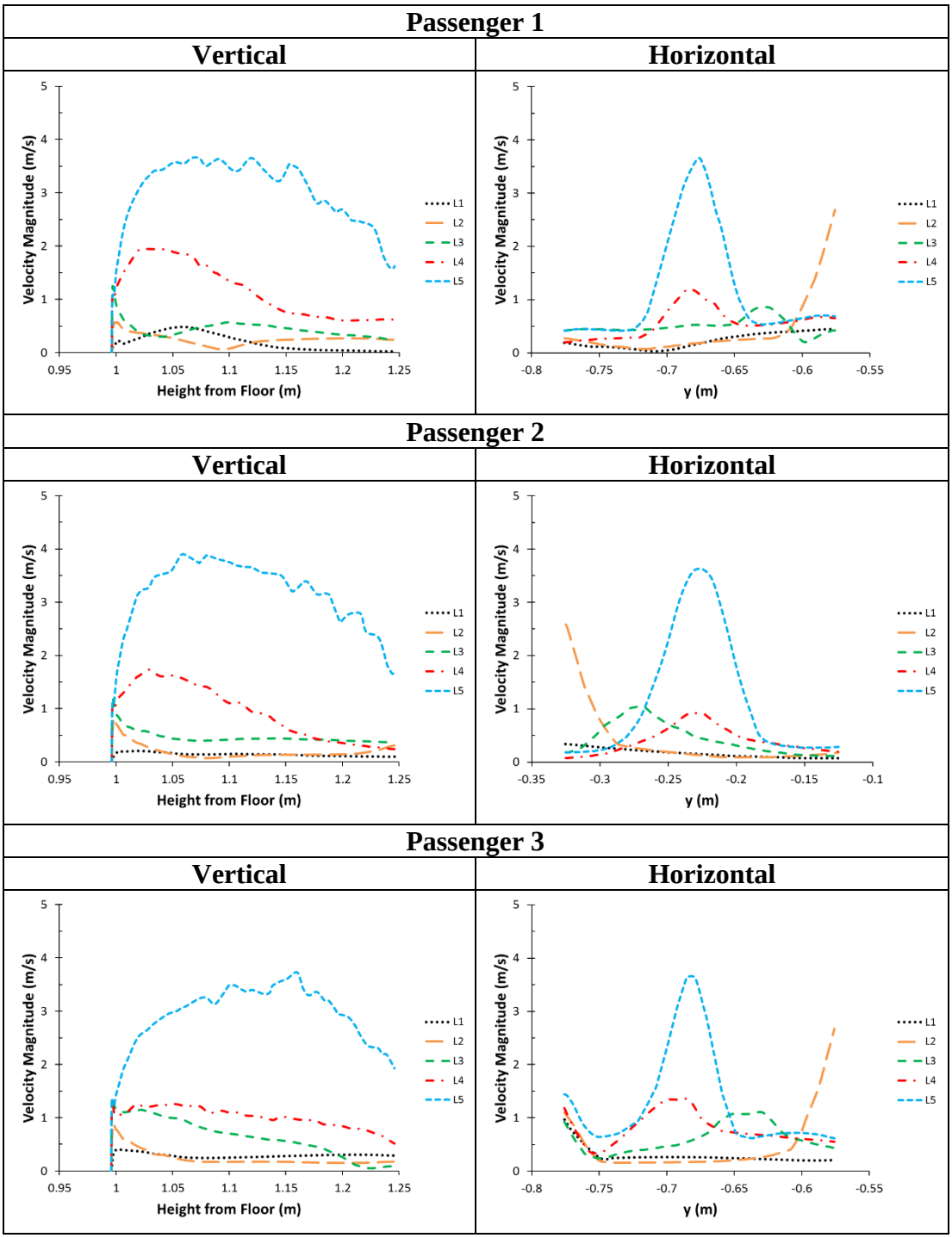

Figure 6-2 Velocity magnitudes on vertical and horizontal lines for L1 to L5 gasper locations

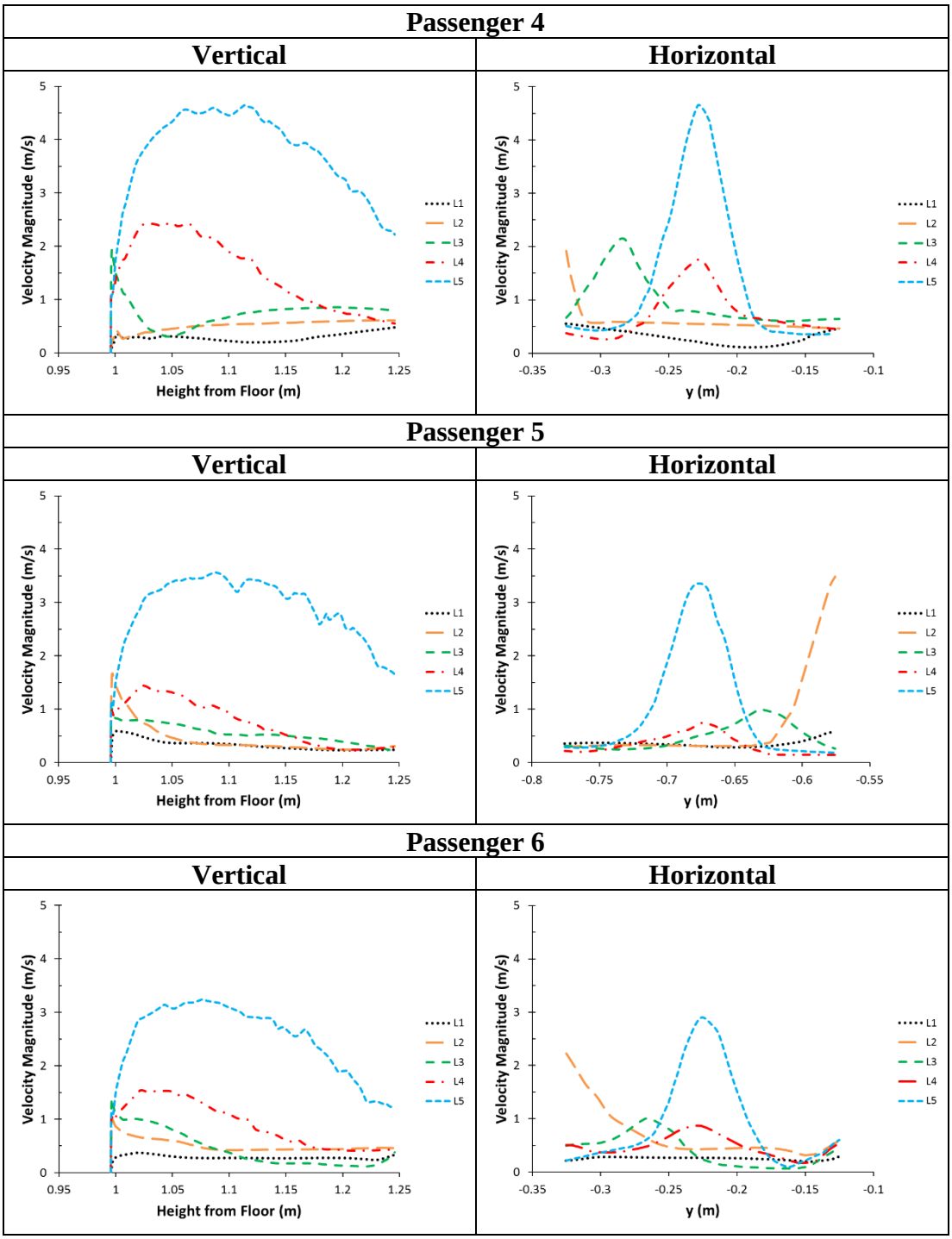

Figure 6-2 (Cont'd) Velocity magnitudes on vertical and horizontal lines for L1 to L5 gasper locations

Evaluation of horizontal velocity lines mainly shows that for the order of air inlet velocity magnitudes of the existing gasper design, 11 m/s, jet flow creates a high velocity region at its downstream but a narrow one. At the boundary region of the jet, velocity magnitudes drop drastically and outside of the jet region, velocity magnitudes are almost same for all five investigated locations as being much less than 1 m/s. That jet profile can be observed by investigating velocity magnitude profiles on horizontal lines of all locations except L1 which cannot create a high velocity region since its location is such far away from the faces of the passengers that the jet flow totally loses its momentum. For the gasper locations L4 and L5, high differences between peak velocities are observed in the middle part of the horizontal lines. Although the distance between L4 and L5 is just 20 mm in longitudinal direction, the difference between peak velocities is more than 2 m/s. That justifies the inference of jets to be mainly effective in a narrow region.

6.2.2 Flow Patterns

Velocity magnitude contours are observed for L4 and L5 which are able to create air motion in the vicinity of the faces of the passengers around the comfort range. Figure 6-3 and Figure 6-4 show velocity magnitude contours on the vertical planes which pass through the middle of the faces of the passengers sitting at the window side seats and interior seats, respectively. Moreover, it should be noted that these planes also pass through the centers of the gaspers for the L4 and L5 locations. When presenting velocity contours, the color range is narrowed to 0 m/s – 3 m/s to evaluate flow field more clearly. Hence, the velocities of 3 m/s and higher are presented with the same color.

Considering the velocity contours on the vertical planes presented in Figure 6-3 and Figure 6-4, it can be observed that the air jet emerging from the gasper flows vertically down with its initial high momentum without spreading too much such that it does not impinge on the face of the passenger whom it is dedicated. The jet velocity decreases to the order of 3 m/s just at the seat level; that is, it is excessively high at the head level. Both for L4 and L5, it is observed that although the jet velocity is excessively high at the head level, air flow is not sufficient to create a

thermally comfortably environment especially at the upper half of the passenger's face because of the distance between the gasper and passenger.

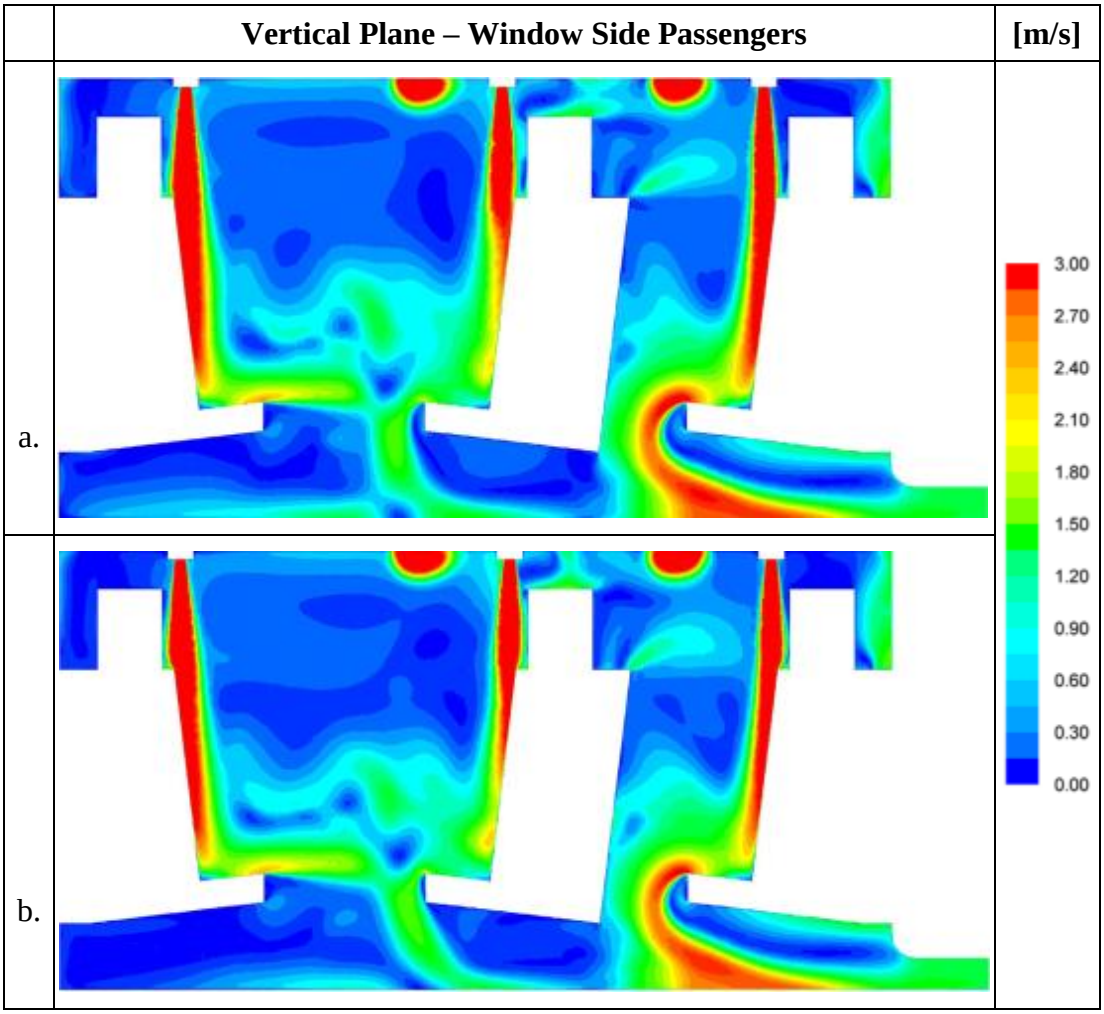

Figure 6-3 Velocity magnitude contours for the passengers sitting at the window side seats for; (a) L4; (b) L5

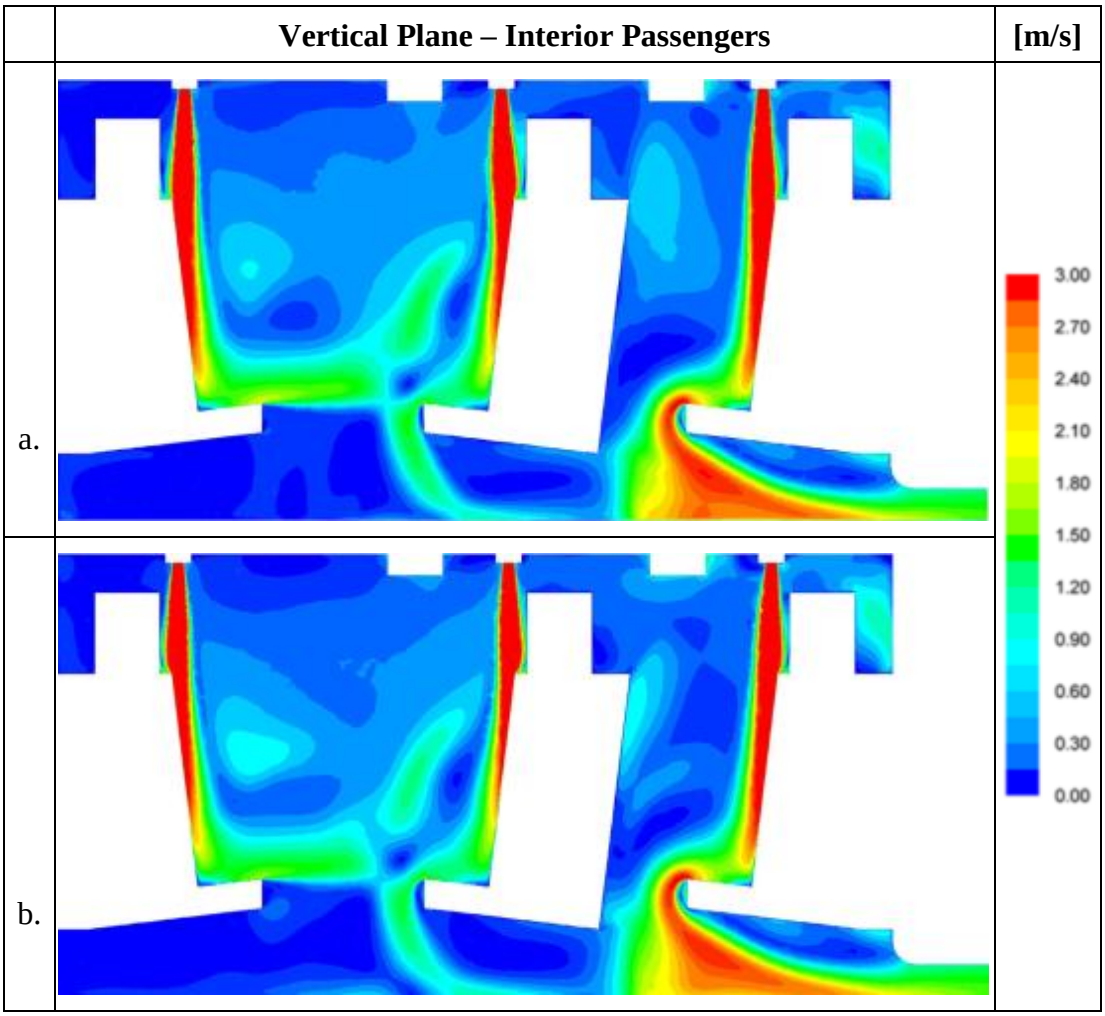

Figure 6-4 Velocity magnitude contours for the passengers sitting at the interior seats for; (a) L4; (b) L5

Moreover, velocity contours are observed on the horizontal planes which are located at three different head levels. The locations of the horizontal planes are indicated in Figure 6-5 and the corresponding velocity magnitude contours are shown in Figure 6-6 and Figure 6-7 for L4 and L5, respectively.

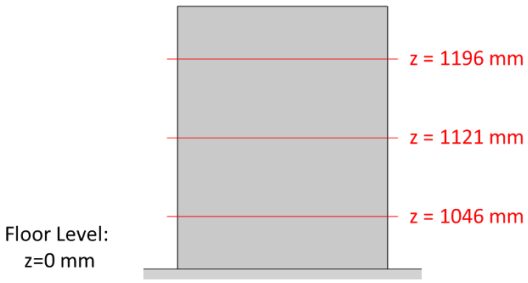

Figure 6-5 Horizontal planes located at the head level

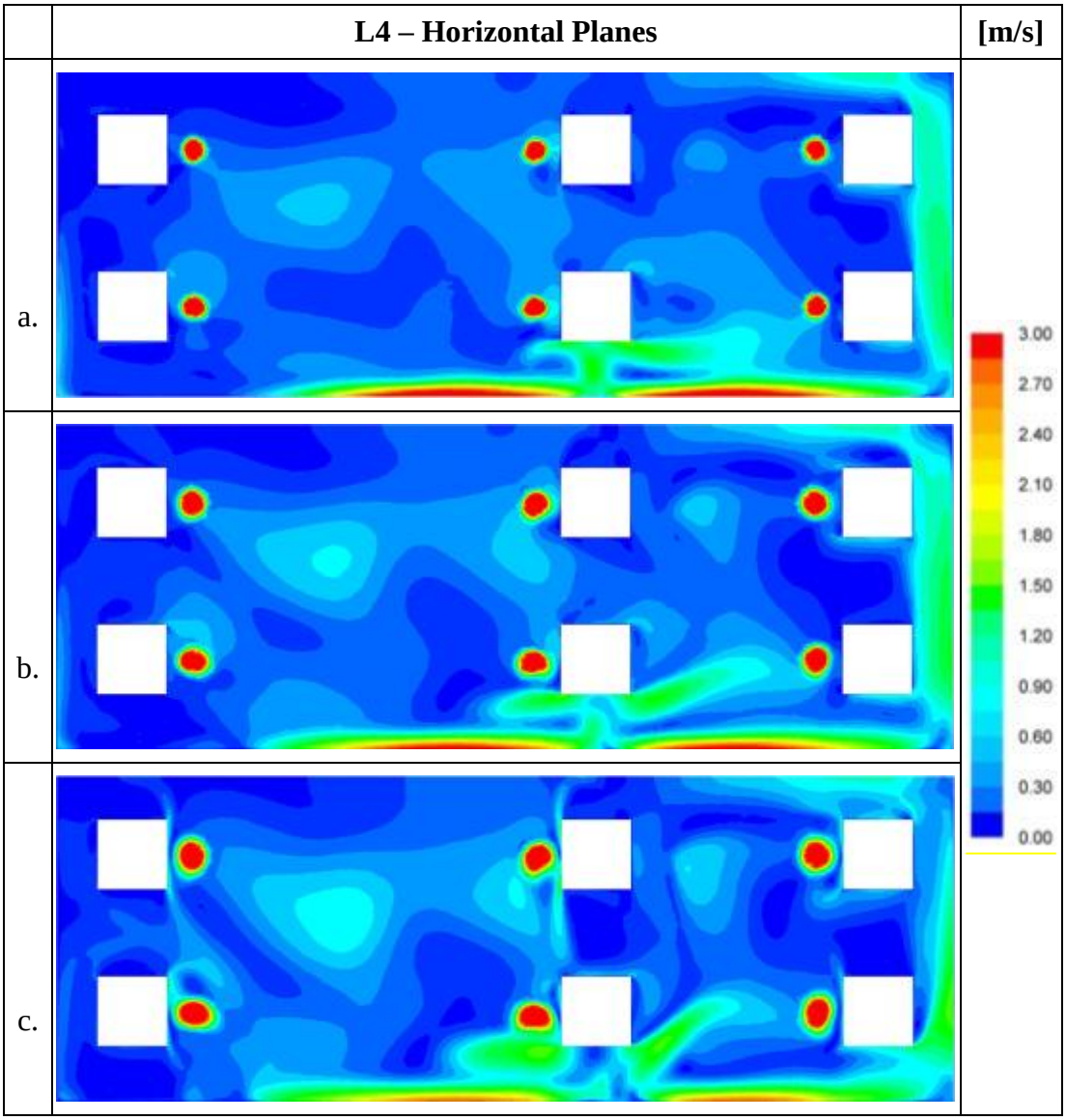

Figure 6-6 Velocity magnitude contours for L4 on the horizontal plane at; (a) z=1196 mm; (b) z=1121 mm; (c) z=1046 mm

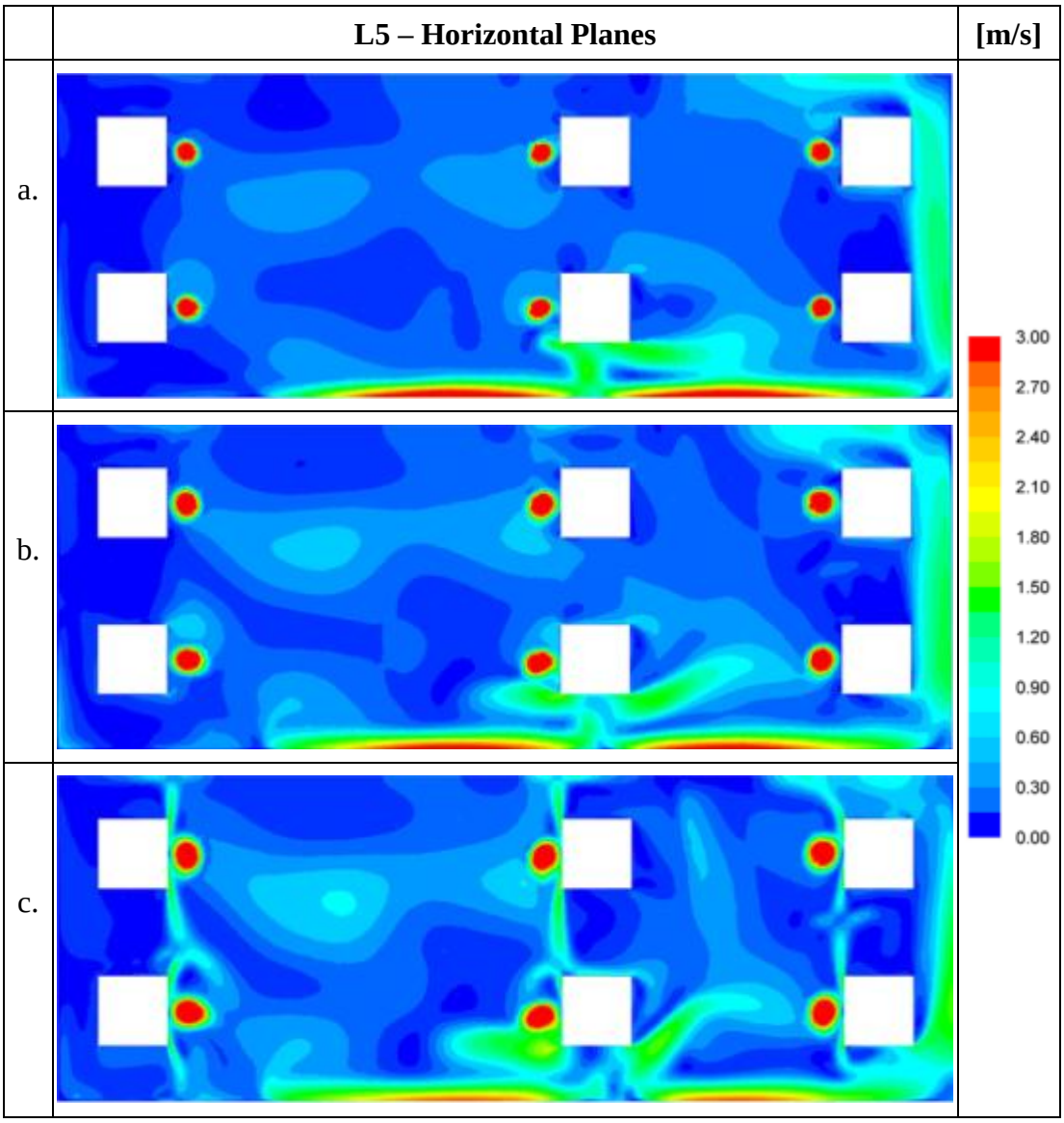

Figure 6-7 Velocity magnitude contours for L5 on the horizontal plane at; (a) z=1196 mm; (b) z=1121 mm; (c) z=1046 mm

Considering the velocity magnitude contours on the horizontal planes presented in Figure 6-6 and Figure 6-7, the conical shape of gasper jets is clearly observed with increasing its area as it travels vertically down. Inside the cone, the jet velocity is higher than the comfort limits and outside of that area, it suddenly decreases. Figure 6-6 and Figure 6-7 indicate that the jet flow is effective in a narrow region which was previously observed by the velocity profiles of the horizontal lines. By considering the upper and middle head level horizontal planes, both for L4 and L5, velocity

magnitudes near the passengers are quite low. In fact, for L4, at all three height levels, velocity magnitudes near the faces of passengers are generally much less than 1 m/s. Therefore, it is concluded that L4 cannot create sufficiently comfortable environment for the passengers. It should also be noted that the velocity magnitudes around P3 are higher than the other passengers' vicinity since the location of P3 is close to the wall region where main inlet jet impinges. However, these values are at most 1 m/s which justify the inference of the main inlets not having a direct impact on passengers.

To observe and comprehend the flow field just near the faces of passengers, as an illustration, flow structure around P1 is investigated for L5 design case. Figure 6-8 shows velocity contours and velocity vectors fields on the vertical plane which is the plane used in Figure 6-3. When presenting velocity contours and velocity vector fields, the color range is narrowed to 0 m/s – 3 m/s to observe the vectors fields of this range more clearly. Additionally, vector fields of 0 m/s – 11 m/s color range is also presented in Figure 6-8 to quantitatively observe the jet momentum loss occurring as a result of the shear force applied by the surrounding stagnant air.

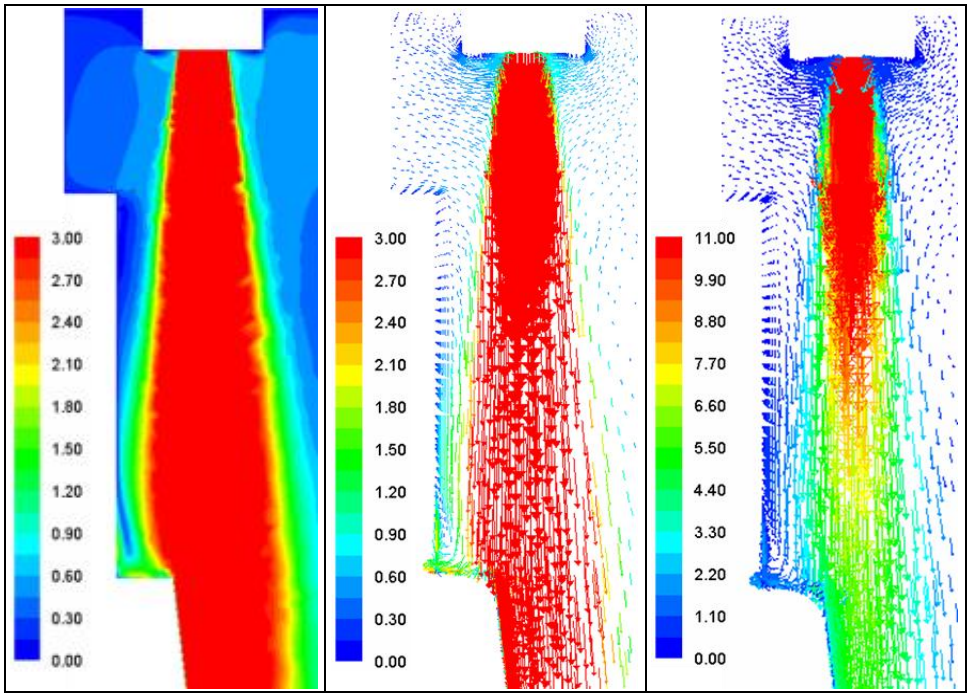

Figure 6-8 Velocity contours and vector fields for P1 for L5 case on vertical plane

By considering 0 m/s – 3 m/s color-range vector fields of Figure 6-8, it is observed that the jet emerging from the gasper spreads along the way from inlet to the lower head levels by joining neighboring fluid particles to it. It is observed that the jet flow does not spread too much up to reaching to the lower head levels and cannot create velocity magnitudes near the passenger's face in the comfort range. As travelling down from the middle head height, a portion of the jet flow which is closer to the passenger' face confronts with the body part of the modeled passenger dummy. Passenger body behaves as an obstacle; therefore, collapsing jet portion loses its momentum. The collapsing fluid particle slows the fluid particle coming after it and this occurs for all impinging particles, successively. As a result, a stagnant zone is formed near the contact region. The main portion of the jet flows vertically down whereas collapsing part spreads outwards by creating two recirculation zones in front of the passenger, at the two sides of the jet as shown in Figure 6-9. As observed by the vector fields of Figure 6-9, the collapsing jet portion interacts with the passenger's face; however, cannot create the desired velocity magnitudes.

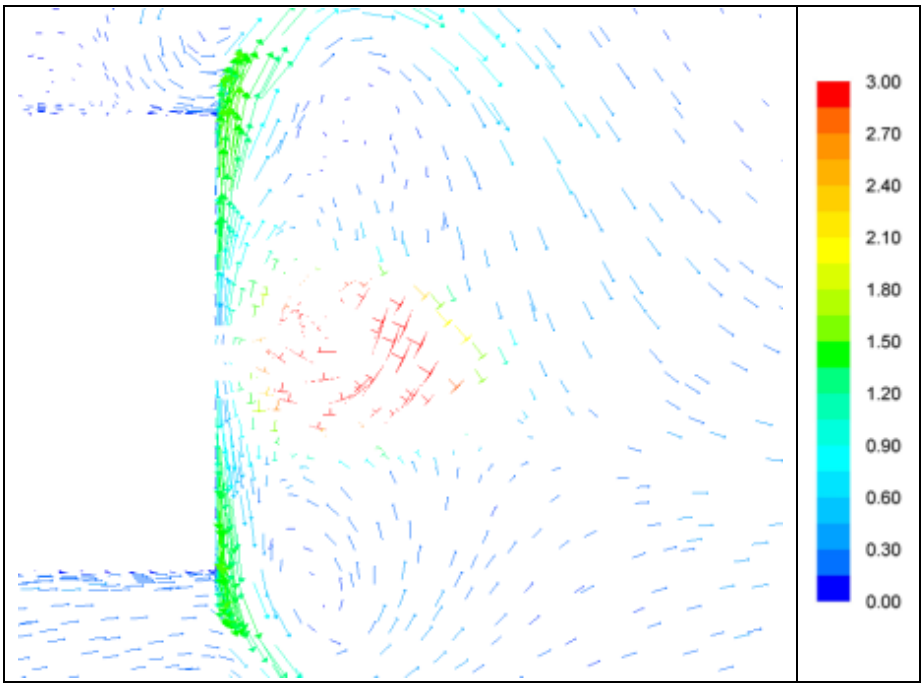

Figure 6-9 Velocity vector fields for P1 for L5 case on the horizontal plane at the middle head level

6.3 Discussion on Possible Gasper Modifications Based on the Results of the Investigated Cases

By processing five additional gasper locations, a design providing sufficient air movement around the faces of the passengers according to the flow performance requirements cannot be reached; however, the region information to focus on is obtained for the further design improvement studies to enhance thermal comfort. By considering all of the presented line plots, velocity contours and velocity vector fields, it can be concluded that, to create a comfortable environment in the vicinity of the faces of the passengers, modifications should be applied on the design of the gaspers and also on the locations of the gaspers relative to the passengers.

One of the modifications that should be applied is to locate the gaspers closer to the passengers whom they are dedicated. However, the sharp velocity change at the boundary of the jet cone, clearly observed in Figure 6-6 and Figure 6-7, makes fine location arrangement in longitudinal direction with the existing gasper design risky since an improper positioning may result in feeling of stagnation or local draft.

In addition to the first modification, jet inlet velocity should be decreased since the order of magnitude of 11 m/s inlet velocity is too high to lose its momentum to the desired levels when reaching to the head level. Applying this proposed modification also makes the application of the first modification more feasible since it would reduce the velocity gradient at the jet cone boundaries.

As the third modification, gasper inlet area should be enlarged to increase the effective area of the passenger face under the control of the personalized air distribution system. It should be noted that, mass flow rate of gaspers would not be affected significantly by the gasper geometry modification since flow rate highly depends on the pilot/copilot control and the air ducting line design located at the upstream of the gaspers. Hence, mass flow rate of the gaspers can be considered as not changing. Moreover, it should be noticed that increasing the gasper inlet area has also contribution to the secondly proposed modification since increasing the area with keeping the flow rate same results in inlet velocity decrement.

CHAPTER 7

THERMAL COMFORT IMPROVEMENT STUDY IN THE HELICOPTER CABIN WITH IMPROVING THE DESIGN OF THE GASPERS

In this chapter, details of the study performed on the purpose of improving thermal comfort conditions of the passengers are presented which are based on the conclusions drawn in Chapter 6.

7.1 Details of the Gasper Design Improvement Study

In Chapter 6, according to results of the investigation, three modifications are proposed; namely, gasper inlet area enlargement, gasper inlet velocity reduction and locating gasper closer to the passenger.

In this design stage, similar approach with Chapter 6 is followed. For a gasper design case, CFD analysis is performed to investigate passengers' thermal comfort condition. According to the results of CFD analysis, the gasper design is improved by modifying inlet area and shape or changing location whichever is required or both. In this part of the thesis study, location L5 is considered as the base since according to the investigation results of the Chapter 6, locating the gaspers in the vicinity of L5 would provide the desired air flow around the faces of the passengers.

In this part of the study, firstly, four different gasper designs are iterated up to obtaining a design satisfying the thermal comfort requirements related to air flow. During the iteration process, gasper locations are also changed when it is deemed as necessary according to the evaluation of the flow fields. The investigation is performed according to the existing air ducting design where the total air is evenly divided between the main inlet lines and the gasper line. The locations of the

investigated gaspers and the path followed during the design iterations are shown in Figure 7-1 for P1 and P2. It should be noted that L6, the first investigated gasper design of this part of the study, has the center location coincident with the center of base, L5. The L5 design is also included into the Figure 7-1 and its boundaries can be observed inside of the area of L6.

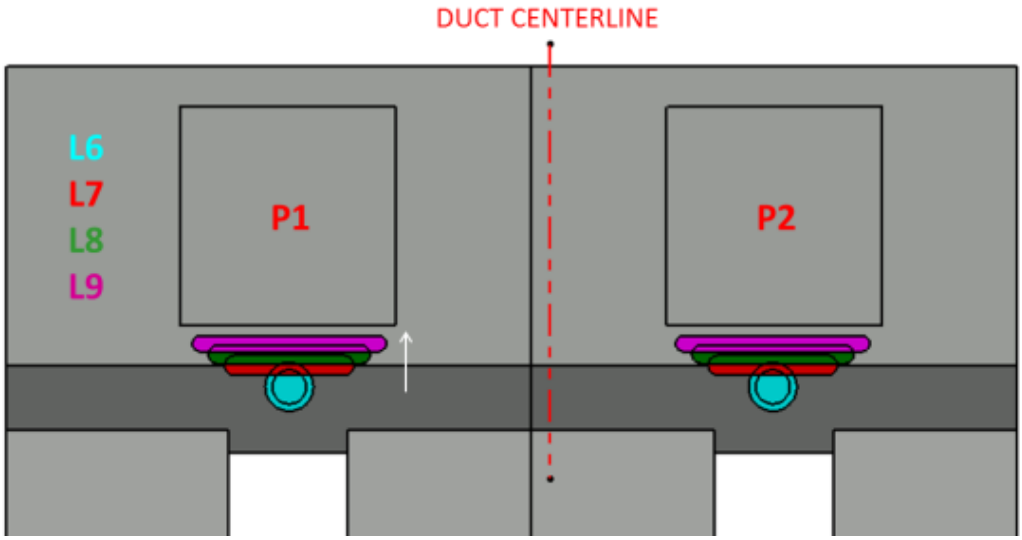

Figure 7-1 Newly designed gaspers for P1 and P2 and the followed design path

Geometric parameters, corresponding air inlet velocities and location information of the newly designed gaspers are summarized in Table 7-1.

After obtaining a design providing the desired velocity magnitudes in the vicinity of the faces of the passengers and blowing air as covering sufficiently broad area on the faces of the passenger, L9, the three different flow rate distribution cases introduced in Chapter 5, namely, %50-50, %60-40 and %70-30 are investigated to obtain more alternatives for the temperature field investigation which is carried out subsequently. In this step, the three cases are investigated for the same air inlet velocity, 3.25 m/s, since a thermally comfortable environment is obtained by that inlet velocity in terms of air flow. Hence, increasing the flow rates of the main inlets is achieved by reducing gasper area. It should be mentioned that, as an assumption, reducing the gasper area by narrowing the width more than the L9's value, 15 mm, is considered

as an unrealistic design. Therefore, the modifications are applied to the gaspers as reducing their lengths. The gasper design L9 and its two extension designs are shown in Figure 7-2. Moreover, geometric parameters of the gaspers and inlet velocities are tabulated in Table 7-2.

Table 7-1 Geometric parameters, inlet velocities and location information of the newly designed gaspers

GASPERS	**Shape**	**Area (mm^2)**	**Length – Width (mm)**	**Inlet Velocity (m/s)**	**Horizontal Position in x-direction; Origin => Passenger Face, (+) Value => To Front of Passengers (mm)**
L6	Circular	1583	44.9 – 44.9	5.5	57.5
L7	Elongated Hole	2169	120 - 18.7	4	37.5
L8	Elongated Hole	2482	150 – 16.95	3.5	27.5
L9	Elongated Hole	2670	180 - 15.11	3.25	17.5

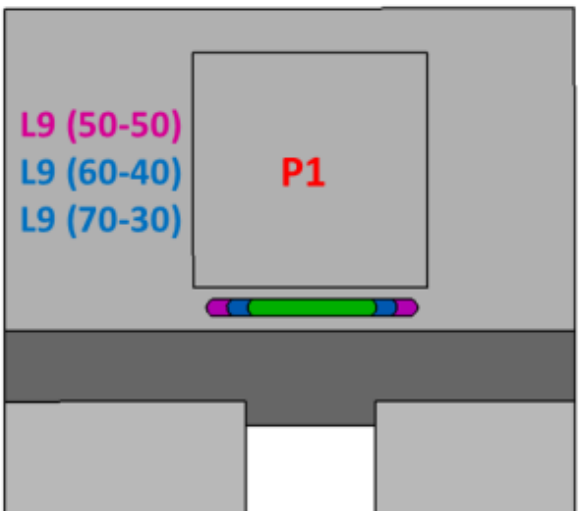

Figure 7-2 Locations of the design extensions of L9

Table 7-2 Geometric parameters of the gaspers and inlet velocities of L9 and its extensions

Flow Rate Ratio (Main Inlet-Gasper)	Gasper Geometric Parameters (mm)		Air Inlet Velocity (m/s)	
	Length	Width	Gasper	Main Inlet
50-50	180	15.11	3.25	7.2
60-40	145	15.11	3.25	8.6
70-30	110	15.11	3.25	10.1

By evaluating the air flow in the vicinity of the passengers, the gasper designs which are considered as proper designs in terms of air flow are further investigated by considering thermal comfort requirements related to temperature distribution.

7.2 Results of the Gasper Design Improvement Study

7.2.1 Air Flow Investigation

To examine the L9 and its extension designs, velocity contours and velocity vector fields are used to observe the flow field around the faces of passengers in detail. Velocity magnitude contours of L9 and its extensions are presented in Figure 7-3 and Figure 7-4 on the vertical plane which passes thought the middle of the faces of the passengers sitting at the interior seats and on the horizontal plane which passes through the middle of the passengers' head level, respectively. It should be noted that, in this stage of the design, to evaluate the performances of the investigated designs according to the comfort requirements in more detail, velocity magnitude range is narrowed to 1 m/s – 3 m/s.

Considering the velocity contours, it can be observed that L9 (50-50) and L9 (60-40) create thermally comfortable environment for the passengers whereas L9 (70-30) cannot. The lower mass flow rate of L9 (70-30) results in lower jet momentum and insufficient air movement around the faces of the passengers. As a result, the further temperature distribution investigation inside of the cabin is performed for L9 (50-50) and L9 (60-40) cases.

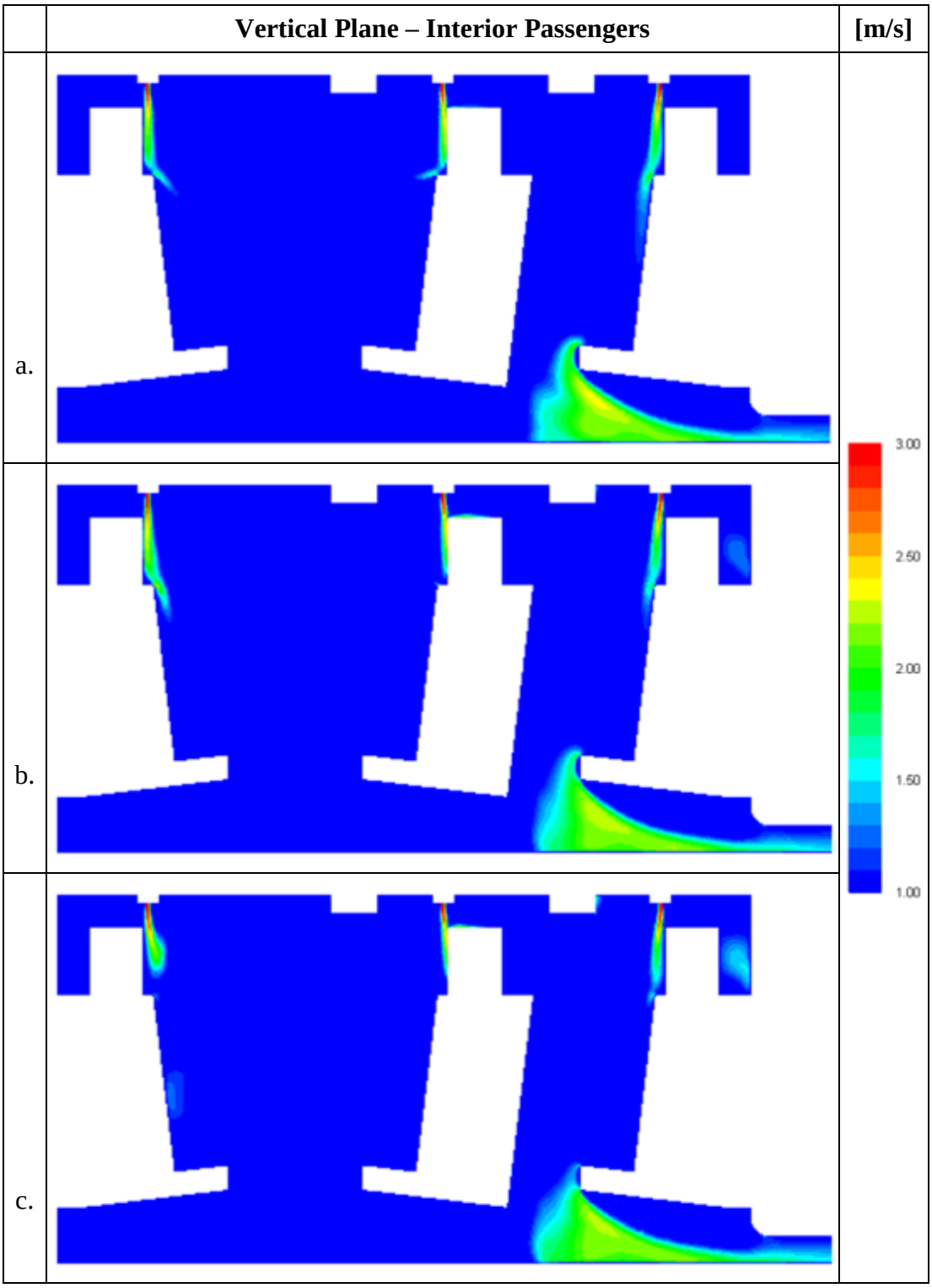

Figure 7-3 Velocity magnitude contours for the passengers sitting at the interior seats for; (a) L9 (50-50); (b) L9 (60-40); (c) L9 (70-30)

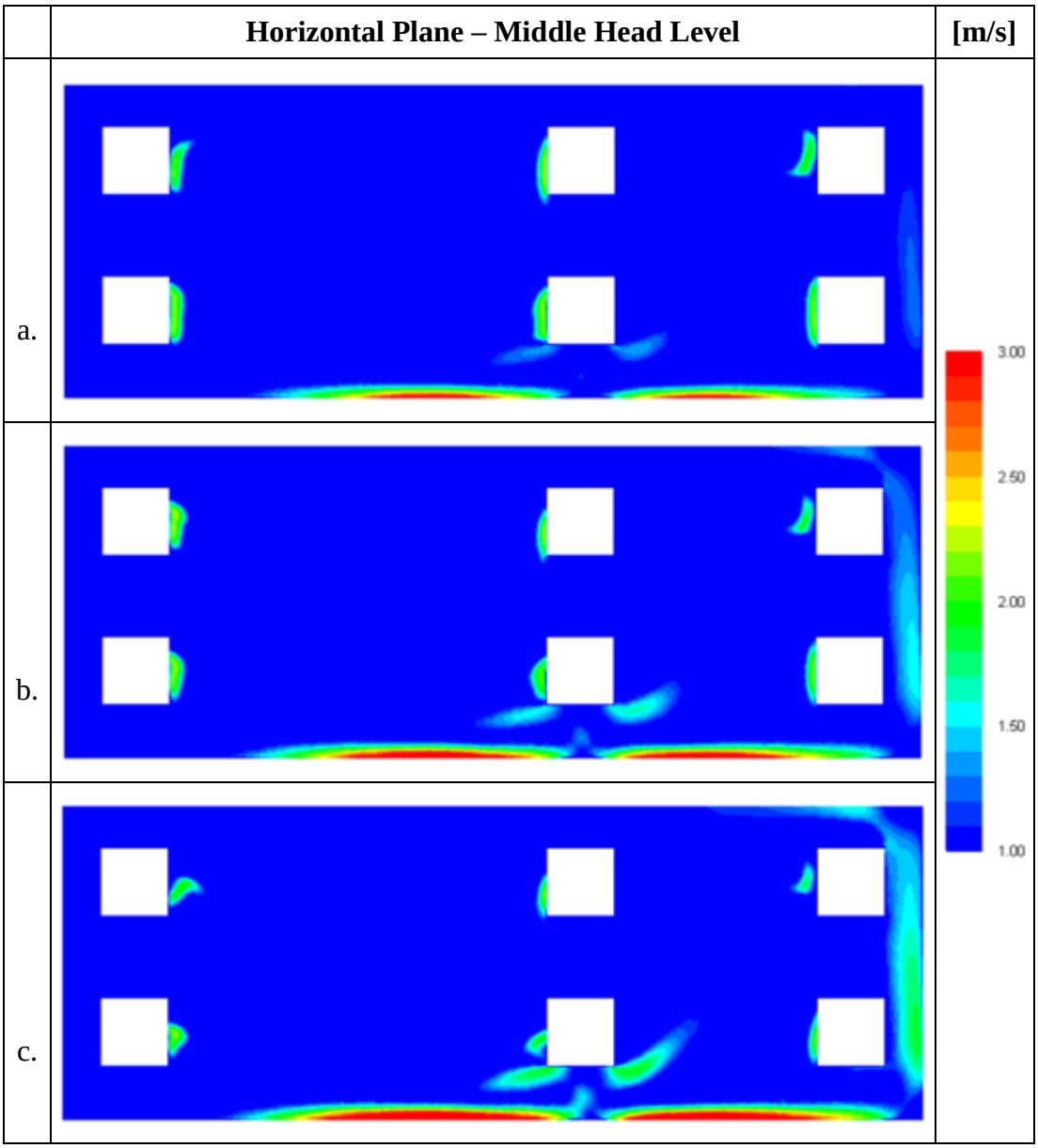

Figure 7-4 Velocity magnitude contours on the horizontal plane at the middle head level for; (a) L9 (50-50); (b) L9 (60-40); (c) L9 (70-30)

7.2.2 Temperature Distribution Investigation

For the temperature distribution investigation, in addition to L9 (50-50) and L9 (60-40) cases, existing gasper design, L0, is also included to examine whether improvement is shown up by the new designs. The flow rate ratio and inlet velocity information of the cases included into the temperature distribution investigation are tabulated in Table 7-3.

Table 7-3 Flow rate ratio and inlet velocities of the cases included into the temperature distribution investigation

Location	Flow Rate Ratio (Main Inlet-Gasper)	Air Inlet Velocity (m/s)	
		Gasper	Main Inlet
L0	50-50	11	7.2
L9	50-50	3.25	7.2
L9	60-40	3.25	8.6

To examine the L9 designs which satisfy air flow requirements, according to the temperature requirement defined in Chapter 5 and to observe the temperature fields, seven vertical planes are determined on which the evaluation to be performed. The planes are determined as; four are passing through the middle of the legs of two neighbor passengers, two are passing through the middle of the faces of two neighbor passengers and one is passing through the contact surface of two neighbor passengers. The projection of the seven vertical planes and corresponding indexes are shown in Figure 7-5. It should be noted that the upper and lower z-coordinates of the vertical planes are determined according to the statement of the temperature variation requirement.

By considering the temperature requirement, uniformity of the temperature distribution is examined by using temperature root mean square (rms) values. When evaluating the temperature rms results, it is important to multiply values by two for

reasonable evaluation since temperature rms value represents the standard deviation from the average whereas the temperature requirement defines the total range of the allowable variation. The plot presenting the temperature rms values of the seven planes is shown in Figure 7-6. In this figure, x-axis shows the indexes of the vertical planes and y-axis shows the temperature rms values.

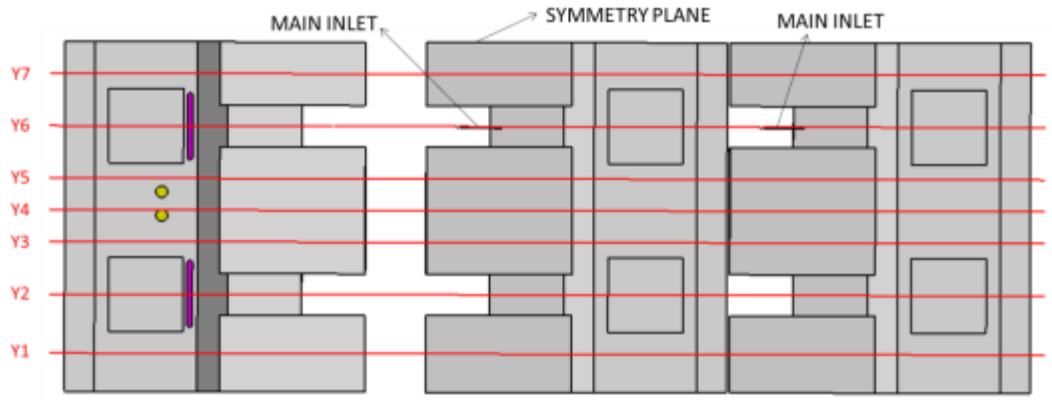

Figure 7-5 Locations and indexes of the temperature field investigation planes

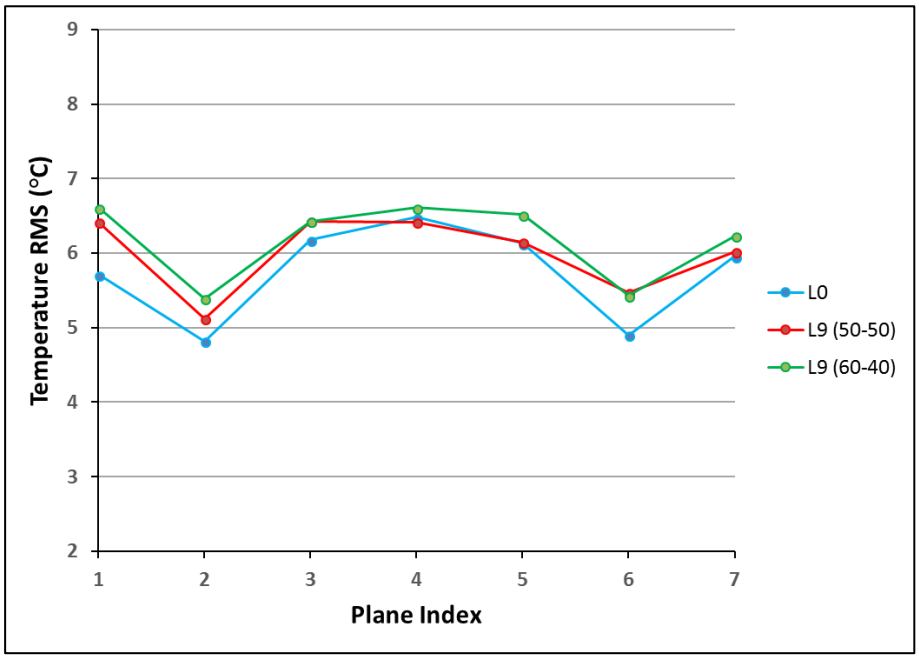

Figure 7-6 Temperature RMS values of the investigated planes

By the Figure 7-6, it can be observed that both the existing design and the proposed designs have the values outside of the range defined by the requirement as the temperature variation measured in a vertical plane from 5 cm above floor level to seated head height should not exceed 2.8°C.

To examine the existence of high temperature rms values and the temperature distribution in more detail, temperature contours are utilized. To illustrate, in Figure 7-7, temperature contours are shown on Y4 plane, located just near the gaspers of L0 case and in Figure 7-8, temperature contours are shown on Y6 plane, passing through the center of the gaspers of both L9 designs. When presenting the temperature contours, the color range is adjusted to evaluate contours more clearly. By considering both figures, it can be obviously seen that the temperature differences between the upper and lower parts of the planes are quite high.

The temperature distribution at the upper region of the cabin can be considered as more crucial for the thermal comfort conditions of the passengers since the faces and most of the body parts of the passengers exist in that region. By considering this issue and the observed high temperature difference, dividing vertical planes into two as upper and lower regions would be more convenient for thermal comfort investigation and would not be an unrealistic approach. This division plane is shown in Figure 7-9.

Figure 7-10, shows the average temperature values of the upper and lower regions of the seven vertical planes. In Figure 7-10, by considering each plane separately, it is observed that the differences between the average temperatures of the upper and lower parts of the planes are more than 3°C for Y2 and Y6 planes, located on the air passage on the way of outlet and more than 5°C for the other planes. The figure clearly indicates the reason of the existence of higher temperature rms values than the desired.

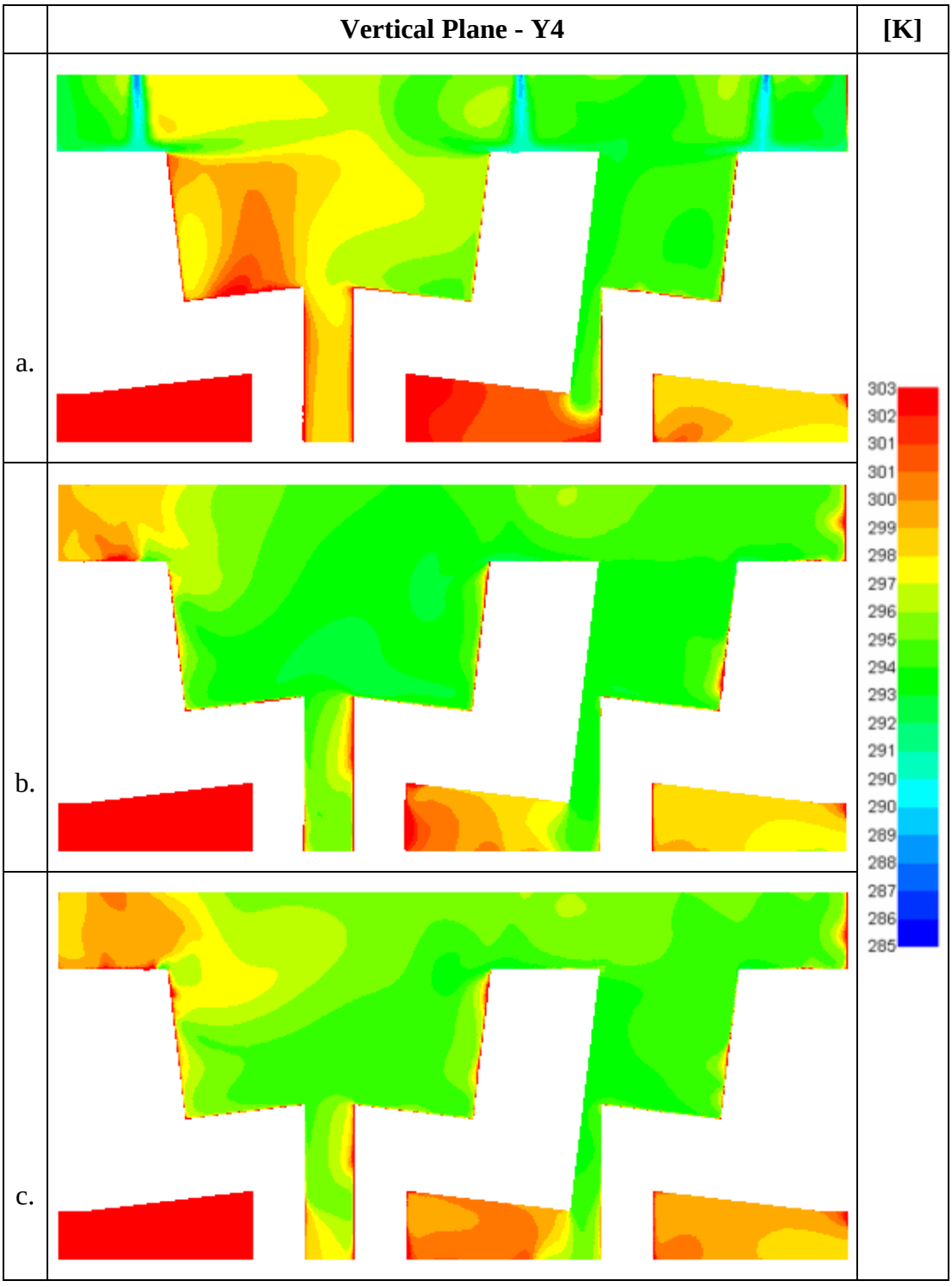

Figure 7-7 Temperature contours on Y4 for; (a) L0; (b) L9 (50-50); (c) L9 (60-40)

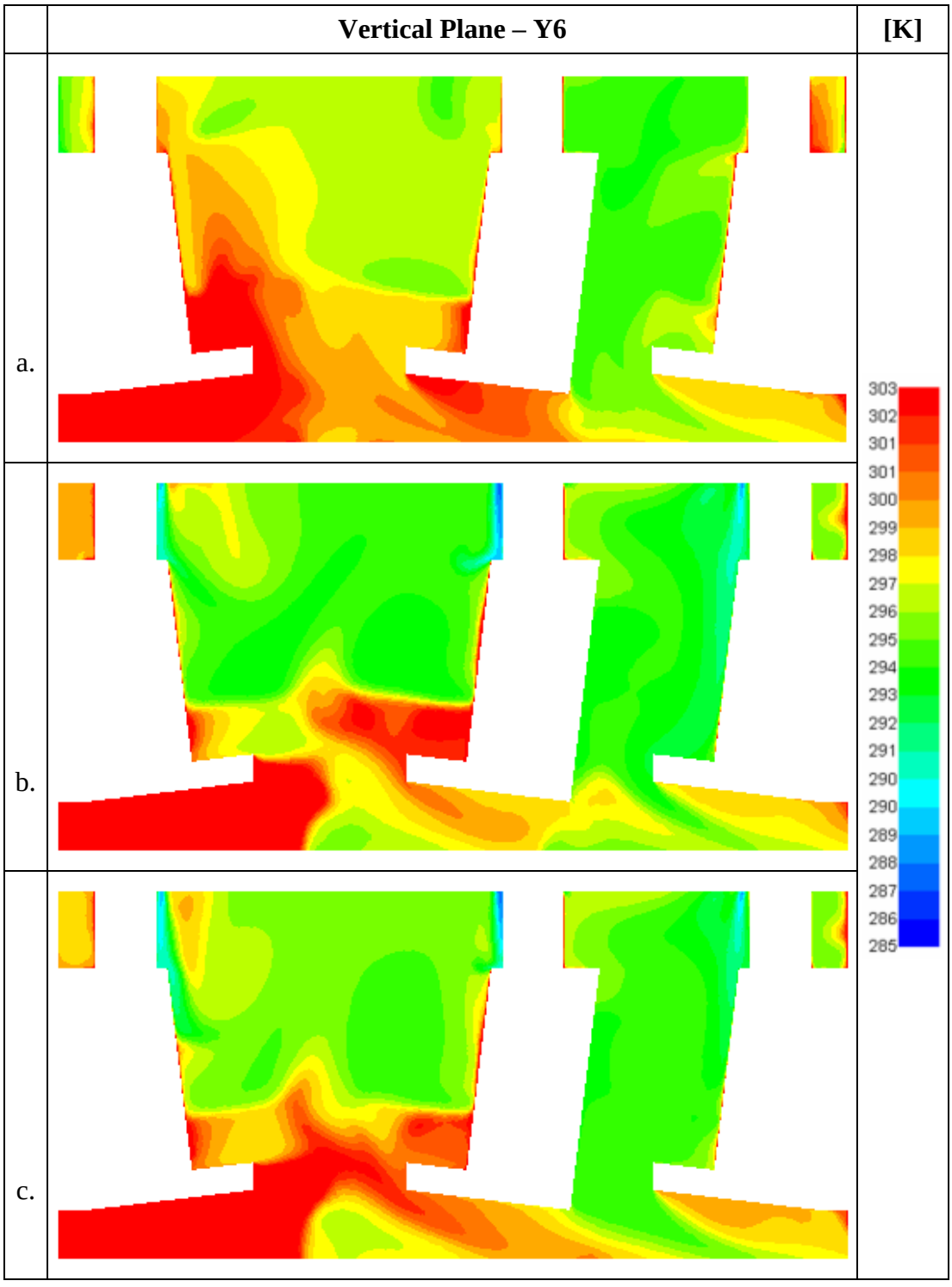

Figure 7-8 Temperature contours on Y6 for; (a) L0; (b) L9 (50-50); (c) L9 (60-40)

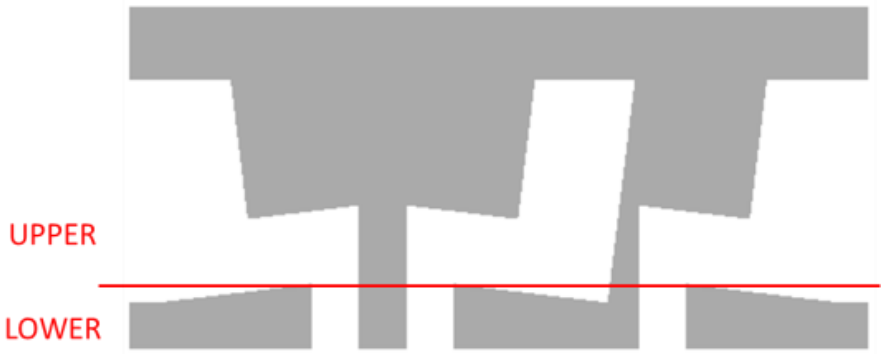

Figure 7-9 Division plane used to investigate temperature uniformity

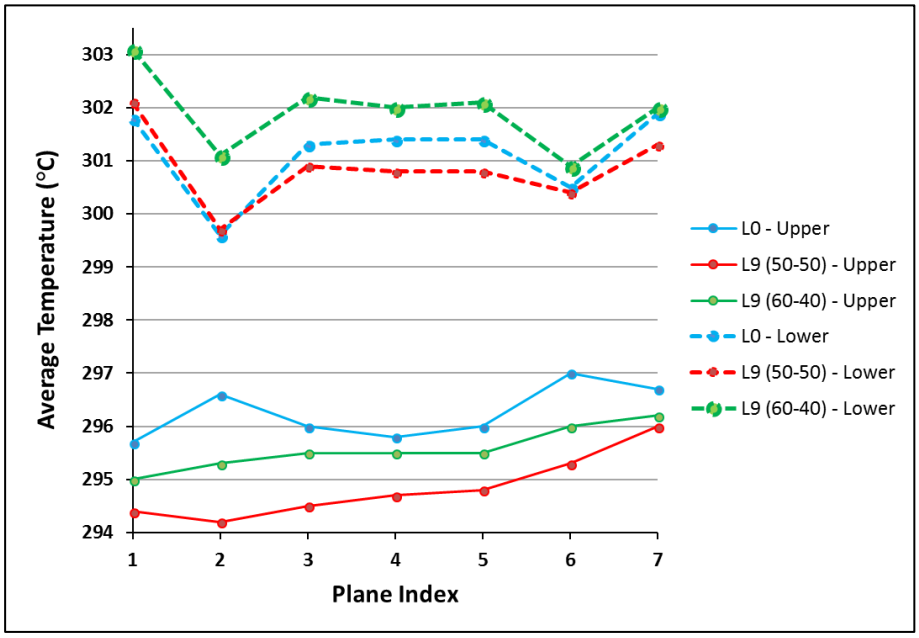

Figure 7-10 Average temperature values of the investigated planes – Upper and lower cabin region

By considering the upper regions of the all seven vertical planes, average temperature values of both new gasper designs, L9 (50-50) and L9 (60-40), are less than the existing design, L0. In fact, L9 (50-50) provides almost 1°C colder air temperatures than L0 (60-40) despite releasing less amount of air from the main inlet. This shows that gaspers may become primarily effective in the cabin flow depending upon their location and design. The reason of L0 not being able to create sufficient air movement in the upper region which results in lack of cooling

performance is related to its location and geometry. To observe this inference in more detail, vector field are used. In Figure 7-11, velocity vector fields colored by temperature are compared on Y4 for L0 and L9 (50-50) cases. It should also be noted that, for these two cases, main inlet velocities are same.

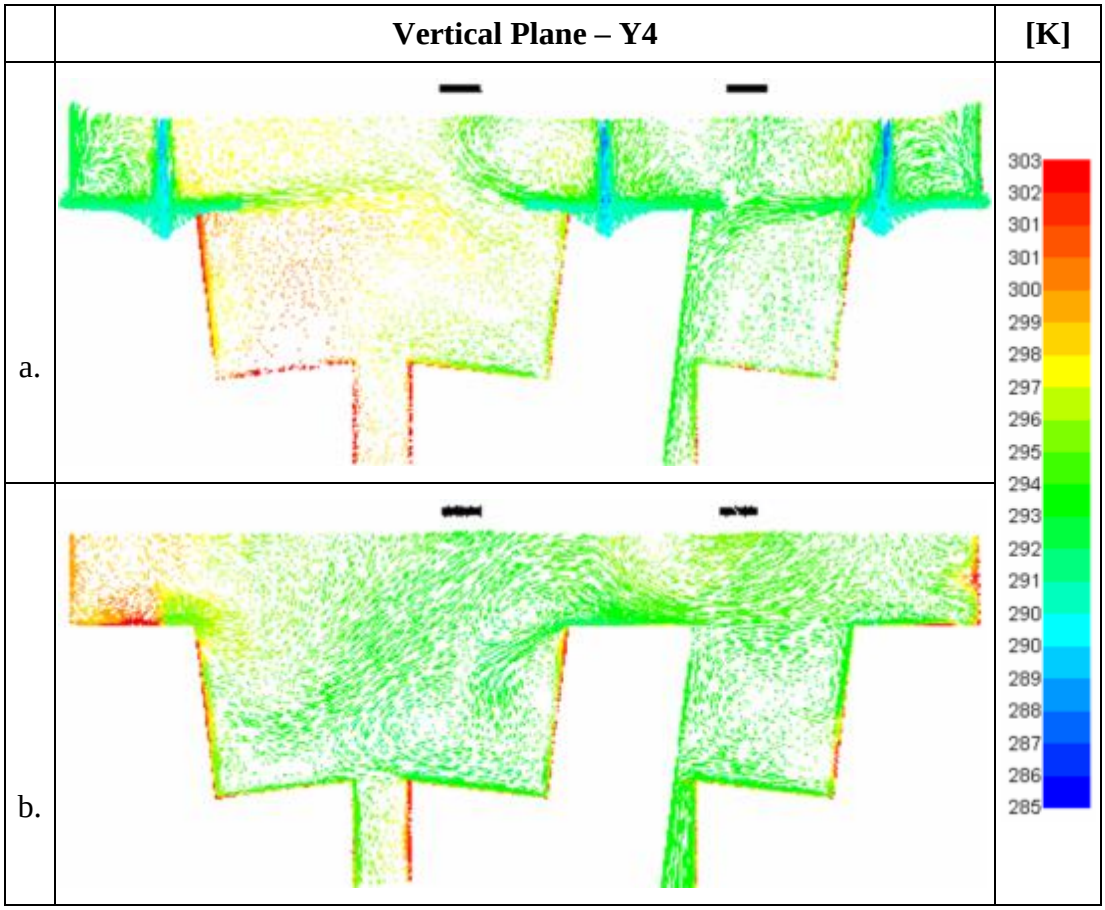

Figure 7-11 Velocity vector fields colored by temperature on Y4 plane for; (a) L0; (b) L9 (50-50)

By considering the vector field magnitudes of both compared cases, it is observed that, although Y4 plane is very close to the gaspers of L0 and air inlet velocities of L0 gaspers are much higher than the L9 (50-50), as a consequence of its location and geometry, L0 cannot create sufficient air movement. As observed from the vector fields of L0, jet flow arising from the gasper impinges on the body of the passenger and spreads radially before going towards to the upper parts of the cabin. Since

gasper jets do not go through the bodies of passengers directly, temperature values are much higher around the bodies of passengers. On the other hand, since the velocity magnitudes are higher in L9 (50-50) case almost on whole plane, it can be observed that conditioned air is distributed throughout the plane more uniformly. In Figure 7-11, the locations of main inlets are also included to give an idea about the effect of main inlets on to the flow field.

To expand the flow field comparison, for the same cases, L0 and L9 (50-50), an observation is done on Y6 plane which is located between the legs of the passengers sitting at the interior seats and on the air passage on the way of outlet. Velocity vector fields on Y6 plane colored by temperature are shown in Figure 7-12.

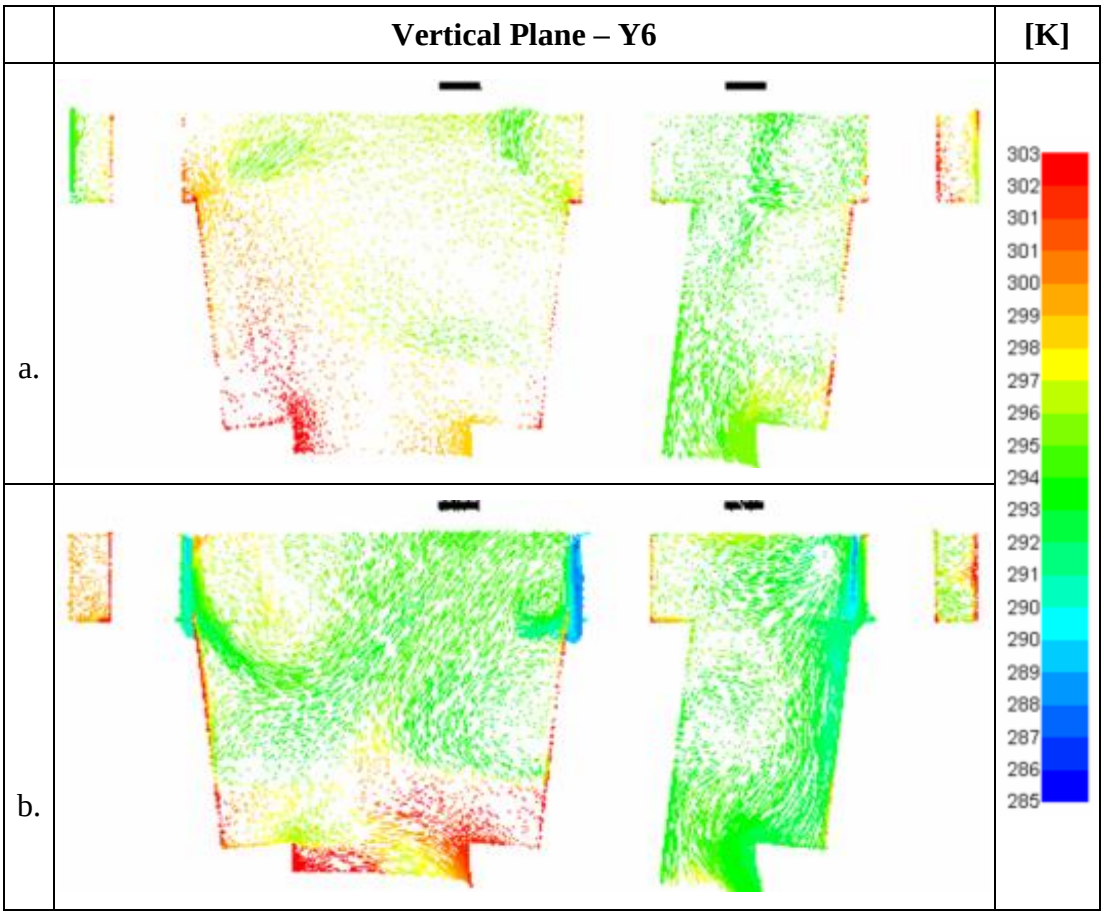

Figure 7-12 Velocity vector fields colored by temperature on Y6 plane for; (a) L0; (b) L9 (50-50)

It can be observed that, for L0 case, because of the low flow velocities, the hot air between the legs of the passengers sitting in the first and second rows penetrates to the upper region of the cabin by a thermal plume effect because of the density difference; therefore, upper part becomes hotter and more non-uniform. On the other hand, although a hotter region exists around the passenger sitting at the third row, the temperature distribution is not as non-uniform as the forward part of the cabin since flow emerging from the gaspers of that region ultimately passes around the third-row sitting passenger's body because of physical feature of the cabin. For the L9 (50-50) case of the same figure, it can be observed that flow velocities are much higher and temperature values are much lower. The hot air between the legs of passengers are restrained by the jet flow; therefore, could not heat up the upper part of the bodies of the passengers.

To evaluate the temperature distribution uniformity, in Figure 7-13 and Figure 7-14, temperature rms values for upper and lower cabin regions are presented for seven investigated planes, respectively.

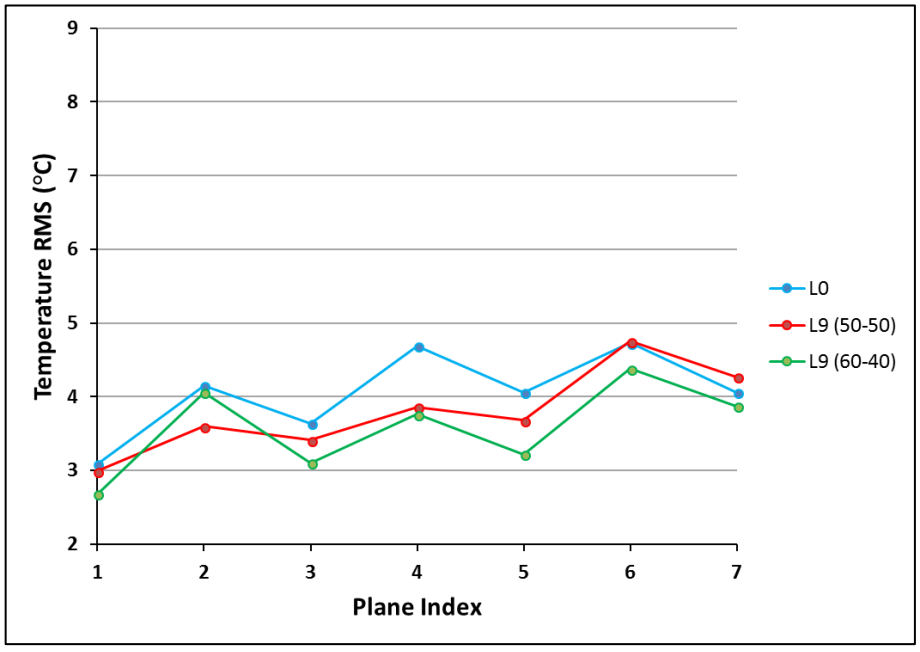

Figure 7-13 Temperature RMS values of the investigated planes – Upper cabin region

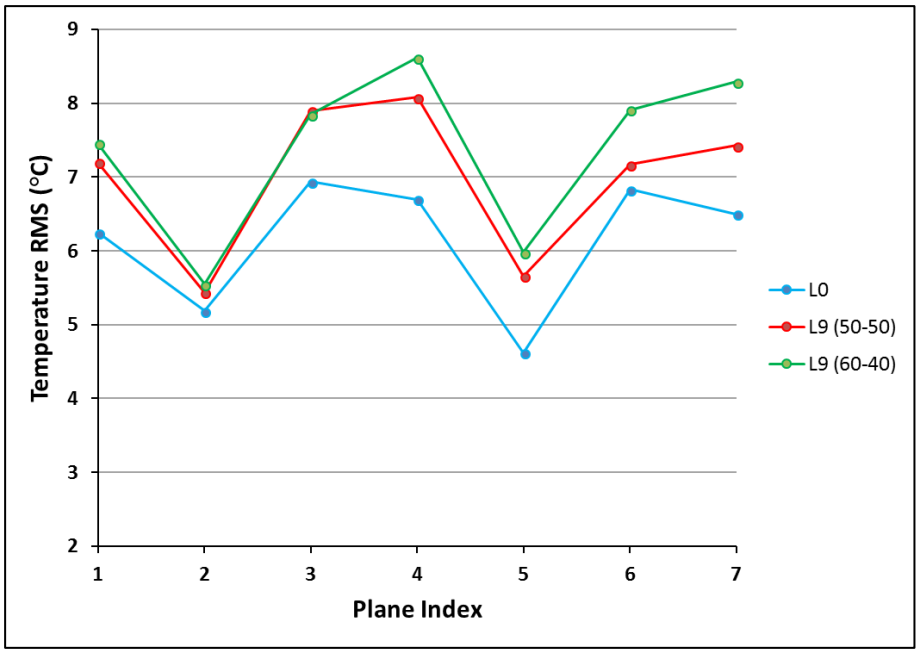

Figure 7-14 Temperature RMS values of the investigated planes – Lower cabin region

By comparing the temperature rms values of Figure 7-13 with the values of Figure 7-14, for all design cases, it can be observed that temperature rms values are less than 5°C for the upper part of the cabin whereas for the lower part of the cabin, values are higher as reaching up to 9°C. Moreover, temperature differences among all seven planes are much lower for the upper region. These results reveal that for all gasper design cases, upper part of the cabin is much more uniform than the lower part. This shows the feasibility of the thermal comfort investigation approach of dividing cabin into two as upper and lower.

The reason of having high rms temperature values in the lower region of the cabin is that the airflow coming from the upper region passes through the narrow spaces between the legs of the passengers and directly goes towards to the outlet without spreading sufficiently. As a consequence of insufficient air movement, stagnant and hot regions exist at the lower part of the cabin resulting in non-uniform temperature profile. It can also be observed that, in the lower region, the temperature rms values are relatively lower for the Y2 and Y6 planes since the air directed towards the cabin

outlet passes through these planes and makes the temperature distribution more uniform. Both having a non-uniform temperature profile and accumulation of high temperature because of the lack of hot air release, lower region also makes temperature rms values of the undivided planes much higher, which is formerly presented in Figure 7-6.

Considering the upper region of the cabin, in Figure 7-13, comparison of the three cases shows that the temperature rms values of both L9 designs are lower than the L0's which means that the new designs provide more uniform temperature in the upper region of the cabin.

By considering temperature variation requirement, it can be interpreted that because of the complex geometry and dense occupancy features of the cabin, showing exact compliance with the requirement is quite difficult by improving air inlet design. However, the evaluation of thermal comfort conditions of the passengers can be performed by stretching the performance criteria by applying realisic approaches.

By considering temperature rms values of undivided planes and the average temperature values of upper and lower cabin regions distinctly, it can be concluded that the reason of L0 case having lower rms values is the lack of cooling performance of L0 in the upper region. Since the upper parts are hotter in L0 case, the temperature difference between hotter lower region is less. That results in existence of lower temperature rms values for L0 case which does not make sense and reflect reality in terms of thermal comfort conditions of the passengers. In fact, it can be concluded that by creating more air movement, the new gasper designs (L9s) show improvement in terms of temperature distribution uniformity in the upper region of the cabin.

7.3 General Evaluation and Proposal of the Best Gasper Design

By comparing the new gasper designs with the existing design, it is revealed that by the new designs, L9 (50-50) and L9 (60-40), desired air velocity magnitudes are obtained in the vicinity of the faces of the passengers. In terms of temperature

distribution, although the temperature variation requirement cannot be directly satisfied, the results showed that by the new designs, an improvement is shown up in the upper part of the cabin where is considered as crucial for the thermal comfort of the passengers. It should be noted that, the improvement is shown up by much lower gasper inlet velocities; that is, locating gaspers in proper locations is more crucial than having high inlet velocities. By the proper gasper locations of the new designs, higher air velocities are obtained inside the cabin, the cooling performance is enhanced and the temperature distribution becomes more uniform.

By considering the two new designs, L0 (50-50) and L0 (60-40), both shows similar success in terms of creating uniform temperature profiles. On the other hand, L9 (50-50) case makes cabin environment nearly 1°C cooler. Moreover, owing to its geometry, L9 (50-50) case distributes air in a broader area on the faces of the passengers. As a result, it is concluded that, a personalized air distribution design having the geometry and location of the L0 (50-50) case with an upstream ducting design distributing air evenly between personalized air inlets and main inlets will improve the thermal comfort conditions of the passengers.

CHAPTER 8

CONCLUSION AND FUTURE WORKS

8.1 Summary and Conclusions

In this study, thermal comfort conditions of the passengers are numerically investigated in a newly designed passenger transportation helicopter by using CFD modeling. The simulations are performed by using standard k-ε turbulence model whose performance competence is confirmed by the experimental and numerical results of Günther et al. [9].

For the existing air supply system, thermal comfort levels of the passengers are investigated and the results revealed the inadequacy of the existing system in creating comfortable environment to the passengers. To improve the thermal comfort of the passengers, a design process is performed by adjusting the locations and changing the design of the gaspers. The procedures followed during the design are clearly explained. By the study, a new design providing the desired air velocities around the faces of the passengers and showing up improvement in terms of temperature distribution is proposed.

By this study, effects of the designs and locations of the air inlets to the flow field are investigated in detail for various cases by quantitative and qualitative evaluation. Moreover, by this study, gasper design parameters are provided to be utilized in the design of any passenger transportation type helicopter.

The following conclusions can be drawn from the present study;

- Gasper, having an inlet velocity in the order of 11 m/s, creates a jet cone inside which air velocity is much higher than the comfort range; however, at the boundary of the cone, air velocity sharply decreases as being below 1 m/s,

the lower limit of the comfort range, outside of the cone. To obtain the desired velocities in the vicinity of the faces of the passenger, gasper inlet velocity should be around 3 m/s.

- For the investigated helicopter cabin, the locations of the gaspers shall be in front of the passenger as being 1 cm away from the faces. For, the same order of inlet velocities, the position parameters supplied in this study can be used universally to locate gasper.
- To increase the effective area of the passenger face under the control of personalized air distribution system, the length of the gaspers should be increased in the lateral direction. For the investigated helicopter, increasing the length of the gaspers also provides reduction of the velocity magnitudes into the comfort range around the faces of the passengers. Broadening gasper length also provides sitting position flexibility to the passengers.
- For the investigated helicopter cabin, personalized air flow has a higher effect on the flow field than the main inlet flow. To illustrate, for the existing design, although the locations of the gaspers are not proper in terms of thermal comfort, a higher air movement in the vicinity of the faces of passengers is observed in the case which personalized air flow is the highest among all.
- For the investigated helicopter cabin, it is observed that the main inlets do not have a direct impact on the passengers' thermal comfort which is a desired property of a main air supply design.
- By high personalized air flow and locating gaspers in proper locations as allowing jets to spread without contacting with an obstacle, a higher air movement and as a result, a more uniform temperature distribution is obtained. Indeed, it is found that the locations of gaspers are more crucial than the inlet velocities to obtain a higher air movement. For the investigated helicopter cabin, the design which the gaspers are located properly as their jets do not impinge on the bodies of the passengers with a 3.25 m/s inlet velocity provides a more uniform temperature distribution than the case in

which the gaspers jets impinge on the shoulders of the passengers with an inlet velocity of 11 m/s.

- The high-density feature of the investigated helicopter cabin creates a barrier as keeping air from cooling the lower regions of the existing helicopter. This causes the existence of a higher temperature difference between the upper and lower regions of cabin. However, temperature distribution of upper parts of the cabin, considered as more crucial on the comfort of the passengers, is more uniform.
- Higher air movement obtained by higher gasper flow also enhances the cooling performance of the ECS.

8.2 Future Works

With regarding to future work, the present study can be further improved in the following ways:

- With a higher computing power source, investigation can be detailed by using a detailed human body model including all physical properties. In addition, when developing CFD model, heat dissipation can be distributed on the surface of the passenger dummies according to the each body part's specific heat generation characteristic.
- With a higher computing power source, simulations can be performed by using actual geometry of the main inlets and gaspers.
- In the thermal comfort point of view, humidity distribution in the cabin for the improved design can be investigated.
- In the health point of view, contaminant concentration distribution and transportation in the cabin for the improved design can be investigated.

REFERENCES

[1] "Airport Council International Europe," Feb. 2018. [Online]. Available: www.aci-europe.org. [Accessed February 2008].

[2] X. Du, B. Li, H. Liu, Y. Wu and T. Cheng, "The appropriate airflow rate for a nozzle in commercial aircraft cabins based on thermal comfort experiments," *Building and Environment,* vol. 112, pp. 132-143, Feb. 2017.

[3] Feb. 2018. [Online]. Available: http://www.hse.gov.uk.

[4] M. Kühn , J. Bosbach and C. Wagner, "Experimental parametric study of forced and mixed convection in a passenger aircraft cabin mock-up," *Building and Environment,* vol. 44, no. 5, p. 961–970, May 2009.

[5] V. Bianco, O. Manca, S. Nardini and M. Roma, "Numerical investigation of transient thermal and fluidynamic fields in an executive aircraft cabin," *Applied Thermal Engineering,* vol. 29, no. 16, p. 3418–3425, Nov. 2009.

[6] Z. Fang, H. Liu, B. Li, A. Baldwin, J. Wang and K. Xia, "Experimental investigation of personal air supply nozzle use in aircraft cabins," *Applied Ergonomics,* vol. 47, pp. 193-202, Mar. 2015.

[7] R. You, J. Chen, Z. Shi, W. Liu, C.-H. Lin, D. Wei and Q. Chen, "Experimental and Numerical Study of Airflow Distribution in an Aircraft Cabin Mockup with a Gasper On," *Building Performance Simulation,* vol. 9, no. 5, pp. 555-566, Jan. 2016.

[8] J. Niu, N. Gao, M. Phoebe and Z. Huigang, "Experimental study on a chair-based personalized ventilation system," *Building and Environment,* vol. 42, no. 2, pp. 913-925, Feb. 2007.

[9] G. Günther, J. Bosbach, J. Pennecot, C. Wagner, T. Lerche and I. Gores, "Experimental and numerical simulations of idealized aircraft cabin flows," *Aerospace Science and Technology,* vol. 10, no. 7, p. 563–573, Oct. 2006.

[10] Z. Zhai, Z. Zhang, W. Zhang and Q. Chen, "Evaluation of Various Turbulence Models in Predicting Airflow and Turbulence in Enclosed Environments by CFD: Part-1: Summary of Prevalent Turbulence Models," *HVAC&R Research,*

vol. 13, no. 6, pp. 853-870, Aug. 2007.

[11] Z. Zhang, W. Zhang, Z. J. Zhai and Q. Y. Chen, "Evaluation of Various Turbulence Models in Predicting Airflow and Turbulence in Enclosed Environments by CFD: Part 2—Comparison with Experimental Data from Literature," *HVAC&R Research,* vol. 13, no. 6, pp. 871-886, Aug. 2007.

[12] M. Wang and Q. Chen, "Assessment of Various Turbulence Models for Transitional Flows in an Enclosed Environment (RP-1271)," *HVAC&R Research,* vol. 15, no. 6, pp. 1099-1119, Nov. 2009.

[13] J. Li, C. Xiaodong, L. Junjie, W. Congcong and Z. Yongzhi, "Global airflow field distribution in a cabin mock-up measured via large-scale 2D-PIV," *Building and Environment,* vol. 93, no. 2, pp. 234-244, Aug. 2015.

[14] W. Liu, J. Wen, J. Chao, W. Yin, C. Shen, D. Lai, C.-H. Lin, J. Liu, H. Sun and Q. Chen, "Accurate and High-Resolution Boundary Conditions and Flow Fields in the First-Class Cabin of an MD-82 Commercial Airliner," *Atmospheric Environment,* vol. 56, pp. 33-44, Sep. 2012.

[15] W. Liu, J. Wen, C.-H. Lin, J. Liu, Z. Long and Q. Chen, "Evaluation of Various Categories of Turbulence Models for Predicting Air Distribution in an Airliner Cabin," *Building and Environment,* vol. 65, pp. 118-131, July 2013.

[16] J. Bosbach, J. Pennecot, C. Wagner, M. Raffel, T. Lerche and S. Repp, "Experimental and numerical simulations of turbulent ventilation in aircraft cabins," *Energy,* vol. 31, no. 5, pp. 694-705, Apr. 2006.

[17] W. Yan, Y. Zhang, Y. Sun and D. Li, "Experimental and CFD study of unsteady airborne pollutant transport within an aircraft cabin mock-up," *Building and Environment,* vol. 44, no. 1, p. 34–43, Jan. 2009.

[18] Z. Zhang, X. Chen, S. Mazumdar, T. Zhang and Q. Chen, "Experimental and Numerical Investigation of Airflow and Contaminant Transport in an Airliner Cabin Mockup," *Building and Environment,* vol. 44, no. 1, pp. 85-94, Jan. 2009.

[19] A. J. Baker , M. B. Taylor , N. S. Winowich and M. R. Heller, "Prediction of the Distribution of Indoor Air Quality and Comfort in Aircraft Cabins Using Computational Fluid Dynamics (CFD)," in *Air Quality and Comfort in Airliner Cabins*, N. L. Nagda, Ed., ASTM SP 1393, 2000.

[20] S. Liu, L. Xu, J. Chao, C. Shen, J. Liu, H. Sun, X. Xiao and G. Nan, "Thermal

environment around passengers in an aircraft cabin," *HVAC&R Research,* vol. 19, no. 5, pp. 627-634, July 2013.

[21] S. Yin and T. T. Zhang, "A new under-aisle displacement air distribution system for wide-body aircraft cabins," in *Building Simulation 2009,* Glasgow, Scotland, 2009.

[22] W. Liu, R. Duan, C. Chen, C.-H. Lin and Q. Chen, "Inverse design of the thermal environment in an airliner cabin by use of the CFD-based adjoint method," *Energy and Buildings,* vol. 104, p. 147–155, Oct. 2015.

[23] C. Wang, J. Liu, J. Li, Y. Guo and N. Jiang, "Turbulence characterization of instantaneous airflow in an aisle of an aircraft cabin mockup," *Building and Environment,* vol. 116, pp. 207-217, May 2017.

[24] Z. Yao, X. Zhang, C. Yang and F. He, "Flow Characteristics and Turbulence Simulation for an Aircraft Cabin Environment," *Procedia Engineering,* vol. 121, p. 1266 – 1273, 2015.

[25] C. H. Lin, T. T. Wu, R. H. Horstman, P. A. Lebbin, M. H. Hosni, B. W. Jones and B. T. Beck, "Comparison of Large Eddy Simulation Predictions with Particle Image Velocimetry Data for the Airflow in a Generic Cabin Model," *HVAC&R Research,* vol. 12, no. 3, pp. 935-951, Apr. 2006.

[26] A. J. Baker, S. C. Ericson, J. A. Orzechowski, K. L. Wong and R. P. Garner, "Aircraft Passenger Cabin ECS-Generated Ventilation Velocity and Mass Transport CFD Simulation: Velocity Field Validation," *Journal of the IEST,* vol. 49, no. 2, p. 51–83, Oct. 2006.

[27] B. A. J., "Validation for CFD prediction of mass transport in an aircraft passenger cabin," University of Tennessee, Knoxville, 2005.

[28] B. Li, J. Li, Y. Huang, H. Yin, C.-H. Lin, D. Wei, X. Shen, J. Liu and Q. Chen, "Experimental studies of thermal environment and contaminant transport in a commercial aircraft cabin with gaspers on," *Indoor Air,* vol. 26, no. 5, p. 806–819, Nov. 2015.

[29] T. Zhang and Q. Y. Chen, "Novel air distribution systems for commercial aircraft cabins," *Building and Environment,* vol. 42, no. 4, pp. 1675-1684, Apr. 2007.

[30] J. Fiser and M. Jícha, "Impact of air distribution system on quality of ventilation

in small aircraft cabin," *Building and Environment,* vol. 69, pp. 171-182, Nov. 2013.

[31] R. You, W. Liu, J. Chen, C.-H. Lin, D. Wei and Q. Chen, "Predicting airflow distribution and contaminant transport in aircraft cabins with a simplified gasper model," *Building Performance Simulation,* vol. 9, no. 6, pp. 699-708, June 2016.

[32] C.-H. Lin, R. Horstman, M. Ahlers, L. Sedgwick, K. Dunn, J. Topmiller, J. Bennett and S. Wirogo, "Numerical simulation of airflow and airborne pathogen transport in aircraft cabins - Part II: Numerical simulation of airborne pathogen transport," *ASHRAE Transactions,* vol. 111, pp. 755-763, Jan. 2005.

[33] P. Zítek, T. Vyhlídal, G. Simeunovic, L. Nováková and J. Cízek, "Novel personalized and humidified air supply for airliner passengers," *Building and Environment,* vol. 45, no. 11, pp. 2345-2353, Nov. 2010.

[34] T. T. Zhang, P. Li and S. Wang, "A Personal Air Distribution System with Air Terminals Embedded in Chair Armrests on Commercial Airplanes," *Building and Environment,* vol. 47, no. 1, pp. 89-99, Jan. 2012.

[35] H. E. Khalifa, M. I. Janos and J. F. Dannenhoffer, "Experimental investigation of reduced-mixing personal ventilation jets," *Building and Environment,* vol. 44, no. 8, p. 1551–1558, Aug. 2009.

[36] J. S. Russo, T. Q. Dang and H. E. Khalifa, "Computational analysis of reduced-mixing personal ventilation jets," *Building and Environment,* vol. 44, no. 8, p. 1559–1567, Aug. 2009.

[37] R. You, J. Chen, C.-H. Lin, D. Wei and Q. Chen, "Investigating the impact of gaspers on cabin air quality in commercial airliners with a hybrid turbulence model," *Building and Environment,* vol. 111, pp. 110-122, Jan. 2017.

[38] B. E. Launder and D. B. Spalding, in *Lectures in Mathematical Models of Turbulence,* London, Academic Press, 1972, p. 169.

[39] ANSYS, Inc, *ANSYS Fluent 15.0 Theory Guide,* 2013.

[40] M. Wolfstein, "The velocity and temperature distribution in one-dimensional flow with turbulence augmentation and pressure gradient," *International Journal of Heat and Mass Transfer,* vol. 12, no. 3, pp. 301-308, Mar. 1969.

[41] B. A. Kader, "Temperature and concentration profiles in fully turbulent boundary layers," *International Journal of Heat and Mass Transfer*, vol. 24, no. 9, pp. 1541-1544, Sep. 1981.

[42] ANSYS, Inc, *Introduction to ANSYS Fluent 16.0 - Solver Settings,* 2015.

[43] ANSYS, Inc, *Introduction to ANSYS Fluent 16.0 - Turbulence Modeling,* 2015.

[44] SAE International, *SAE AIR 1168/3: Aerospace Information Report - Aerothermodynamic Systems Engineering and Design,* 2011.

[45] ANSYS, Inc, *ANSYS Fluent 12.0 User's Guide*, 2009.

[46] SAE International, *SAE ARP292 - Environmental Control Systems for Helicopters,* C ed., 2003.

APPENDICES

A.1 Mesh Independence Results of the Helicopter Cabin Investigation

In this part, mesh independence result of the helicopter cabin investigation is presented.

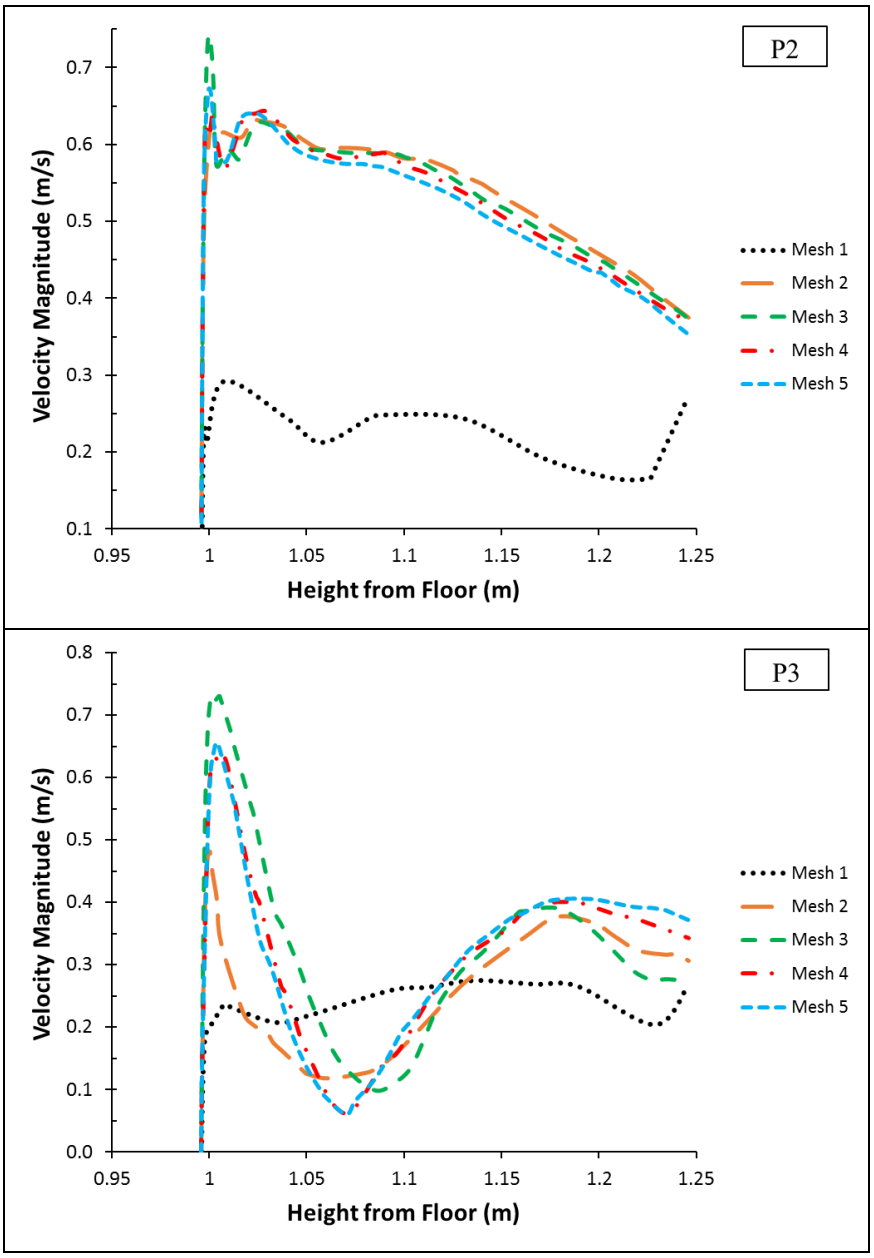

Figure A-1 Mesh independence results for velocity magnitude on vertical lines

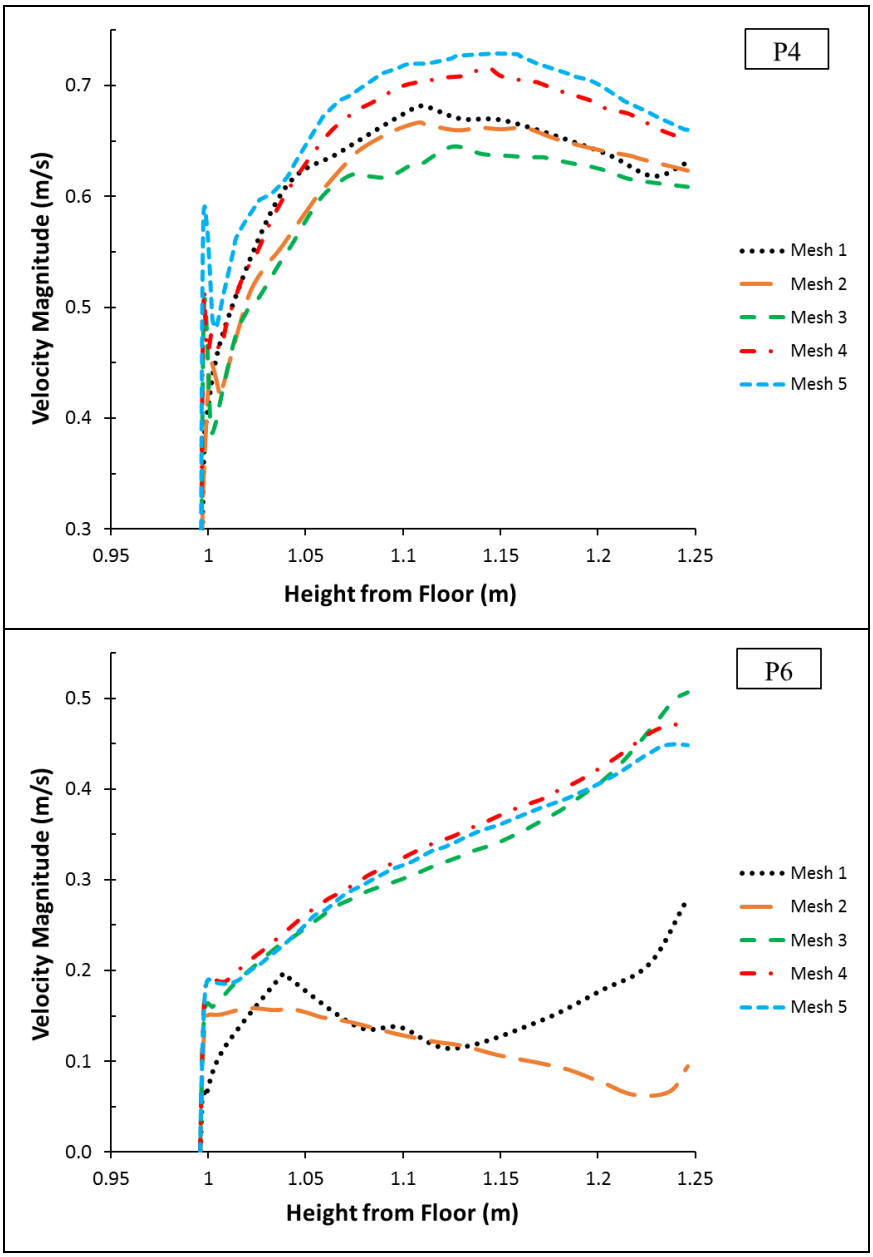

Figure A-1 (Cont'd) Mesh independence results for velocity magnitude on vertical lines

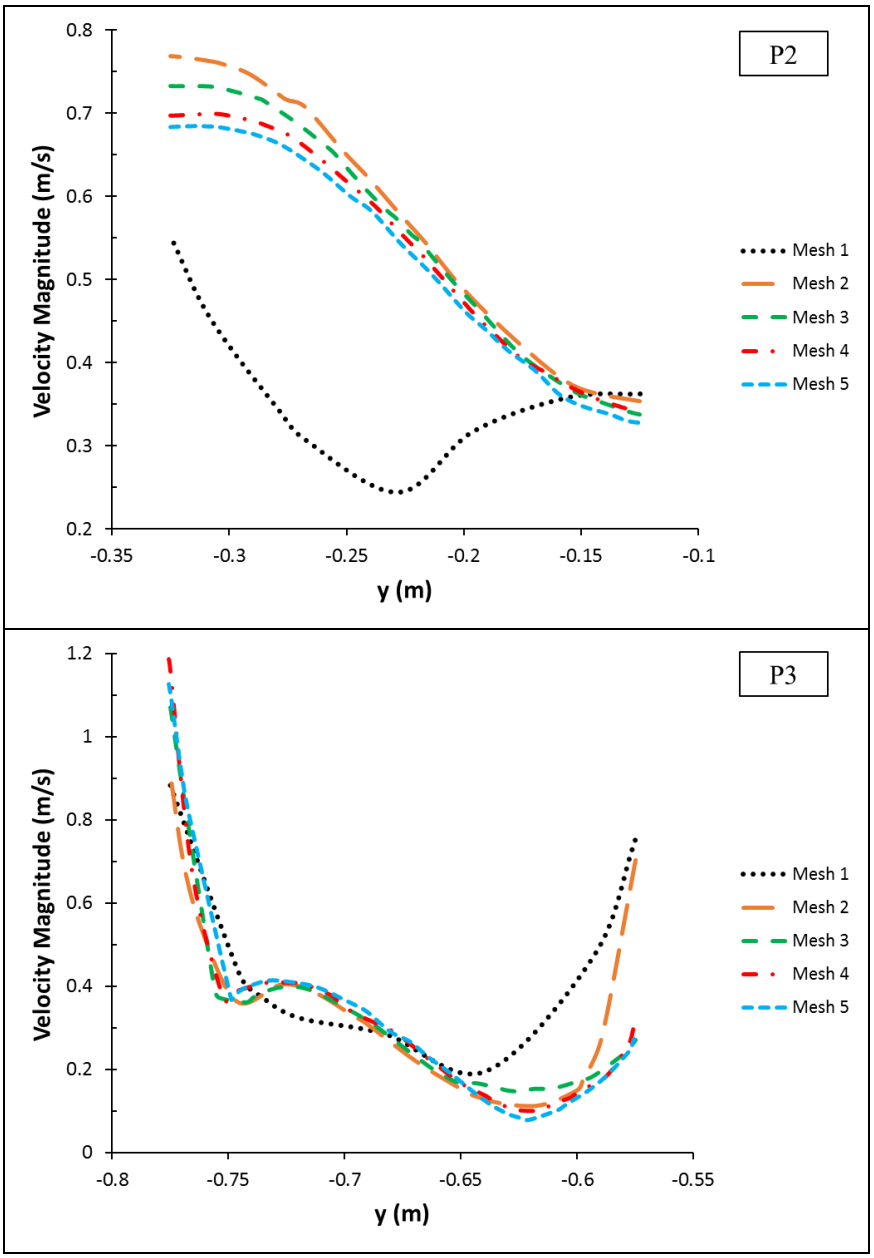

Figure A-2 Mesh independence results for velocity magnitude on horizontal lines

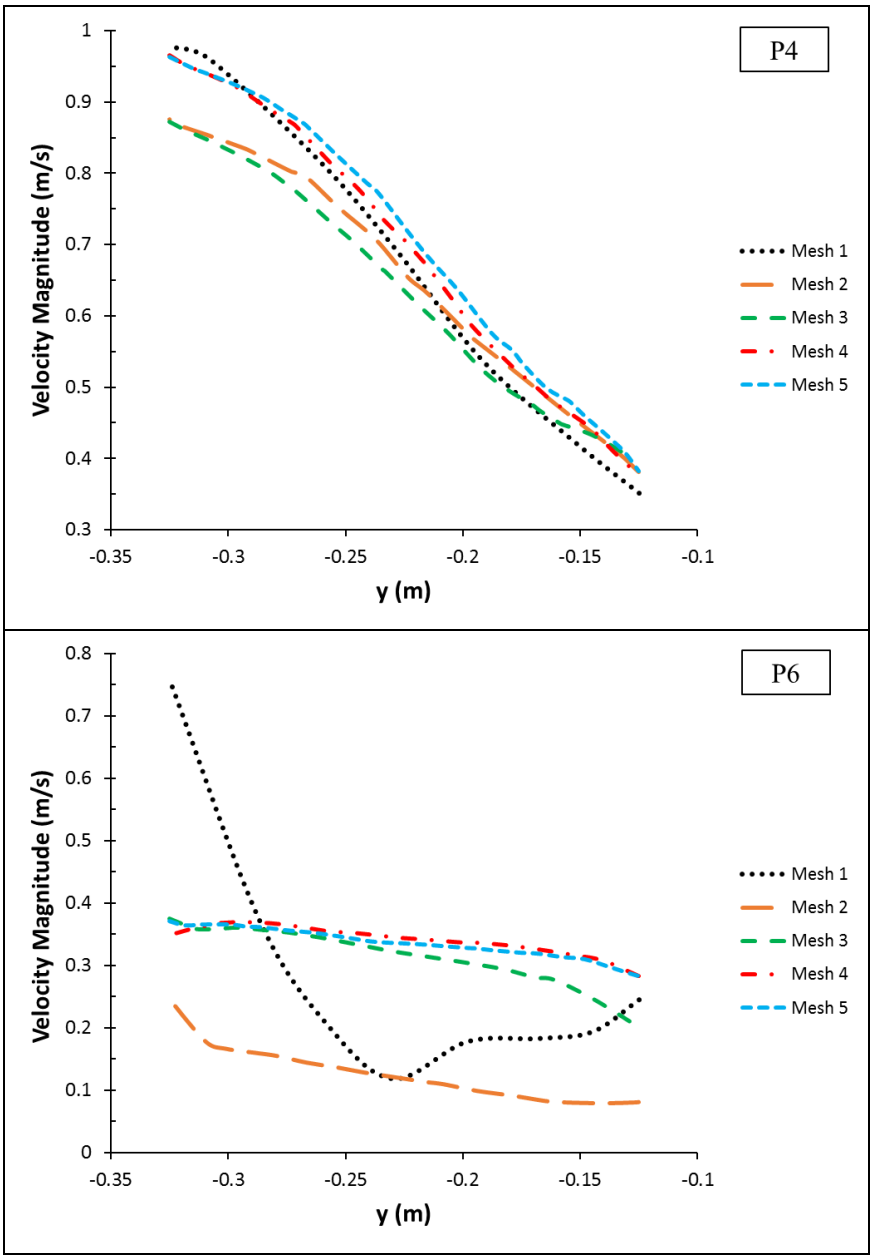

Figure A-2 (Cont'd) Mesh independence results for velocity magnitude on horizontal lines

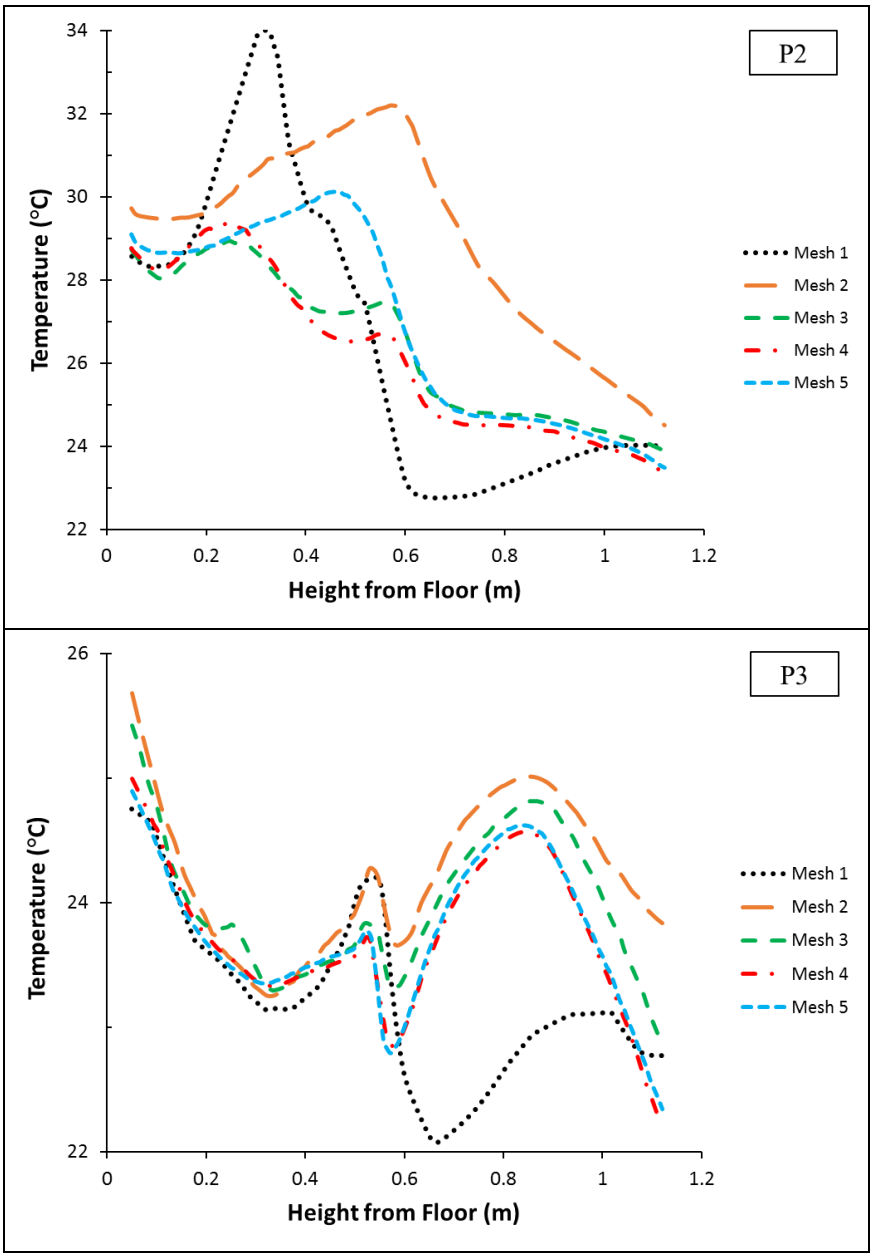

Figure A-3 Mesh independence results for temperature value

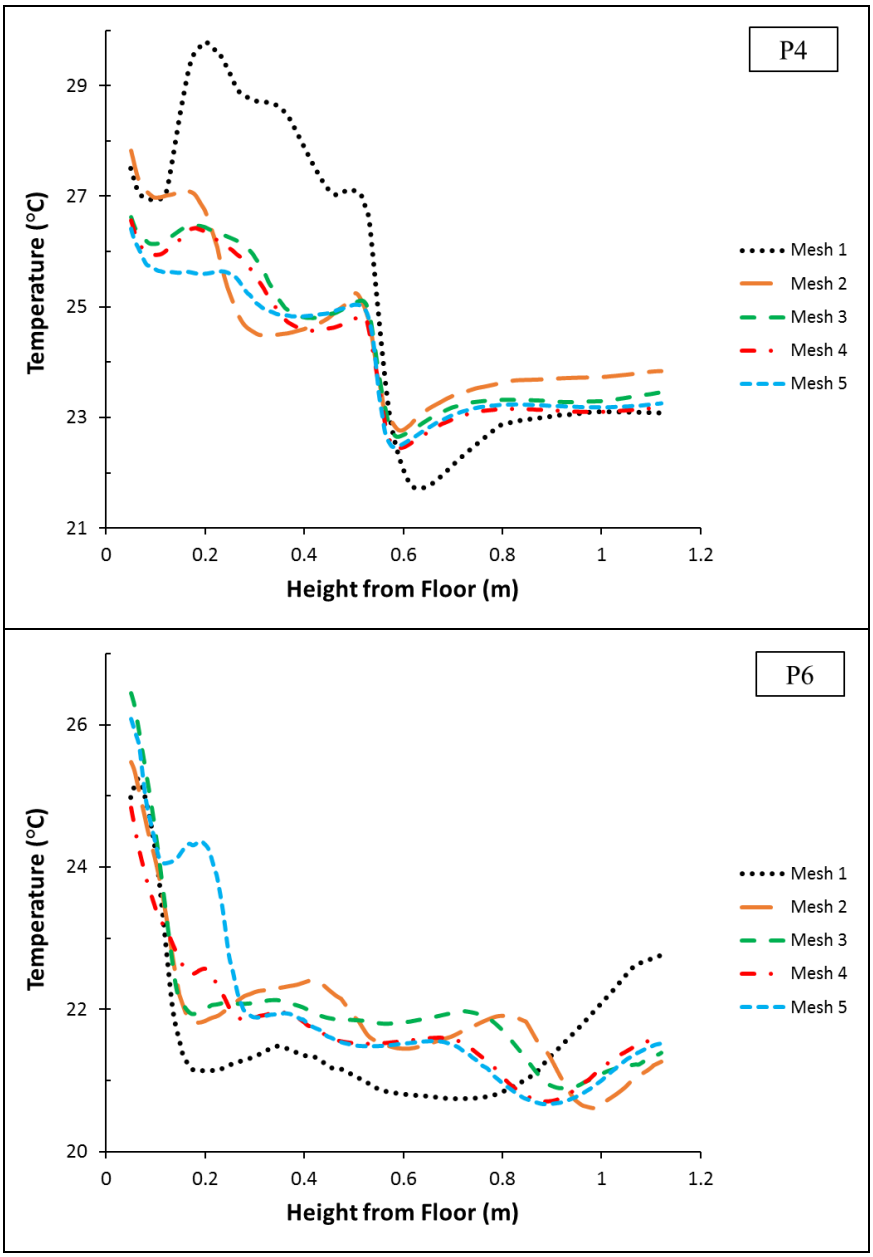

Figure A-3 (Cont'd) Mesh independence results for temperature value